UCRL-20248

c. 2

K^+d INTERACTIONS FROM 865 TO 1365 MeV/c

Allan Akira Hirata
(Ph. D. Thesis)

October 1970

AEC Contract No. W-7405-eng-48

LAWRENCE RADIATION LABORATORY
UNIVERSITY of CALIFORNIA BERKELEY

UCRL-20248

c. 2

DISCLAIMER

K^+d INTERACTIONS FROM 865 TO 1365 MeV/c

Contents

K^+d INTERACTIONS FROM 865 TO 1365 MeV/c

Allan Akira Hirata

Lawrence Radiation Laboratory
University of California
Berkeley, California 94720

October 1, 1970

ABSTRACT

In this paper we present some detailed experimental results on the K^+d interactions from 865 to 1365 MeV/c incident beam momentum. We present measurements on several K^+d partial cross sections and calculate most of the others using relations derived from isospin conservation and data from other experiments. The most striking feature of the cross section data is the abrupt rise of the total single-pion-production cross section near 1200 MeV/c. We also extract isospin-0 KN partial cross sections and find a rapid increase of $\sigma_o(KN\pi)$ at the threshold for the quasi-two-body reaction $K\,N \rightarrow K^*N$. As in the case of the isospin-1 K^+N system, it appears that the structure around 1200 MeV/c in the total cross section for the isospin-0 K^+N system is well reconstructed by the sum of three smoothly varying, non-peaked channel cross sections $\sigma_o(KN)$, $\sigma_o(KN\pi)$, and $\sigma_o(KN\pi\pi)$. We compare the charge exchange data with the predictions of a Regge model and find them to be consistent with the results of high-energy fits. We study the reaction $K\,N \rightarrow K^*N$ near threshold and find that the data can be easily interpreted in terms of t-channel phenomena.

I. INTRODUCTION

In 1963 the Bevatron Scheduling Committee approved a low energy K^+d experiment as a companion to a high statistics, low energy K^+p experiment. These experiments were intended to study in detail the K^+p and K^+n interactions in the region of the single pion production threshold and to search for $\kappa(725)$ meson production at momenta just below the threshold for production of other resonances [e.g., $K^*(891)$]. In the spring and summer of 1964, the Lawrence Radiation Laboratory 25-inch bubble chamber was used in a 600 000 picture exposure of K^+p interactions and a 100 000 picture exposure of K^+d interactions at selected momenta in the region from 860 to 1600 MeV/c incident K^+ meson momentum. The results of the low-energy K^+p experiment have been reported by Bland et al.[1-8] We report here the results of our analysis of the low energy K^+d data.

Since the film was taken we have been further motivated in this experiment by the very accurate K^+p and K^+d total cross section measurements made in this region by Cool et al.[9] at Brookhaven and Bugg et al.[10] at Rutherford Laboratory. Their measurements show a clear peak in the K^+p cross section at $P_K \approx 1250$ MeV/c as well as a more pronounced peak in the K^+d cross section at $P_K \approx 1150$ MeV/c, (Fig. 1, we have included the new total cross section measurements recently reported by the Arizona group[11] in the region 360 to 720 MeV/c.) The structure in each channel appears 600 to 700 MeV/c above the single-pion production threshold.

The K^+p cross section is the isospin-1 K^+N cross section [we denote the nucleon doublet by $N \equiv (p,n)$]. The isospin-0 cross section is extracted from the K^+p and K^+d cross sections as follows. If one assumes the impulse approximation as well as the Glauber-Wilkin[12-15] shading effect, then one can calculate a "folded" K^+n cross section from the relation

$$"\sigma(K^+n)" = \sigma(K^+d) - "\sigma(K^+p)" + \sigma_{GW}, \qquad (1)$$

where $\sigma(K^+d)$ is the measured K^+d cross section, $"\sigma(K^+p)"$ is the measured K^+p cross section folded into the nucleon momentum distribution in deuterium, and σ_{GW} is the Glauber-Wilkin shading correction. The

isospin-0 K^+N cross section is then obtained from

$$\text{"}\sigma_o\text{"} = 2\,\text{"}\sigma(K^+n)\text{"} - \text{"}\sigma(K^+p)\text{"}$$
$$= 2\,\sigma(K^+d) - 3\,\text{"}\sigma(K^+p)\text{"} + 2\,\sigma_{GW}, \qquad (2)$$

which gives σ_o on unfolding. The isospin-0 total K^+N cross section so deduced is shown in Fig. 2 along with the isospin-1 total K^+N cross section. Both distributions show distinct enhancements around 1200 MeV/c.

Peaks or structure in total cross sections that have been observed in πN and $\bar{K}N$ systems have usually been attributed to the presence of s-channel resonances in these systems. If one then speculates that similarly the enhancements observed in the K^+N system may be due to the presence of two new resonances, they would have the following approximate properties:

Name	P (MeV/c)	Mass (MeV)	Width (MeV)	I	Y	S	Bump (mb)	(J+1/2)x	SU_3
Z_0^*	1150	1863	150	0	2	1	8	0.55	$\overline{10}$
Z_1^*	1250	1910	180	1	2	1	4	0.31	27

However, from the point of view of the quark model, such particles would be unique for the following reason. All well-established strongly-interacting particles and resonances have quantum numbers that permit their classification as quark-antiquark ($q\bar{q}$) states for mesons or as triple-quark (qqq) states for baryons. The Z^*'s, on the other hand, would have to be constructed out of five quarks ($qqqq\bar{q}$) and would be considered exotic.

Bland et al.[1-8] have studied the K^+p reactions around 1 GeV/c and observe the cross section behavior shown in Fig. 3. They find that the peak at 1250 MeV/c in the K^+p system is very well reconstructed by the sum of three smoothly varying, non-peaked channel cross sections. The rise of the total cross section above 800 MeV/c is associated with the rapidly rising single-pion production cross section which, incidently, appears to be dominated by the quasi-two-body channels $K\Delta(1236)$ and $K^*(891)N$. The maximum in the K^+p total cross section is reached when the rate of rise of the single-pion production cross section is just balanced

by the rate of fall of the elastic cross section. This maximum is followed by a drop as the single-pion production cross section levels off while the elastic cross section continues to fall. Finally, this drop is arrested when the double-pion production cross section begins to rise around 1500 MeV/c. Thus the structure in the K^+p total cross section at 1250 MeV/c does not appear to arise from structure in any single partial cross section, but rather it seems to be a consequence of the sharp rises of the single- and double-pion production channels at widely separated thresholds. Bland et al. emphasize that although this interpretation of the structure in the K^+p total cross section is at variance with the conventional resonance interpretation it does appear to be completely in accord with their observations that the detailed behavior of angular distributions and polarizations in the inelastic channels appear to be smooth even through the momentum region in which the structure in the total cross section appears.

Several partial-wave analyses of the K^+p elastic scattering have been recently reported.[16] Each of these analyses finds more than one solution to choose from, indicating that the data are not presently good enough to eliminate some of the possibilities. Each analysis gets at least one solution with a P_{13} amplitude traversing the Argand plot in a counterclockwise direction. Some analyses claim a resonant P_{13}[16e, g, i, j, k] whereas other analyses claim a resonance interpretation is not required.[16c, b, f] Another possible way to describe the P_{13} amplitude would be in terms of a coupled-channel threshold effect, i.e., the KN amplitude becomes rapidly absorptive as it feeds the rapidly increasing $K\Delta$ channel. At present the question as to whether there is or is not a resonance in the K^+p system is still not answered. If there is a resonance, its elasticity is small (~ 0.2) and it decays mainly into $K\Delta$.

We have attempted a similar analysis of the structure in the isospin-0 total cross section by measuring some of the partial K^+d cross sections. In Section II we shall give a brief description of the experiment and the associated scanning and measuring procedures used in the analysis of the data. In Section III we show the cross sections for those K^+d channels directly measured, together with other cross sections derived

from them through the use of isospin conservation. In Section IV we study the charge exchange reaction $K^+d \rightarrow K^0pp$. In Section V we consider the various single-pion production reactions $K^+d \rightarrow K\pi NN$. Finally in Section VI we summarize the results of this experiment. Some of our results have been previously reported elsewhere.[17-19]

II. DESCRIPTION OF THE EXPERIMENT

A. The Beam

The experiment consists of a 100 000 picture exposure of the Lawrence Radiation Laboratory 25-inch deuterium-filled bubble chamber to a two-stage variable momentum mass-separated K^+ beam at the Bevatron. Since the performance characteristics of the beam have been described elsewhere,[20] our description will be brief. The physical layout of the beam is shown in Fig. 4. A copper target was placed in an extracted proton beam, external to the Bevatron field, which enabled the beam to operate for positive or negative beam particles over a wide range of momenta. The two mass separation stages each consisted of an electrostatic separator and a vertical mass slit. The central beam momentum and momentum bite were defined at the first horizontal focus by the horizontal aperture of Slit 1. The beam was designed to operate for K mesons in the momentum region from 800 to 1600 MeV/c. Exposures for this experiment were taken at the following four momenta: 863, 968, 1211, and 1364 MeV/c, which correspond to the average fitted beam momentum at the point of the K^+ interaction or decay. Hereafter we shall refer to these four momentum regions by the nominal momenta of 865, 970, 1210, and 1365 MeV/c.

B. Scanning, Measuring, and Selection of Events

The film was scanned twice for events with a vee (corresponding to $K_1^0 \rightarrow \pi^+\pi^-$) or with more than two outgoing charged tracks. The topologies scanned are shown in Fig. 5. Those events with an odd number of outgoing charged tracks were either a K^+ decay or a K^+d interaction in which the proton in the deuteron was a spectator to an interaction on the neutron and did not have enough momentum (less than ~80 MeV/c) to make a visible track. In the latter case, the absence of a track constitutes a measurement (in the sense that one can place an upper limit on its momentum), and in fitting we have assigned to the unseen proton a momentum of zero with an uncertainty appropriate to a proton too slow to be visible.

The initial measurements for this experiment were made on the Berkeley Flying Spot Digitizer (FSD),[21] an automatic film-plane digitizer

measuring at a rate of about 100 events per hour. The FSD requires that a rough-digitized three point "road" be made in advance for each track of an event to be measured. The procedure we adopted was to scan and rough digitize the events as they were found. This proceeded at a rate of about 20 events per hour. As the FSD had difficulty measuring short tracks, additional measurements and remeasurements were made by two "Franckenstein" film-plane measuring projectors, at a rate of about four events per hour.

The measurements from the FSD or Franckenstein were processed through the reconstruction and fitting program SIOUX and the analysis program ARROW.[22] All events were then either accepted, rejected as one of a number of distinct reject types listed below, or remeasured. The chi-squared cutoff for the acceptance of a hypothesis was taken to be five times the number of constraints for that hypothesis; this corresponds to a probability of about 2% for one-constraint events and slightly less than 1% for the other constraint classes. At the energies spanned by this experiment, events fitting more than one hypothesis could be resolved unambiguously by looking at track ionization. Events were rejected for the following reasons:

Not A Beam Track. We required beam tracks to have a measured momentum within three standard deviations of the central beam momentum and to have dip and azimuthal angles within three standard deviations of preset bounds.

Too Many Tracks. Events found in frames in which there were more than thirty beam tracks were not measured.

Not to be Measured. Immeasurable events, e.g., events obscured by passing tracks, chamber distortion, or film damage.

False Event. This category includes duplicate events, phony events, etc.

Outside the Production Fiducial Volume. We required that the K^+ interaction take place within a preset volume of the bubble chamber.

Outside the Decay Fiducial Volume. We required that the K^0 decay within a preset volume of the bubble chamber.

Vee Too Short. $K_1^0 \rightarrow \pi^+\pi^-$ decays within 2 mm of the production vertex

were excluded due to difficulties in finding and measuring close decays.

Vee Scatter. K^0's that scattered before decay were excluded from analysis since the point of the secondary scatter usually could not be determined.

Vee Not a K_1^0. These events were either $K_2^0 \rightarrow \pi^+\pi^-\pi^0$, or $\Lambda^0 \rightarrow p\pi^-$ from associated production from an incident π^+.

Failing events were remeasured until their number was reduced to an insignificant level (less than 5% for all topologies.)

In this manner, we found 3169 events with a K^+ and 5509 events with a K^0 in the final state. The cross sections which we calculate in the next section were normalized to 2730 $K^+ \rightarrow \pi^+\pi^-\pi^+$ decays. In obtaining the cross sections, K^0 events were corrected for 1) decay into neutrals and K_2^0, 2) decay outside the decay fiducial volume, and 3) decay too close to the production vertex (decay less than 2 mm from the production vertex). Since the scanning efficiency after two complete scans of the film proved to be better than 98% we have not corrected for scanning biases. Furthermore, since the unresolved events were found to be channel independent and since their number was less than the statistical error in most channels we have not corrected for these events. The final source of bias is contamination from incident π^+ interactions. Events with a vee in the final state were predominantly $K_1^0 \rightarrow \pi^+\pi^-$ decays resulting from interactions of incident K^+ mesons. The $\Lambda^0 \rightarrow p\pi^-$ decays resulting from incident π^+ interactions could be clearly separated from the $K_1^0 \rightarrow \pi^+\pi^-$ decays. Therefore pion contamination to the K^0 channels is negligible. The only channel that is seriously affected by pion contamination is $K^+d \rightarrow K^+\pi^-pp$ which must be separated from $\pi^+d \rightarrow \pi^+\pi^-pp$. Each of these events was looked at on the scan table to insure that the selected hypothesis was consistent with the ionization of the secondary tracks. We estimate that the contamination to this channel from pion interactions is less than 5%.

III. CROSS SECTIONS

In this section we present our measurements of some of the K^+d partial cross sections and our calculations of most of the others using relations derived from isospin conservation and data from Bland et al.[7] and the total cross section data of Cool et al.[9] and Bugg et al.[10] We also determine the isospin-0 KN partial cross sections.

A. Directly Measured K^+d Cross Sections

The reactions that occur at the energies spanned by this experiment are:

$$
\begin{aligned}
K^+d \rightarrow KNN \rightarrow\ & K^+pn & & & * \\
\rightarrow\ & K^0pp & & & * \\
\rightarrow KNN\pi \rightarrow\ & K^+nn\pi^+ & \Big\} & \sigma_c & * \\
\rightarrow\ & K^0pn\pi^+ & & & * \\
\rightarrow\ & K^+pp\pi^- & \Big\} & & * \\
\rightarrow\ & K^+pn\pi^0 & \Big\} & \sigma_o & * \\
\rightarrow\ & K^0pp\pi^0 & & & * \\
\rightarrow KNN\pi\pi \rightarrow\ & K^0nn\pi^+\pi^+ & \Big\} & \sigma_{cc} & * \\
\rightarrow\ & K^+pn\pi^+\pi^- & & & * \\
\rightarrow\ & K^0pp\pi^+\pi^- & \Big\} & & * \\
\rightarrow\ & K^+nn\pi^+\pi^0 & \Big\} & \sigma_{co} & * \\
\rightarrow\ & K^0pn\pi^+\pi^0 & & & * \\
\rightarrow\ & K^+pp\pi^-\pi^0 & \Big\} & & * \\
\rightarrow\ & K^+pn\pi^0\pi^0 & \Big\} & \sigma_{oo} & * \\
\rightarrow\ & K^0pp\pi^0\pi^0 & & &
\end{aligned}
\qquad (3)
$$

Reactions in which the deuteron is left intact are implicitly included with those with a proton and a neutron in the final state. The topologies we scanned lead to cross sections for the reactions marked with an asterisk. The reactions listed above are arranged according to the charge states of the pions. The symbol σ_{co}, for example, represents the sum of all cross sections leading to one charged and one neutral pion. Thus the total $K^+d \rightarrow KNN\pi$ and $K^+d \rightarrow KNN\pi\pi$ cross sections are:

$$\sigma(KNN\pi) = \sigma_c + \sigma_o \qquad (4a)$$

$$\sigma(KNN\pi\pi) = \sigma_{cc} + \sigma_{co} + \sigma_{oo} \ . \qquad (4b)$$

Table I lists the number of events found in the channels we have directly measured for each of the four momenta studied. We have calculated cross sections using the following relation

$$\sigma = \frac{f}{\eta c \tau} \times \frac{A_d}{\rho_d N_A} \times \frac{N_{interactions}}{N_{decays}} \qquad (5)$$

$$= \frac{1}{0.544} \times \frac{1}{P_K(MeV/c)} \times \frac{N_{interactions}}{N_{decays}} , \qquad (5)$$

where

A_d (Atomic weight of deuterium) = 2.015 amu

N_A (Avogadro's number) = 6.02252×10^{23} mole^{-1}

ρ_d (Density of deuterium in the bubble chamber)

= 0.1352 g/cm^3 (Ref. 23)

$\eta = P_K(beam)/M_K$

τ (K^+ lifetime) = 1.234×10^{-8} sec

f (K^+ branching ratio into the τ-decay mode) = 0.0557.

Figure 6(a) and Table II show the cross sections we have measured. The quoted errors are statistical only. The charge exchange ($K^+d \rightarrow K^0pp$) cross section falls off smoothly with increasing momentum. The single-pion production cross sections rise rapidly until about 1200 MeV/c, then level off; they all have roughly the same shape, though they differ in size. The double-pion production cross sections (only the sum of the measured cross sections—i. e., six of the eight possible channels—is shown) are extremely small until 1200 MeV/c, after which they begin to rise. The thresholds for single and double pion production on deuterons are 450 and 700 MeV/c. (On free nucleons, the thresholds are 510 and 810 MeV/c.) The cross sections are small until well above these thresholds.

To determine the cross sections for K^+ interactions on free nucleons from the cross sections for K^+d interactions, one must invoke the impulse approximation.[24] In the impulse approximation one assumes that one nucleon in the deuteron is only a spectator to the interaction of the incident K^+ with the other nucleon. In reactions such as $K^+d \to K^0pp$, $K^+d \to K^0pp\pi^0$, and $K^+d \to K^+pp\pi^-$ with two protons in the final state, the K^+ must necessarily have interacted with the neutron, for these reactions the K^+d cross sections give a somewhat distorted picture of free-neutron cross sections. For example, $\sigma(K^+d \to K^0pp)$ is approximately $\sigma(K^+n \to K^0p)$. In contrast, the $K^0pn\pi^+$ final state can come from the interaction of the K^+ with either of the target nucleons. The simplest way to make the division is to take the slower nucleon to be the spectator. This overestimates the smaller $K^+n(p) \to K^0\pi^+n(p)$ cross section and underestimates the larger $K^+p(n) \to K^0\pi^+p(n)$. We have corrected for this effect by the following prescription: We first exclude all $K^+d \to K^0pn\pi^+$ events with both nucleon momenta greater than 150 MeV/c. For the remaining events we take the slower nucleon to be the spectator and then calculate the fraction of events that are proton spectator events and the fraction of events that are neutron spectator events. Finally <u>all</u> the $K^+d \to K^0pn\pi^+$ events are then divided according to the fractions determined from the sample with a 150 MeV/c spectator momentum cut.

Figure 6(b) shows the division of the $K^+d \to K^0pn\pi^+$ cross section with the spectator nucleon indicated by parenthesis. Also shown is the $K^+d \to K^0d\pi^+$ cross section which appears to be flat over the energy range covered by this experiment. The $K^+p \to K^0\pi^+p$ cross section as measured by Bland et al.[6,7] is also shown. The difference between the $K^+p \to K^0\pi^+p$ and $K^+p(n) \to K^0\pi^+p(n)$ cross sections is small and is consistent with a rough calculation of the effect of eclipsing and motion of nucleons within the deuteron. The ratio of the two measurements from low to high momentum are 1.14 ± 0.14, 1.28 ± 0.11, 1.07 ± 0.06, and 1.12 ± 0.10 at 865, 970, 1210, and 1365 MeV/c respectively. The $K^+p \to K^0\pi^+p$ data of Bland et al. will be used again as a check on the systematics of this K^+d experiment.

Therefore Fig. 6. gives those cross sections we have directly measured. In the next section we derive relations from isospin conservation

that will allow us to calculate other cross sections.

B. Isospin Conservation and K^+d Reactions

Isospin conservation provides one (and only one) linear relation between the $K^+d \to KNN\pi$ cross sections and one between the $K^+d \to KNN\pi\pi$ cross sections; namely,

$$\sigma_c = 2\sigma_o \tag{6a}$$

$$2\sigma_{cc} = 4\sigma_{oo} + \sigma_{co} \ . \tag{6b}$$

These relations (derived in the Appendix) can then be used to write the total $K^+d \to KNN\pi$ and $K^+d \to KNN\pi\pi$ cross sections in various ways, eliminating one or the other of the constituent parts:

$$\sigma(KNN\pi) = \sigma_c + \sigma_o \tag{7a}$$

$$= 3\sigma_o \tag{7b}$$

$$= \frac{3}{2}\,\sigma_c \tag{7c}$$

and

$$\sigma(KNN\pi\pi) = \sigma_{cc} + \sigma_{co} + \sigma_{oo} \tag{8a}$$

$$= 3(\sigma_{cc} - \sigma_{oo}) \tag{8b}$$

$$= \frac{3}{2}(\sigma_{co} + 2\sigma_{oo}) \tag{8c}$$

$$= \frac{3}{4}(\sigma_{co} + 2\sigma_{cc}) \ . \tag{8d}$$

Note that we have not measured all of either σ_c or σ_o, nor have we measured all of any two of σ_{cc}, σ_{co}, and σ_{oo}. However, we can still use these equations to obtain $\sigma(KNN\pi)$ and $\sigma(KNN\pi\pi)$.

Consider first the total cross section for single-pion production $\sigma(KNN\pi)$. To complete σ_c we need the $K^+d \to K^+nn\pi^+$ cross section (see the list of reactions in Section IIIA). In the spirit of the impulse approximation, the K^+ interaction in this channel is with the proton. Therefore we assume

$$\sigma(K^+d \to K^+nn\pi^+) \approx \sigma(K^+p \to K^+\pi^+n). \tag{9}$$

In view of the comparison made in Fig. 6(b) we expect this approximation

to be good to 10 or 20%. The $K^+p \to K^+n\pi^+$ cross section has been measured by Bland et al.[6,7] It is small, being never more than one-tenth the sum of the other, directly measured parts of σ_c. Since the latter is measured to about 5%, Eq. (9) would have to be wrong by 50% to affect the value of σ_c obtained using it by as much as a standard deviation. Thus we have used Eq. 9 (doubling the quoted errors on $\sigma(K^+p \to K^+\pi^+n)$) to complete σ_c and use Eq. (7c) to calculate $\sigma(KNN\pi)$.

Consider next the isospin relations for $\sigma(KNN\pi\pi)$. The Eqs. (8a-d) become inequalities if we put on the right just the parts of σ_{cc}, σ_{co}, and σ_{oo} that we have measured. Since all of σ_{cc} has been measured, Eq. (8b) gives an upper limit of $\sigma(KNN\pi\pi)$. The other three inequalities give lower limits, from which we may choose whichever is most restrictive [which in our case was Eq. (8d)]. We then assign to $\sigma(KNN\pi\pi)$ the value midway between the upper and lower limits, and fold together half the difference between the limits and the statistical uncertainty on them for an error.

Finally, by subtracting the pion-production cross sections from the total cross section we obtain the $K^+d \to KNN$ cross section. Subtracting the measured $K^+d \to K^0pp$ cross section from this gives the $K^+d \to K^+pn$ cross section (this includes $K^+d \to K^+d$).

Figure 7 and Table II show the results of these calculations. Also shown are the total cross section data of Cool et al.[9] and Bugg et al.[10] and some partial cross section data from Slater et al.[25] and Butterworth et al.[26] The most striking feature is the abrupt rise of the single-pion production cross section to 15 mb at 1200 MeV/c. Since this rise is accompanied by a less steep fall of the $K^+d \to KNN$ cross section, the total cross section increases by only about 10 mb. The onset of double-pion production, by which time the single-pion production cross section has leveled off, causes no marked change of the total cross section.

C. Isospin Conservation and K^+N Reactions

In order to study the structure in the isospin-0 total cross section, we must obtain a relation for the isospin-0 single-pion production cross section off nucleons.

There are seven charge states for single-pion production in the K^+N reactions:

$$\left.\begin{aligned} K^+p &\to K^0\pi^+p \\ &\to K^+\pi^+n \\ &\to K^+\pi^0p \end{aligned}\right\} \quad \sigma_p \tag{10}$$

$$\left.\begin{aligned} K^+n &\to K^0\pi^+n \\ &\to K^0\pi^0p \\ &\to K^+\pi^0n \\ &\to K^+\pi^-p \end{aligned}\right\} \quad \sigma_n , \tag{11}$$

where σ_p and σ_n are the sums of the K^+p and K^+n cross sections. There eleven charge states for double-pion production:

$$\left.\begin{aligned} K^+p &\to K^0n\,\pi^+\pi^+ \\ &\to K^+p\,\pi^+\pi^- \\ &\to K^0n\,\pi^+\pi^0 \\ &\to K^0p\,\pi^+\pi^0 \\ &\to K^+p\,\pi^0\pi^0 \end{aligned}\right\} \sigma_p \tag{12}$$

$$\left.\begin{aligned} K^+n &\to K^+n\,\pi^+\pi^- \\ &\to K^0p\,\pi^+\pi^- \\ &\to K^0n\,\pi^+\pi^0 \\ &\to K^+p\,\pi^-\pi^0 \\ &\to K^+n\,\pi^0\pi^0 \\ &\to K^0p\,\pi^0\pi^0 \end{aligned}\right\} \sigma_n . \tag{13}$$

As before, isospin conservation provides one linear relation between the $KN \to KN\pi$ cross sections and one between the $KN \to KN\pi\pi$ cross sections. If we refer to the above sets of cross sections in terms of the charge states of the pions we get, as before:

$$\sigma_c = 2\sigma_o \tag{14a}$$

$$2\sigma_{cc} = 4\sigma_{oo} + \sigma_{co} . \tag{14b}$$

Consider single-pion production. The cross sections for single-pion production through the isospin-1 and isospin-0 channels are respectively:

$$\sigma_1(KN\pi) = \sigma_p \tag{15a}$$

$$\sigma_0(KN\pi) = 2\sigma_n - \sigma_p \,. \tag{15b}$$

From Eqs. (15b) and (14a) one can obtain the relation

$$\sigma_o(KN\pi) = 3[\sigma(K^+n \to K^0\pi^+n) + \sigma(K^+n \to K^+\pi^-p) - \sigma(K^+p \to K^+\pi^0p)] \,, \tag{16}$$

in which only three of the seven $KN \to KN\pi$ cross sections appear. The $K^+p \to K^+\pi^0p$ cross section has been measured by Bland et al.[6,7] The other two are approximately equal to the $K^+n(p) \to K^0\pi^+n(p)$ and $K^+d \to K^+\pi^-pp$ cross sections shown in Fig. 6. To get free-neutron cross sections from these, we have multiplied them at each momentum by the corresponding ratio of the $K^+p \to K^0\pi^+p$ to $K^+p(n) \to K^0\pi^+p(n)$ cross sections shown in Fig. 6(b). Although it is not strictly valid to apply to one channel the free-to-bound-nucleon cross section ratios found in another, the errors on the ratios are probably large enough to encompass channel-to-channel variations, and they are propagated.

Figure 8 and Table III show the values of $\sigma_0(KN\pi)$ we obtain. Also shown are total cross sections from Carter[27] and isospin-1 partial cross sections from a compilation made by Bland et al.[6,7] The smooth curve labelled $\sigma_0(KN\pi)$ was subtracted from σ_o (total) to get the elastic scattering cross section $\sigma_o(KN)$. We were unable to extract reliable values of $\sigma_o(KN\pi\pi)$, but even at 1365 MeV/c it is too small to do more than slightly reduce $\sigma_o(KN)$. In the region of the peak and below, the values of σ_o(total) that appear in the literature are in only qualitative agreement.[9,10,11,27] Below 1 GeV/c even the statistical errors alone amount to 1 or 2 mb, and therefore the elastic cross section we calculate is correspondingly uncertain. Recently several new unfoldings of the isospin-0 total cross sections have been performed incorporating the new low energy total cross section data of the Arizona group.[11,28] Cool[28a] and Dowell[28b] report similar results: Both obtain two possible results for the isospin-0 total cross section which differ by as much a 4 or 5 mb in the region from 0.7 to 1.0 GeV/c. The choice of two possibilities arises mostly from the disagreement between the data in this region and depends very little on the method of unfolding.[28c]

At low momenta, the total and elastic cross sections are equal (as the inelastic cross section is zero), and their qualitative behavior is given in terms of the S-wave zero-effective-range scattering length, A, by

$$\sigma = 4\pi A^2 . \qquad (17)$$

The isospin-0 and isospin-1 scattering lengths are respectively

$$A_0 = 0.04 \pm 0.04 \text{ F} \qquad \text{(Ref. 29)}$$

and

$$A_1 = -0.30 \pm 0.01 \text{ F} \qquad \text{(Ref. 30)}$$

which, in turn, give the following cross sections

$$\sigma_0 = 0.2^{+0.6}_{-0.2} \text{ mb}$$

and

$$\sigma_1 = 11.3 \pm 0.8 \text{ mb.}$$

This shows that σ_0(total), in contract to σ_1(total), does in fact fall off rapidly at low momenta as indicated in Fig. 8. This rapid fall-off in σ_0(total) at low energies is confirmed by the recent analyses of the new low energy total cross section data of the Arizona group.[28]

The rapid increase of $\sigma_0(KN\pi)$ comes at the threshold for the quasi-two-body reaction $KN \rightarrow K^*N$. It appears to come at a slightly higher momentum than does the increase of $\sigma_1(KN\pi)$. This is reasonable, because the reaction $KN \rightarrow K\Delta$, for which the threshold is slightly lower and which is known to be a major part of $\sigma_1(KN\pi)$ in this region, is forbidden to the isospin-0 channel. It is surprising then how similar in magnitude $\sigma_0(KN\pi)$ and $\sigma_1(KN\pi)$ quickly become. The rapid increase of $\sigma_0(KN\pi)$ is accompanied by a turnover of $\sigma_0(KN)$ Note that $\sigma_0(KN)$ falls off more rapidly than $\sigma_1(KN)$ but no faster than does the kinematic factor $4\pi\lambda^2$ where λ is the reduced wavelength in the KN center-of-mass system.

As in the case of the isospin-1 K^+N system, it appears that the peak around 1200 MeV/c in the total cross section for the isospin-0 K^+N system is well reconstructed by the sum of three smoothly varying, non-

peaked channel cross sections $\sigma_0(KN)$, $\sigma_0(KN\pi)$, and $\sigma_0(KN\pi\pi)$. On the other hand, the behavior of $\sigma_0(KN)$ at low energies is intriguing. It rises rather rapidly from 0 up to about 20 mb around 800 MeV/c at which point it turns over and falls roughly as $4\pi\lambda^2$. Abrams et al.[31] and also J. Dowell[28b] have suggested that this peak in $\sigma_0(KN)$ might be due to the existence of a Z_0^* with $M(KN) \approx 1780$ MeV and $\Gamma \approx 565$ MeV. The existence or nonexistence of this Z^* will have to wait until a reliable phase shift analysis is performed in the isospin-0 K^+N system in this region. In order to eliminate ambiguities, this analysis will require polarization measurements in the $K^+d \to K^0pp$ and $K^+d \to K^+pn$ reactions.

D. A Formal Discussion of K^+N Cross Sections As Deduced from K^+d Cross Sections

In the preceding section we determined $\sigma_0(KN\pi)$ by using values of $\sigma(K^+n \to K^0\pi^+n)$ and $\sigma(K^+n \to K^+\pi^-p)$ obtained by scaling the cross sections for $K^+n(p) \to K^0\pi^+n(p)$ and $K^+d \to K^+\pi^-pp$, measured in deuterium, by the ratio of the cross sections for $K^+p \to K^0\pi^+p$ as measured in hydrogen and deuterium

$$R_c = \sigma(K^+p \to K^0\pi^+p)/\sigma[K^+p(n) \to K^0\pi^+p(n)]. \qquad (18)$$

In this section we shall compare this crude "empirical" method of correcting for effects of a deuteron target with a more formal analysis of the problems associated with the determination of K^+-nucleon cross sections from measured K^+d cross sections. Those readers uninterested in the machinations associated with experiments in deuterium may wish to skip this section.

As mentioned above, the spirit behind the extraction of free nucleon cross sections from interactions off complex nuclei is embodied in the impulse approximation.[24] In this approximation the amplitude for scattering off a complex nucleus is represented as a superposition of amplitudies for scattering off free nucleons which have the same momentum distribution as the actual bound nucleons. It is based on the following assumptions:

a,) The range of the force between the incident particle and the nucleons

is shorter than the average distance between the two nucleons.

b. The nucleus is rather "transparent" to the incident wave so that the amplitude falling on each nucleon is approximately the same as if the nucleon were alone.

c. Multiple scattering processes have a small probability.

d. The forces that bind the nucleons only have the effect of giving to each nucleon a certain distribution of momentum.

The very small binding energy of the deuteron provides one with a unique set of circumstances such that the conditions of the impulse approximation are fairly well satisfied.

In practice, one usually applies the impulse approximation to meson scattering experiments in deuterium in roughly the following manner. For a given reaction in deuterium in which there are two nucleons in the final state one first looks at the momenta of the two nucleons and calls the slower nucleon the "spectator" and the faster nucleon the "struck" or "target" nucleon. Having made this separation one then looks at the momentum and angular distributions of the spectator nucleon in the rest frame of the deuteron and compares these with the predictions obtained from the deuteron wave function. This gives one a measure of the extent to which the conditions of the impulse approximation are satisfied. Finally, one corrects this sample of events for the following effects:

a) Smearing effects to the total energy by the Fermi motion of the nucleons.

b) Glauber shielding effects and double scattering.

c) Effects of the Pauli principle.

We shall follow this approach in this section.

1. Spectator Nucleon Distributions

The deuteron is a loosely bound composite of a proton and a neutron with a binding energy of 2.226 MeV. The ground state is mainly an S state, with a small amount of D state whose presence can be ignored for our purposes. Among the several wave functions used to describe the $^3S_1$ ground state we shall use that proposed by Hulthén[32]

$$\Psi_D(r) = N(e^{-\alpha r} - e^{-\beta r})/r \qquad (19)$$

where r is the inter-nucleon distance and

$$\alpha = 45.7 \text{ MeV/c}$$
$$\beta = 7\alpha .$$

The normalization constant is

$$N = [\alpha\beta(\alpha + \beta)/4\pi(\beta-\alpha)^2]^{1/2} . \tag{20}$$

The Fourier transform of $\Psi_D(r)$ gives the distribution $\Phi_D(p)$ of the momentum of the two nucleons in the deuteron

$$\Phi_D(p) = N\sqrt{\frac{2}{\pi}}\left(\frac{1}{\alpha^2 + p^2} - \frac{1}{\beta^2 + p^2}\right) \tag{21}$$

such that $4\pi p^2 \Phi_D^2(p)\,dp$ is the probability that the momentum of the nucleons will be between p and p + dp. By imposing the impulse approximation one can measure this probability distribution experimentally. For K^+d interactions, the K^+ is assumed to interact with only one of the nucleons (the target nucleon) in the deuteron, the other nucleon going off after the collision with the same momentum it had before the collision. Figures 9 to 12 show the spectator distributions for the reactions directly measured in this experiment.

Consider first the spectator momentum distributions. The curves shown are the predictions of the Hulthén distribution normalized to the number of events with spectator momentum less than 300 MeV/c. For the reactions

$$K^+d \rightarrow K^0pp$$
$$K^+d \rightarrow K^+\pi^-pp$$
$$K^+d \rightarrow K^0\pi^+p(n)$$

one can either directly measure or kinematically fit for the spectator momentum and angles. In this case the data agree well with the Hulthén predictions in the region with spectator momentum less than 300 MeV/c. On the other hand, for

$$K^+d \rightarrow K^0\pi^0pp$$
$$K^+d \rightarrow K^0\pi^+n(p)$$

the reaction is kinematically underconstrained when the spectator proton is unseen. We circumvent this problem, as described above, by setting the components of the momentum of the unseen spectator equal to zero with errors commensurate with the Hulthén distribution ($\Delta P_x = 30$, $\Delta P_y = 30$, $\Delta P_z = 40$ MeV/c). This has the unfortunate effect of distorting the spectator momentum distribution toward zero momentum and also distorts the spectator angular distribution in an unnatural way. However, within the limited statistics in these two channels, we observe no noticeable distortion of any distributions not involving the spectator proton.

For all reactions there appears to be a deviation from the predictions of the Hulthén wave function which is exhibited as an excess of events with high spectator momentum. The Hulthén distribution predicts that 1% of the events should have their spectator momentum greater than 300 MeV/c whereas experimentally we observe 5 to 15% (see Table IV). One can conjecture that this excess of high momentum spectators could be due to one or more of the following causes:

a) a breakdown of the impulse approximation, i.e., high momentum spectators arising from collisions on the entire dueteron,

b) rescattering of one or more of the final state particles on the spectator nucleon,

c) inadequacy of the Hulthén wave function.

All experiments in a deuterium bubble chamber find such an excess of high momentum spectators, but experimentors vary in their treatment of these events. In some experiments all events are used in cross sections and differential cross sections, whereas other experiments use only events with spectator momenta less than 250 or 300 MeV/c. Since it is not clear to us how much of the excess of high momentum spectators is due to a breakdown of the impulse approximation or rescattering and how much is simply due to an inadequacy of the Hulthén wave function, we have chosen to do the following: We use all events in each channel to determine total cross sections and list in Table IV the percentage in that channel of events with spectator momentum greater than 150 and 300 MeV/c. Likewise all events are used in differential cross sections

for the charge exchange reaction $K^+d \to K^0pp$. For single-pion production channels we have taken a cut of spectator momenta less than 150 MeV/c for differential distributions and have scaled these up to the total channel cross section when necessary to quote absolute differential cross sections. The cut at 150 MeV/c is necessitated by the separation (described in the previous section) for the channel $K^+d \to K^0\pi^+np$, and for consistency we have used the same cut for the other single-pion production channels. Figure 13 shows a scatter plot of the proton momentum as a function of the neutron momentum for the channel $K^+d \to K^0\pi^+pn$ at 1210 MeV/c, illustrating the separation of proton spectators from neutron spectators.

Consider next the spectator angular distributions. The internal (Fermi) motion of the two nucleons bound in the deuteron gives rise to two interesting effects. The first is on the experimentally measured angle between the incident kaon and the recoiling spectator, which we discuss here. The second effect is a smearing of the center-of-mass energy and will be discussed in the following section.

Prior to the interaction, the neutron and proton bound in the deuteron move at random in opposite directions with spatial and momentum distributions given by the Hulthén wave function. Due to the random nature of this motion, one may be led to assume that the measured angle, θ_{sp}, between the incident beam and the recoiling spectator nucleon should have an isotropic distribution. This is misleading since one must take into account the fact that when the target particle is moving toward the beam, there is a greater particle flux and hence a higher reaction rate than when the target is receding from the beam, i.e., a Doppler effect of sorts. Since conservation of momentum requires the target nucleon and spectator nucleon in the deuteron to move in opposite directions, one should expect that there will be more events for which $\cos\theta_{sp}$ is greater than zero than for $\cos\theta_{sp}$ less than zero. Taking into account this Doppler effect the predicted spectator distribution is of the form[33]

$$W(\cos\theta_{sp}) \approx 1 + \frac{\beta}{\beta_K}\cos\theta_{sp} \qquad (22a)$$

$$\approx 1 + \frac{\langle P \rangle}{\left(\frac{M}{M_K}\right) P_K} \cos \theta_{sp}, \qquad (22b)$$

where M is the nucleon mass, $\beta\,(\beta_K)$ is the spectator (beam) velocity and $\langle P \rangle$ is the mean spectator momentum. To this one should add a correction for the binding energy of the deuteron, so that[33]

$$W(\cos \theta_{sp}) \approx 1 + \left[\frac{\langle P \rangle}{\left(\frac{M}{M_K}\right) P_K} + 2 \left\langle \frac{P + BM}{P P_T} \right\rangle \right] \cos \theta_{sp}, \qquad (23)$$

where P_T is the target nucleon momentum and B is the deuteron binding energy.

Since the number of events observed is proportional to the particle flux times the cross section, the above prediction for the distribution of $\cos \theta_{sp}$ should be valid only if the cross section is assumed to be constant over the range of center-of-mass energies produced in the collisions. In the energy region covered by this experiment, the charge exchange cross section $\sigma(K^+d \to K^0pp)$ appears to be falling while the single-pion production cross sections $\sigma(K^+d \to K\pi NN)$ appear to be rising rapidly. These cross section variations should manifest themselves as a slight excess of backward spectators for the charge exchange reaction and an excess in the forward direction for spectators associated with the single-pion production reactions.

Experimentally, our spectator angular distributions, in general, agree qualitatively with what one might expect from a combination of these two effects—i. e., the Doppler effect and the rapid cross-section variation. The exception is in the channel $K^+n(p) \to K^0\pi^+n(p)$, where the spectator distributions are distorted due to the manner in which normally underconstrained events were fitted by the kinematic fitting process and to which we alluded earlier. Surprisingly, this distortion is not as marked in the channel $K^+d \to K^0\pi^0p(p)$ which was similarly treated. The only difference between these two reactions is that when one fits for an unseen spectator proton one is also fitting for a neutron in the first case

and a neutral pion in the second. How this reflects in the spectator distribution is not clear. One additional process that should distort the expected spectator angular distributions in all channels is double scattering.

2. Smearing of the Total Energy by the Fermi Motion of the Nucleons

Another effect arising from the motion of the nucleons bound in the deuteron is a smearing of the total counter-of-mass energy distribution. For a collision of a beam off stationary target nucleons, there is a unique center-of-mass energy corresponding to the incident beam momentum. On the other hand, if one of the nucleons in the deuteron is the target, there results a distribution of center-of-mass energies, f(E), due to the fact that the target nucleon has a range of momenta and is moving in a random direction with respect to the beam. Therefore, the cross section for a given channel measured in deuterium represents an average over this distribution in center-of-mass energy

$$\sigma(Kd \to X N_T N_S) = \frac{\int \sigma(E, KN \to X N_T)\, f(E) dE}{\int f(E) dE} - \sigma_{corr}, \qquad (24)$$

where X represents one of the following K, Kπ, K$\pi\pi$, and where $N_T(N_S)$ is the target (spectator) nucleon and σ_{corr} is the Glauber shielding and Pauli principle corrections discussed in the following sections. Ideally one then determines $\sigma(E, KN \to X N_T)$ by unfolding this expression. Unfortunately, the exposures in this experiment were separated by 105 to 250 MeV/c. This fact together with the limited statistics in most channels, does not make the above procedure practicable. Therefore, we choose to treat the exposure at each momentum as a separate experiment and quote a cross section for the central value of the energy corresponding to the incident momentum. These cross sections, averaged over the Hulthén distribution,

$$\sigma(KN \to X N_T) \simeq \sigma(K^+ d \to X N_T(N_S)) + \sigma_{corr}, \qquad (25)$$

can then be corrected for the effects considered below.

3. Glauber Shielding Effects and Double Scattering

In general, the total cross section for scattering off deuterons is less than the sum of the cross sections for scattering off each of the two nucleons in the deuteron separately. If the two nucleons are viewed as black discs, then part of the time one disc will obscure the other, thus reducing the effective cross section. Glauber,[12] using an eikonal method, showed that the total cross section for scattering off deuterons could be approximated as the sum of cross sections off protons and neutrons minus a shadow (shielding, screening) term, so that in our case

$$\sigma_{K^+d} = \sigma_{K^+p} + \sigma_{K^+n} - \frac{1}{4\pi}\left[\sigma_{K^+p}\,\sigma_{K^+n}\right]\langle r^{-2}\rangle , \qquad (26)$$

where the parameter $\langle r^{-2}\rangle$ represents the mean inverse squared neutron-proton separation in the deuteron ground state. Wilkin[13] has subsequently shown that this form violates charge independence and has derived an alternative formula which in our case takes the form

$$\sigma_{K^+d} = \sigma_{K^+p} + \sigma_{K^+n} - \sigma_{GW} \qquad (27)$$

where

$$\sigma_{GW} = \frac{1}{4\pi}\left\{(1-\gamma_n\gamma_p)\sigma_{K^+n}\sigma_{K^+p} - \frac{1}{2}\left[(\sigma_{K^+n} - \sigma_{K^+p})^2 - (\gamma_n\sigma_{K^+n} - \gamma_p\sigma_{K^+p})^2\right]\right\}\langle r^{-2}\rangle \qquad (28)$$

and

$$\gamma_i = \mathrm{Re}\, f_i(0)/\mathrm{I_m}\, f_i(0) \qquad i = n, p \qquad (29)$$

are the ratios of the real and imaginary parts of the scattering amplitudes. There is some uncertainty in the value to be taken for $\langle r^{-2}\rangle$ ranging from a value of 0.020 mb^{-1} (Ref. 34) to the value 0.034 mb^{-1} (Ref. 10) obtained from the Hulthén wave function. To get an estimate of the shielding correction we have used a value $\langle r^{-2}\rangle \approx 0.03$ mb^{-1} with an uncertainty of ± 0.01 mb^{-1}. To get σ_{K^+p} and σ_{K^+n} at our energies we have drawn a smooth curve through the points of Cool et al.[9] and Bugg et al.[10] and have assigned errors commensurate with the errors on neighboring points. We get γ_p and γ_n from the dispersion relation values for γ_0

and γ_1 of Carter[27] and use the relations $\gamma_p = \gamma_1$ and $\gamma_n = \frac{1}{2}(\gamma_1 + \gamma_0)$. Estimates of the Glauber-Wilkin screening correction so calculated are shown in Table V and are found to be typically of the order of 2% of the total K^+d cross section.

It is not clear how this correction to the total cross section should be distributed among the various channel cross sections. We have assumed that each final state is depleted by the same fraction. In all channels, this correction of ~2% is much smaller than the statistical error in the channel. When applied in this manner, the Glauber-Wilkin shielding correction does not seem to account for all of the difference we observe between the cross sections $\sigma(K^+p \rightarrow K^0\pi^+p)$ measured in hydrogen and $\sigma[K^+p(n) \rightarrow K^0\pi^+p(n)]$ measured in deuterium. The observed spread in the total center-of-mass energy for the reaction $K^+p(n) \rightarrow K^0\pi^+p(n)$ is about 60 MeV full width at half maximum. A shift in total energy of 30 MeV will cause the observed ratio, R_c, of Eq. 18 to change by about one standard deviation.

Since the shielding correction is intimately connected to double scattering in the final state, and since this double scattering is clearly channel dependent, a proper treatment of such corrections should involve a detailed study of double scattering contributions in each final state.[14] In view of the limited data, such an approach has not been attempted here.

4. Effects of the Pauli Principle

For charge exchange reactions, $K^+d \rightarrow X^0p(p)$ (where $X^0 = K^0$, $K^+\pi^-$, $K^0\pi^0$), with two protons in the final state, one must also consider the effects of the Paul exclusion principle. For such reactions, the interaction of the incident kaon must necessarily be off the neutron. Consider charge exchange collisions in the very forward direction ($t \simeq 0$) and suppose, hypothetically, that the spin of the struck neutron is not flipped. After the collision the two protons are close together in an S-wave spin-1 configuration (ignoring the small D-wave component of the deuteron). This configuration of two identical fermions is, however, symmetric and is therefore forbidden by the Pauli exclusion principle. Thus in the limit of zero momentum transfer, charge exchange collisions

cannot occur without nucleon spin-flip. However, such spin-flip contributions should go to zero in the forward direction. Therefore, for charge exchange scattering off deuterons, the differential cross section should go to zero in the forward direction.

By invoking the impulse and closure approximations[24] one can express the observed $K^+d \to X^0p(p)$ distribution, $(d\sigma/dt)_d$, in terms of the free neutron $K^+n \to X^0 p$ cross section $(d\sigma/dt)_n$ as[35]

$$(d\sigma/dt)_d = \left(\frac{d\sigma}{dt}\right)_n^{\text{non-spin-flip}} [1-H(t)] + \left(\frac{d\sigma}{dt}\right)_n^{\text{spin-flip}} \left[1-\frac{1}{3}H(t)\right]$$

$$= \left(\frac{d\sigma}{dt}\right)_n \frac{1-H+R(1-H/3)}{1+R}, \tag{30}$$

where

$$R = \frac{\left(\frac{d\sigma}{dt}\right)_n^{\text{spin-flip}}}{\left(\frac{d\sigma}{dt}\right)_n^{\text{non-spin-flip}}} \tag{31}$$

and

$$H(t) \int |\Psi_D(r)|^2 e^{-i\vec{q}\cdot\vec{r}}\, d\vec{r} \tag{32}$$

is the deuteron form factor and q is the three momentum transfer in the laboratory system. Note that for $t = 0$ one has $H = 1$ and $R = 0$, thus causing $(d\sigma/dt)_d$ to vanish in the forward direction whether or not the two-body cross section vanishes. As $-t$ increases, $H(t)$ approaches zero, falling to about 0.1 at $-t = 0.13$ $(\text{GeV}/c)^2$, causing $(d\sigma/dt)_d$ to approach $(d\sigma/dt)_n$.

Thus only the most forward bins of the charge exchange differential cross sections are noticably affected by the Pauli principle. Following Danburg,[36] one can define suppression factors

$$f^{\text{non-spin-flip}} = 1 - H(t) \tag{33a}$$

$$f^{\text{spin-flip}} = 1 - \frac{1}{3} H(t). \tag{33b}$$

These suppression factors can be treated as detection efficiencies, the events in a given differential interval being divided by an appropriate combination of factors to get the number of events that would be found in that interval if the collision had been off of free neutrons. However, to make such a correction one must know the relative amounts of the spin-flip and non-spin-flip cross sections, i.e., the ratio R in Eq. 31. One can hope to get an indication of the relative importance of the spin-flip and non-spin-flip contributions by invoking models that describe the shapes of the differential cross sections.

The Pauli principle correction estimates for the charge exchange reactions in this experiment are shown in Table VI. The ratio of spin-flip to non-spin-flip for the reaction $K^+d \to K^0p(p)$ has been estimated using a Regge model and the resulting Pauli principle corrections are of the order of 3% in the total channel cross section. We have assumed pion exchange dominance, i.e., spin-flip, for the single-pion production reactions $K^+d \to K^+\pi^-p(p)$ and $K^+d \to K^0\pi^0p(p)$. Since we are not far above the threshold for single-pion production, the kinematics of the single-pion production reaction do not allow the momentum transfer to the proton to get too small, so the Pauli principle corrections for such reactions will be small at our energies. As an example, the minimum value to -t for the reaction $K^+d \to K^{*0}p(p)$ at 1210 and 1365 MeV/c is 0.11 and 0.07 $(GeV/c)^2$ respectively. We find the Pauli principle correction for the single-pion production charge exchange reactions to be typically of the order of 3% in the channel cross section.

The channel cross section for the reactions $KN \to XN$, correcting for the Glauber-Wilkin shielding and the Pauli principle, are calculated by using the relation

$$\sigma(KN \to XN) = [1 + C_{GW} + C_{PP}]\, \sigma(K^+d \to XNN), \qquad (34)$$

where C_{GW} is the Glauber-Wilkin correction factor and C_{PP} is the Pauli principle correction factor. The results are shown in Table VI together with single-pion production cross sections obtained by simply scaling by the ratio R_c of Eq. (18), i.e.,

$$\sigma(KN \to K\pi N) = R_c\ \sigma(Kd \to K\pi N(N)). \qquad (35)$$

The two sets of cross sections are consistent with each other within their errors with the possible exception of the values at 970 MeV/c. When we have occasion to add or compare $K^+n \rightarrow K\pi N$ cross sections with $K^+p \rightarrow K\pi N$ cross sections we choose to use the scaled set of cross sections, thus in effect normalizing to the reaction $K^+p \rightarrow K^0\pi^+p$, measured in hydrogen, and ignoring the Pauli principle correction. Recall this approach was used in the calculation of $\sigma_0(KN\pi)$ in the previous section. We feel that the errors in our data are sufficiently large and the deuteron corrections are sufficiently small so as to justify the use of this crude method of correcting for deuteron effects in the single-pion production reactions.

IV. THE CHARGE EXCHANGE REACTION: $K^+d \to K^0pp$

In this section we consider the K^+ charge exchange reaction $K^+d \to K^0pp$. We first look at the energy dependence of the total channel cross section and then we study the behavior of the differential cross section in some detail. We ignore double scattering effects and confine our attention to the gross features of the data.

A. Total Cross Sections

In Table VII we list the total cross section measurements for the reaction $K^+d \to K^0p(p)$.[25, 26, 37, 38, 39] We have included the recent results of Firestone et al. at 12.0 GeV/c.[39] Figure 14 shows the cross sections plotted as a function of the laboratory momentum of the incident kaon, P_K, for momenta up to 3.0 GeV/c. The cross section rises rapidly from threshold to a value of ~ 7 mb at ~ 600 MeV/c, remains constant until ~ 900 MeV/c, at which point it turns over and falls smoothly to 0.75 mb at ~ 3.0 GeV/c and 0.031 mb at 12.0 GeV/c.

Figure 15 shows a plot of log $\sigma[K^+d \to K^0p(p)]$ as a function of log P_K. Note that on such a log-log plot the cross section falls linearly in the region from 1.0 to 12.0 GeV/c. A fit of the cross sections from 1.21 to 12.0 GeV/c to the form suggested by Morrison:[40]

$$\sigma = A\, P_K^{-n} \tag{36}$$

gives

$$A = 7.3 \pm 0.2 \text{ mb}$$
$$n = 2.10 \pm 0.05 .$$

A similar behavior has been observed by Mathews[41] for the reaction $K^+p \to K^0\Delta^{++}$ and for which he finds A = 6.19 mb and n = 1.88. Firestone et al.,[39] fitting to more data of this latter reaction, find $A = 7.0 \pm 0.2$ mb and $n = 2.00 \pm 0.05$. Figure 16 shows the cross sections for these two reactions plotted together.[42] Note that above 1.5 GeV/c the two sets of cross sections appear identical. Above about 2.0 GeV/c the scattering mechanisms for these two reactions are quite similar in that they appear to be dominated by ρ and A_2 exchanges in the t-channel. We shall attempt to use a similar t-channel exchange model to describe the

scattering at lower energies for the reaction $K^+d \rightarrow K^0p(p)$.

B. Differential Cross Sections

Values of the differential cross section as a function of the momentum transfer from the incident K^+ to the outgoing K^0 are listed in Table VIII. These values are plotted in Fig. 17. The dashed curves represent predictions from the Regge model of Rarita and Schwarzschild[43] and the solid curves are predictions from a modification of this model to fit the data of this experiment.

As pointed out in the previous section, one can express the observed $K^+d \rightarrow K^0p(p)$ distribution, $(d\sigma/dt)_d$, in terms of the free neutron $K^+n \rightarrow K^0p$ charge exchange cross section, $(d\sigma/dt)_n$, as

$$(d\sigma/dt)_d = (d\sigma/dt)_n \left\{\frac{1 - H + R\,(1 - 1/3\,H)}{1+R}\right\} \tag{37}$$

where

$$R(t) = \frac{\left(\frac{d\sigma}{dt}\right)^{\text{spin-flip}}_n}{\left(\frac{d\sigma}{dt}\right)^{\text{non-spin-flip}}_n} \tag{38}$$

and H is the Hulthén deuteron form factor. Rarita and Schwarzschild[43] have successfully fitted the differential cross section for $K^+d \rightarrow K^0p(p)$ at 2.3 GeV/c, using a Regge model for $(d\sigma/dt)_n$ utilizing the well-established ρ and $A_2 = R$ trajectories and a less-well-established ρ' trajectory.[44] Their model also fits the charge exchange data at 3.0[38] and 12.0 GeV/c.[39] This model does not invoke exchange degeneracy of the ρ and A_2 trajectories.

The form of the differential cross section used by Rarita and Schwarzschild is

$$\left(\frac{d\sigma}{dt}\right)_n = \frac{1}{\pi}\left(\frac{1}{4P_K}\right)^2 \left\{\left(1 - \frac{t}{4M^2}\right)|A|^2 - \frac{t}{4M^2}\left[\frac{s + P_K^2}{1-(t/4M^2)} - s\right]|B|^2\right\}, \tag{39}$$

where M is the nucleon mass and P_K is the laboratory momentum of the incident kaon. They have parametrized the Regge helicity-non-flip (A) and helicity-flip (B) amplitudes as

$$A(K^+n \to K^0p) = A^+ - A^- = A_R^+ - A_\rho^- - A_{\rho'}^- \tag{40a}$$

$$B(K^+n \to K^0p) = B^+ - B^- = B_R^+ - B_\rho^- - B_{\rho'}^- \tag{40b}$$

with

$$A_i^\pm = - C_i(t)\,(\alpha_i + 1)\,\frac{(e^{-i\pi\alpha_i} \pm 1)}{\sin \pi\alpha_i}\,\left(\frac{E}{E_0}\right)^{\alpha_i} \tag{41a}$$

$$B_i^\pm = - D_i(t)\,\alpha_i\,(\alpha_i + 1)\,\frac{(e^{-i\pi\alpha_i} \pm 1)}{\sin \pi\alpha_i}\,\left(\frac{E}{E_0}\right)^{\alpha_i} \tag{41b}$$

$i = \rho,\ \rho',\ R,$

where E is the laboratory energy of the incident kaon. The residue functions and trajectories are parametrized as follows:

$$C_\rho(t) = C_\rho^0\,(1 + C_\rho^1\,t) \qquad D_\rho(t) = D_\rho^0 \exp(D_\rho^1 t)$$

$$C_{\rho'}(t) = C_{\rho'}^0 \exp(C_{\rho'}^1\,t) \qquad D_{\rho'}(t) = D_{\rho'}^0 \exp(D_{\rho'}^1\,t) \tag{42}$$

$$C_R(t) = \alpha_R\,C_R^0 \exp(C_R^1 t) \qquad D_R(t) = \alpha_R\,D_R^0 \exp(D_R^1 t)$$

and

$$\alpha_i = \alpha_i^0 + \alpha_i' t\,.$$

Values of the parameters fitted by Rarita and Schwarzschild are shown in Table IX.

Using their formalism, in the form described above, and their parameters without modification, we have obtained predictions for the charge exchange reaction at our momenta (dashed curves in Fig. 17). The model is assumed to be valid only in the pheripheral region, $-t \leq 1.0\ (\mathrm{GeV}/c)^2$. Clearly the model reproduces the shape of the differential cross section reasonably well but is too large in magnitude by about a factor of two. Part of the failing is due to our use of the asymptotic forms of the Rarita-Schwarzschild Regge amplitudes instead of the formulation of their amplitudes expressed in terms of explicit Legendre functions which they point out is more valid at low energies.

We have made two modifications to the asymptotic Regge model described above which seem to have negligible effect at high energies but improve the agreement with the low energy data. The first is a simple change in the formalism that increases the validity of the model at low energies, short of going to the explicit Legendre formulation. In the high energy approximation the laboratory beam energy, E, appears in the Regge amplitudes in the form $A \approx (E/E_0)^{\alpha}$ and $B \approx (E/E_0)^{\alpha-1}$. In our modification we replace E by the more accurate form $E + t/4M$, i.e.,

$$\left(\frac{s-u}{2s_0}\right)^{\alpha} = \left(\frac{E + t/4M}{E_0}\right)^{\alpha} \approx \left(\frac{E}{E_0}\right)^{\alpha} . \tag{43}$$

The correction term (t/4M) is clearly negligible in either the high energy or low momentum transfer limit. However, the shape of the differential cross section below 2.3 GeV/c is appreciably affected. Our second modification is to vary the ρ' spin-flip residue function, $D_{\rho'} = D^0_{\rho'} \exp(D^1_{\rho'} t)$ as follows: $D^0_{\rho'}$ changed in magnitude from 264 to 135 mb and $D^1_{\rho'}$ decreased from 2.95 to 2.30 $(GeV/c)^{-2}$. These changes (solid curves in Fig. 17) decrease the quality of the fit at 2.3 GeV/c, i.e., the predictions are low by about 20%, but give good agreement with the lower energy data down to 865 MeV/c. At 12.0 GeV/c, the predictions of our modified model are about 7% lower than those of the unmodified Rarita-Schwarzschild model.

While we have not performed a complete Regge fit to our charge exchange data, the calculations described here indicate that the Rarita-Schwarzschild fit could easily be extended down to momenta spanning the structure in the isospin-0 and isospin-1 total cross sections near 1.2 GeV/c. It is interesting to note that the Regge model appears to fit low energies both the charge exchange and K^+p elastic scattering data[5] rather well at low energies.

In Table X and Fig. 18 we show the differential cross sections for $K^+d \rightarrow K^0p(p)$ as a function of the K^+ - K^0 scattering angle in the K-nucleon center-of-mass system. Using the values of R determined from the Regge model calculations described above, we have obtained the differential

cross section for scattering off a free neutron using the relation

$$(d\sigma/d\Omega)_n = (d\sigma/d\Omega)_d \Big/ \left\{ \frac{1 - H + R(1 - 1/3\,H)}{1 + R} \right\} \tag{44}$$

and which are shown in Fig. 17 represented by a black dot. The correction is negligible except in the very forward direction. The solid curves represent Legendre polynomial fits to the corrected $(d\sigma/d\Omega)_n$ distributions with errors scaled according to the above equation. For the 1365-MeV/c data, the anomoous point at $\cos\theta = 0.65$ was not included in the fit. A fourth-order fit was necessary and sufficient at 865, 970, and 1210 MeV/c, whereas a fifth-order fit was required at 1365 MeV/c. The Legendre polynomial coefficients, defined by

$$\left(\frac{d\sigma}{d\Omega}\right)_n = \frac{\lambda^2}{4} \sum_{n=0}^{n_{max}} A_n P_n(\cos\theta) \tag{45}$$

with $\lambda = \frac{\hbar}{q_{c.m.}}$, are shown in Table XI and Fig. 19. The coefficients appear to vary smoothly over the momentum range of this experiment. More detailed statements about the charge exchange reaction can be made only after a complete phase shift analysis has been performed on the data: This has not been attempted here.

Finally we compare the forward scattering cross section with that derived from the optical theorm. If the isospin amplitudes for K^+p elastic scattering, K^+n elastic scattering, and K^+n charge exchange scattering (c.e.) are given by

$$A(K^+p \to K^+p) = A_1 \tag{46a}$$

$$A(K^+n \to K^+n) = 1/2(A_1 + A_0) \tag{46b}$$

$$A(K^+n \to K^0p) = 1/2(A_1 - A_0) \tag{46c}$$

then

$$A_{c.e.} = A(K^+n \to K^0p) = A(K^+p \to K^+p) - A(K^+n \to K^+n). \tag{47}$$

From the optical theorm we then obtain

$$(\mathrm{Im}\, A_{c.e.})_{\theta=0} = \frac{k}{4\pi} [\sigma_{tot}(K^+p) - \sigma_{tot}(K^+n)] \tag{48}$$

which yields the inequality

$$\left(\frac{d\sigma}{d\Omega}\right)_n\Bigg]_{\theta=0} \geq \left\{\frac{k}{4\pi}\left[\sigma_{tot}(K^+p) - \sigma_{tot}(K^+n)\right]\right\}^2, \qquad (49)$$

where the equality holds if the K^+n charge exchange amplitude were purely imaginary. Values of the left-hand side of this equation have been obtained from the Legendre polynomial fit to our data and are shown in Table XII together with values of the right-hand side determined from published total cross-section measurements.[9,10] The difference between the values calculated for the two sides of this equation shows that the K^+n charge exchange amplitude must be predominantly real. This effect has been previously observed at 2.3[26] and 3.0 GeV/c[38] and more recently at 12.0 GeV/c[39] and agrees with the dispersion relation calculations of Carter.[27] Based on a Regge model of KN scattering with only ρ and A_2 trajectories exchanged, Phillips and Rarita[45] have predicted that K^+n charge exchange should have a predominantly real amplitude and K^-p charge exchange should have a predominantly imaginary amplitude.

V. SINGLE PION PRODUCTION REACTIONS: $K^+d \to K\pi N(N)$

In this section we shall study the single-pion production reactions measured in this experiment:

$$K^+d = K^+p(n) \to K^0\pi^+p(n) \quad (50a)$$

$$K^+n(p) \to K^0\pi^+n(p) \quad (50b)$$

$$K^+n(p) \to K^+\pi^-p(p) \quad (50c)$$

$$K^+n(p) \to K^0\pi^0p(p) \ , \quad (50d)$$

where we designate the (slower) spectator nucleon by enclosing it within parentheses. In Section III we presented partial cross sections for $K^+d \to K\pi NN$ and isospin-0 $KN \to K\pi N$ reactions at our K^+ momenta of 865, 970, 1210, and 1365 MeV/c. The emphasis of our analysis in this section will be on the isospin-0 $KN \to K\pi N$ channel. Our results show that above the K^*N threshold at 1080 MeV/c most of the isospin-0 $K\pi N$ production proceeds via the K^*N channel and that the main production mechanism is t-channel pion exchange. There is no apparent support for an s-channel resonance interpretation of the total cross section peak.

In this analysis we assign $K^+d \to K\pi NN$ events to $KN \to K\pi N$ channels by discarding events for which the laboratory momentum of both nucleons is greater than 150 MeV/c, and for the remainder we assume that the slower nucleon is a spectator. Since it is almost never true that both nucleons are produced with momenta below 150 MeV/c, this separation should be reliable.

To get an empirical measure of the effects of a spectator nucleon we compare measurements of a K^+p reaction made with and without a spectator neutron. In Fig. 20 we compare the shapes of various distributions for the reaction $K^+p \to K^0\pi^+p$ at 1210 MeV/c, measured by Bland et al.,[6,8] with what we obtain for that reaction from $K^+p(n) \to K^0\pi^+p(n)$ events. Areas under curves being compared are equal. Figures 20(a) and 20(b) compare the $K^0\pi^+$ and $p\pi^+$ invariant mass spectra. Figures 20(c, d, e) compare production and decay angular distributions for events around the K^* peak, from 840 to 940 MeV, treating them as $KN \to K^*N$ with no

attempt to subtract out Δ events. Cos θ is the K^* production-angle cosine $\hat{K}^+ \cdot \hat{K}^*$ in the K^*N center-of-mass, cos α is the polar-decay-angle cosine $\hat{K}^+ \cdot \hat{K}^0$ in the K^* center-of-mass, and ϕ is the Treiman-Yang azimuthal decay angle. Nowhere is there any evidence of distoration of the $K^+p(n) \rightarrow K^0\pi^+p(n)$ events. The overall confidence level that the two sets of measurements are compatible is 85%. Similar results are observed when data at 1365 MeV/c are compared. Because the agreement is good, we assume that the shapes of distributions for other $KN \rightarrow K\pi N$ reactions are likewise not significantly distorted by the presence of a spectator.

At 1210 and 1365 MeV/c the K^* peak in the (isospin-1) reaction $K^+p \rightarrow K^0\pi^+p$ is heavily contaminated with Δ(1236) events because both the Δ-production cross section and the area of the Dalitz plot common to K^* and Δ bands are large. As far as looking for distortions is concerned, it does not matter whether the events are K^* events or not. However, the angular distributions shown in Fig. 20 are similar to those obtained when a more careful selection of K^*'s is made, and they may be used for the qualitative comparison with the K^* angular distributions in the isospin-0 channel given below.

A. Resonance Production Cross Sections

Having convinced ourselves that we can meaningfully assign $K^+d \rightarrow K\pi N(N)$ events to $K^+N \rightarrow K\pi N$ reactions, we have proceeded to determine the resonance production cross sections for the four channels (50a) to (50d). At our energies the possible final states are

$$K^+N \rightarrow K^*N \quad (51a)$$

$$\rightarrow K\Delta \quad (51b)$$

$$\rightarrow K\pi N \text{ nonresonant.} \quad (51c)$$

Note that the Δ can only be from an isospin-1 KN initial state.

The Dalitz plots for these four reactions at our four momenta are shown in Figs. 21 to 24. At the two lower momenta, 865 and 970 MeV/c, we are below the K^* threshold and only Δ production is observed. On the other hand, at 1210 and 1365 MeV/c a considerable amount of K^* is produced. Since the area of the Dalitz plot common to the K^* and Δ bands is large care must be taken in determining the amount of each resonance present in a given channel as it has been shown that interference

effects are important at these energies.[3,6] To draw quantitative conclusions from the Dalitz plots we have considered four models for single-pion production: a non-interference model which is expected to be valid only in the part of the Dalitz plot outside the K^* - Δ overlap region; an empirical model including K^* - Δ interference; a non-interference model and an empirical interference model in both of which the amount of Δ is constrained from isospin considerations. The models adopted are due to Bland et al.[7] and will be briefly described below; for a more detailed discussion of the models see Reference 7.

1. Non-interference Model

In general, one can represent the Dalitz plot density for the production of a single resonance as the product of a Breit-Wigner function, a function specifying the density distribution within the resonance band along a line of fixed resonance mass, and a production angular momentum barrier factor. If the only final states considered are K^*N, $K\Delta$, and non-resonant $K\pi N$, the Dalitz plot density is given by[7]

$$\frac{d^2\sigma}{dM^2_{K\pi}dM^2_{N\pi}} = a + b\, I_{K^*} + c\, I_{\Delta} \tag{52}$$

where the intensities, I, are

$$I_{K^*} = BW_{K^*}(1 + A_{K^*}\cos^2\lambda_{K\pi})\left(\frac{q^2_{K^*}}{q^2_{K^*} + m^2_{x/2}}\right) \tag{53a}$$

$$I_{\Delta} = BW_{\Delta}(1 + A_{\Delta}\cos^2\lambda_{N\pi})\left(\frac{q^2_{\Delta}}{q^2_{\Delta} + m^2_{\rho/2}}\right) . \tag{53b}$$

The first factor in each of the intensities is the appropriate Breit-Wigner form

$$BW = \frac{1}{\sqrt{\pi}}\,\frac{\Gamma\,(p_0/p)\,m_0}{(m^2 - m_0^2)^2 + (\Gamma m_0)^2} , \tag{54}$$

where

$$\Gamma = \Gamma_0\left(\frac{p^2}{p^2 + m^2_{\pi}} \Big/ \frac{p^2_0}{p^2_0 + m^2_{\pi}}\right)\left(\frac{p}{p_0}\right) ; \tag{55}$$

here m_0 and Γ_0 are the nominal resonance mass and width taken as 1236 MeV and 116 MeV for the Δ, and 891 MeV and 50 MeV for the K^*, m is the appropriate diparticle mass, p_0 and p are the two-body center-of-mass momenta corresponding to m_0 and m.

Consider next the second factor. For the $K\pi(N\pi)$ system we define $\lambda_{K\pi}$ ($\lambda_{N\pi}$) as the decay angle, in the $K\pi(N\pi)$ center-of-mass, of the pion with respect to the outgoing nucleon (kaon). Along a line of constant $M^2_{K\pi}$ ($M^2_{N\pi}$), $M^2_{N\pi}$ ($M^2_{K\pi}$) varies linearly with cos $\lambda_{K\pi}$ (cos $\lambda_{N\pi}$), where cos $\lambda_{K\pi} = \pm 1$ (cos $\lambda_{N\pi} = \pm 1$) corresponds to the edges of the Dalitz plot. Since both the K^* and the Δ decay via P waves, their decay distributions in λ are of the form

$$W(\cos\lambda) \approx 1 + A\cos^2\lambda. \tag{56}$$

In this model, the values of A for the two resonances have been left as free parameters to be varied in the fit.

Finally the last factor is a production angular momentum barrier function where q_{K^*} and q_Δ are the K^* and Δ momenta in the overall center-of-mass. Following Bland et al.[7] we have assumed that the final state K^*N and $K\Delta$ systems are in a relative P wave. This assumption may not be valid for the $K^{*0}p$ final states since several partial waves may be important in this case. For the inverse radius of interaction for K^* production, $m_x/\sqrt{2}$, we have taken $m_x = m_\omega$ ($m_x = m_\pi$) for $K^{*+}(K^{*0})$ production because ω-exchange (π-exchange) appears to be the dominant mechanism for $K^{*+}(K^{*0})$ production.[46, 47] In the case of the Δ, we have used $m_\rho/\sqrt{2}$ as suggested by the ρ-exchange hypothesis for Δ production.

2. Empirical Interference Model

Bland et al.[7] have included interference effects in an approximate way, short of a detailed calculation based on a specific choice of amplitudes, by adopting an empirical interference model of the following form:

$$\frac{d^2\sigma}{dM^2_{K\pi}\, dM^2_{N\pi}} = a + b\, I_{K^*} + c\, I_\Delta + 2d\,(bc\, I_{K^*} I_\Delta)^{1/2} \cos(\phi_\Delta - \phi_{K^*} + \phi_0). \tag{57}$$

Here I_{K^*} and I_Δ are the same as in Eq. 53, ϕ_{K^*} and ϕ_Δ are the phases of the K^* and Δ amplitudes due to the complex Breit-Wigner amplitude, and ϕ_0 is an additional constant relative phase, to be varied in the fit. The factor d, also varied in the fit, is introduced to allow for less-than-maximal coherence of the interference between the K^*N and $K\Delta$ amplitudes.

3. Isospin Constrained Models

As we have noted above, the $K\Delta$ final state can come only from an isospin-1 KN initial state: Recall that the K^+p system is pure isospin-1 whereas K^+n is a mixture of isospin-0 and isospin-1. Bland et al. have studied the reaction $K^+p \to K\Delta$ in great detail with very good statistics. Through isotopic spin considerations one can use their results to predict the amount of $K\Delta$ to be expected in the four single-pion production channels studied in this experiment. We have therefore considered a modification of the non-interference model and the empirical interference model, described above, in both of which we have constrained the amount of $K\Delta$ to the value expected from isospin considerations, thus reducing the number of constraints in each case by one.

4. Results of the Fits

We have fitted all of our single-pion production Dalitz plots for fractions of background, Δ-production, and, where appropriate, K^* production. At 865 and 970 MeV/c, where the K^* is absent, we have performed a least-chi-squared fit to the $M^2_{N\pi}$ distributions using the following form

$$\frac{d\sigma}{dM^2_{N\pi}} = \left[a + c\, BW(\Delta)\ \frac{q^2_{N\pi}}{q^2_{N\pi} + m^2_{\rho/2}} \right] \frac{p\, q_{N\pi}}{M_{N\pi}}\ , \qquad (58)$$

where the symbols have the same meaning as in Eqs. 53 to 55. At 1210 and 1365 MeV/c, where the K^* is present, the data have been divided into rectangular bins in $M^2_{N\pi}$ and $M^2_{K\pi}$ and fitted by the least-chi-squared method.

The results for the four different models used in the fitting are given in Table XIII. Clearly the non-interference models do not fit the data. In Table XIV we give the resonance production cross sections obtained by

multiplying the fraction of a given resonance in a given channel times the free nucleon cross section for that channel. The free nucleon cross section used is that obtained by scaling the $K^+d \rightarrow K\pi N(N)$ cross section by the ratio

$$R_c = \sigma (K^+p \rightarrow K^0\pi^+p) \; / \; \sigma (K^+p(n) \rightarrow K^0\pi^+p(n)) \qquad (58)$$

as described above in Section III. We quote results for the empirical interference model both with and without the amount of Δ constrained. To account for uncertainties in the models we have used, we quote errors that are $\sqrt{2}$ times the statistical error at 854 and 970 MeV/c and twice the statistical error at 1210 and 1365 MeV/c. As a check on the systematics, note that the amount of Δ determined from the empirical interference model is consistent with the amount of Δ expected from isospin considerations although admittedly the errors are large. Since the statistics in most of of our data are quite poor and since we are primarily interested in the K^* production in our data, we shall use the cross section values obtained from the empirical interference model with the amount of Δ constrained by isospin for the K^* study described below. The results of these fits are shown in Figs. 25 to 28.

The three K^* production reactions from K^+-nucleon interactions are

$$K^+p \rightarrow K^{*+}p \qquad (59a)$$

$$K^+n \rightarrow K^{*+}n \qquad (59b)$$

$$K^+n \rightarrow K^{*0}p. \qquad (59c)$$

The first is a pure isospin-1 reaction and has been studied extensively by Bland et al.;[6, 7, 8] we shall use their results whenever possible. The other two reactions are a mixture of isospin-0 and isospin-1, and have been measured in this experiment. In the following section we shall show how one can isolate the isospin-0 K^* production and compare it with the isospin-1 K^* production. Our aim is to get a consistent, though qualitative, description of the process $KN \rightarrow K^*N$ near threshold.

Table XV and Fig. 29 show the total K^* production cross sections for the three reactions of Eq. 59. The K^+n points at 2.3 GeV/c are from S. Goldhaber et al.,[46] and the points at 3.0 GeV/c are from Bassompiere et al.[47] The K^+p points are from the compilation of

Price et al.[42] Note the rapid rise of the K^* cross sections near threshold. Figure 30 shows these cross sections replotted on a log-log scale. We include the preliminary results of Firestone et al. at 12.0 GeV/c.[48] Note that for all three reactions the K^* cross sections rise rapidly from threshold until about 1.6 GeV/c, at which point they turn over and fall smoothly to 12.0 GeV/c. Following Morrison[40] we have fitted the data above 1.5 GeV/c to the form

$$\sigma = A\, P_K^{-n} \tag{60}$$

and find $A = 7.4 \pm 0.7$ mb and $n = 1.74 \pm 0.07$ for $K^+p \to K^{*+}p$ and $A = 15.1 \pm 1.0$ mb and $n = 2.34 \pm 0.07$ for $K^+n \to K^{*0}p$. Note that all three K^* production reactions have the same energy dependence, falling roughly as P_K^{-2} at high energy, even though their production mechanisms appear to be quite different, as we shall show in the following sections. Finally note that $\sigma(K^+n \to K^{*0}p) \approx 1.5\ \sigma(K^+p \to K^{*+}p)$ and $\sigma(K^+p \to K^{*+}p) \approx 2\sigma(K^+n \to K^{*+}n)$ from threshold to 3.0 GeV/c.

B. Isospin-0 Resonance Production Cross Sections

1. Methods

a) There is only one independent amplitude in isospin space for the isospin-0 $KN \to K\pi N$ channel because there is only one way that either the initial- or final-state particles can couple to isospin 0. In this channel, the final-state subsystems, $K\pi$, $N\pi$, and KN, have isospins 1/2, 1/2, and 1: Δ production is forbidden. The cross section is given by Eq. 16 of Section III:

$$\sigma_0(KN \to K\pi N) = 3[\sigma(K^+n \to K^0\pi^+n) + \sigma(K^+n \to K^+\pi^-p) - \sigma(K^+p \to K^+\pi^0p)]. \tag{61}$$

The same relation applies to differential distributions such as angular distributions and invariant-mass spectra. Distributions for the reaction $K^+p \to K^+\pi^0p$ have been measured by Bland et al.[6, 7, 8] We extract them for the K^+n reactions from $K^+d \to K^0\pi^+n(p)$ and $K^+d \to K^+\pi^-p(p)$ events. We normalize our distributions as follows:

$$\sigma(KN \to KN\pi) = 3\left\{\frac{N[K^+n(p) \to K^0\pi^+n(p)] + N[K^+n(p) \to K^+\pi^-p(p)]}{N[K^+p(n) \to K^0\pi^+p(n)]}\,\sigma(K^+p \to K^0\pi^+p) - \sigma(K^+p \to K^+\pi^0p)\right\}, \tag{62}$$

where, on the right, the σ ( )'s are cross sections measured in hydrogen, and the N[ ]'s are the numbers of events measured in deuterium subject to a 150-MeV/c spectator cut and corrected, when appropriate, for unseen K^0 decays. By normalizing in this manner, we hope to take account of various corrections encountered when interactions are on a deuteron. The K^*N cross section can be obtained by making the appropriate fit to the $K\pi N$ Dalitz plot from Eq. (62) or to projections of the Dalitz plot.

b) Alternatively, the K^*N cross section can also be determined from

$$\sigma_0(KN \to K^*N) = 3[\sigma(K^+n \to K^{*+}n \to K^0\pi^+n) + \sigma(K^+n \to K^{*0}p \to K^+\pi^-p) - \frac{1}{2}\sigma(K^+p \to K^{*+}p \to K^0\pi^+p)] \quad , \tag{63}$$

in which each appropriate deuterium channel is individually separated into K^*N and the $K^0\pi^+p$ hydrogen channel rather than the $K^+\pi^0p$ state is used to subtract out the isospin-1 $K^{*+}p$ part of the cross section.

For the 865, 970, 1210, and 1365-MeV/c data both procedures (a) and (b) were used, whereas for comparison with data at higher momenta, the availability of only the $K^0\pi^+p$ final state in hydrogen permitted only procedure (b).

B. Results

Figures 31 to 34 show the differential distributions, i.e., invariant mass spectra and K^* angular distributions, for the isospin-0 $KN \to K\pi N$ channel at 1210 and 1365 MeV/c together with the corresponding distributions for the three channels $K^+n \to K^0\pi^+n$, $K^+n \to K^+\pi^-p$, and $K^+p \to K^+\pi^0p$ which are the components of $\sigma_0(KN \to K\pi N)$. The K^* events are taken as those events whose $K\pi$ invariant mass lie in a band from 840 to 940 MeV; no attempt has been made to correct for non-K^* background events included in this band. The angles are defined just as for Fig. 20.

Although the angular distributions shown in Figs. 32 and 34 for the reactions $K^+n \to K^{*0}p \to K^+\pi^-p$, $K^+n \to K^{*+}n \to K^0\pi^+n$, and $K^+p \to K^{*+}p \to K^+\pi^0p$ are contaminated by non-K^* events, they can be used to study qualitatively the production mechanism for the three K^* production

reactions. In the $K^+n \to K^{*0}p \to K^+\pi^-p$ channel, the production angular distributions peak sharply in the forward direction, the polar decay angular distributions have a large $\cos^2\alpha$ component, and the azimuthal decay (Treiman-Yang) angular distributions are essentially flat. In the isospin-1 channel, $K^+p \to K^{*+}p \to K^0\pi^+p$, the production angular distributions are less sharply peaked, the polar decay distributions vary as $\sin^2\alpha$, and the azimuthal decay distributions vary mainly as $\sin^2\phi$. This behavior has previously been observed at 2.3[46] and 3.0 GeV/c[47] and was interpreted as indicating that the reaction $K^+p \to K^{*+}p$ goes predominantly via ω-exchange whereas the reaction $K^+n \to K^{*0}p$ goes predominantly via pion-exchange. The angular distributions for the remaining reaction, $K^+n \to K^{*+}n \to K^0\pi^+n$, appear to be intermediate between those for the other two reactions with no single process appearing to dominate.

Figure 35 shows the $K\pi$ and $N\pi$ invariant mass spectra in the isospin-0 $KN \to K\pi N$ channel for momenta at 970, 1210, and 1365 MeV/c; the corresponding spectra at 865 MeV/c is similar to that at 970 MeV/c. There is no significant structure in the $N\pi$ spectra. Since Δ production is forbidden, the lowest known $N\pi$-resonance that might appear is the $N^*(1470)$; but even at our highest momentum of 1365 MeV/c, the phase space cuts off at 1450 MeV. For this reason the isospin-0 $KN \to K\pi N$ channel is more ideally suited for studying K^* production than any of the component channels. The K^* peak dominates the $K\pi$ spectrum at momenta above the K^*N threshold. Fits of the $K\pi$ spectrum to phase space and a P-wave Breit-Wigner resonance form having mass 891 MeV and width 50 MeV are shown.

Table XVI shows the total isospin-0 $KN \to K\pi N$ and $KN \to K^*N$ cross sections determined using the normalization of Eq. (62);[49] for comparison we list the corresponding isospin-1 $KN \to K\pi N$ and $KN \to K^*N$ cross sections measured by Bland et al.[7] We also give the isospin-0 cross sections for $KN \to K^*N$ determined by the alternative method of Eq. 63 in which we have fitted the Dalitz plots of the three channels $K^+n \to K^0\pi^+n$, $K^+n \to K^+\pi^-p$, and $K^+p \to K^0\pi^+p$ independently for the fraction of K^*N. The cross sections determined by the latter method are systematically lower than those obtained by fitting the projected isospin-0 $K\pi$ spectrum.

Figure 36 shows the energy dependence of the isospin-0 and isospin-1 $KN \to K^*N$ cross sections from threshold to 3.0 GeV/c. The isospin-1 cross sections at 1210, 1365, and 1585 MeV/c are taken from the work of Bland et al.[6,7] Higher momenta data are taken from the compilation of Price et al.[42] The isospin-0 cross sections shown are those calculated using Eq. (63). At 1210, 1365, and 1585 MeV/c we have used the $K^+p \to K^{*+}p \to K^0\pi^+p$ data of Bland et al.[6,7] and the K^+d data of Seeger,[37] and at 3.0 GeV/c we have used the published K^+d data of Bassompiere et al.[47] to calculate the isospin-0 cross sections. A smooth curve has been drawn through the isospin-1 $KN \to K^*N$ cross sections and has been scaled upward by a factor 2.5 to give the smooth curve passing through the isospin-0 $KN \to K^*N$ cross sections. The data indicate that the energy dependency of the isospin-0 and isospin-1 $KN \to K^*N$ cross sections are quite similar in this energy region.

Figure 37 shows the production and decay angular distributions at 1210 and 1365 MeV/c for events around the K^* peak treating them as isospin-0 $KN \to K^*N$ events. As pointed out before, no correction has been made for the non-K^* background events, which amount to about 12% of the selected events at 1210 MeV/c and 7% at 1365 MeV/c. These angular distributions reflect the dominance of the $K^+n \to K^{*0}p$ channel in Eq. 61. Figure 38 shows the isospin-0 K^* differential cross section, $d\sigma/dt$, together with the density matrix elements (Jackson-frame) ρ_{00}, ρ_{1-1}, and Re ρ_{10}. The differential cross-section can be fitted to an exponential

$$d\sigma/dt \approx \exp(bt), \tag{64}$$

with $b = 5.3 \pm 0.4$ $(GeV/c)^{-2}$ at 1210 MeV/c and $b = 4.7 \pm 0.6$ $(GeV/c)^{-2}$ at 1365 MeV/c. Note the rather large value of ρ_{00} indicative of pseudoscalar meson exchange.

The contrast between the K^* angular distributions in the two isospin channels is striking. In the isospin-0 channel, the production angular distributions peak sharply in the forward direction, the polar decay angular distributions vary mainly as $\cos^2\alpha$, and azimithal decay angular distributions are flat. In the isospin-1 channel (Fig. 20 and Reference 8), the production distributions peak much less sharply, the polar decay

distributions vary mainly as $\sin^2\alpha$, and the azimuthal decay distributions vary mainly as $\sin^2\phi$. In the first case, the distributions are characteristic of exchange in the t-channel of a light pseudoscalar meson, as born out by the large value of ρ_{00}; whereas in the second case they are characteristic of a heavier vector meson. All the main features point to π and/or η-exchange being the dominant K^* production mechanism in the isospin-0 channel and ρ- and/or ω-exchange being dominant in the isospin-1 channel.

C. Production Mechanisms for the Reaction $KN \to K^*N$

We summarize our experimental observations for the reaction $KN \to K^*N$ at 1210 and 1365 MeV/c as follows:

1. Cross Sections
   a. $\sigma(K^+p \to K^{*+}p) \approx 2\,\sigma(K^+n \to K^{*+}n)$
   b. $\sigma(K^+n \to K^{*0}p) \approx 1.5\,\sigma(K^+p \to K^{*+}p)$
   c. $\sigma_0(KN \to K^*N) \approx (2.5\text{-}2.7)\,\sigma_1(KN \to K^*N)$
2. Angular Distributions $\to$ Production Mechanisms
   a. $K^+p \to K^{*+}p \to$ dominated by ω-exchange
   b. $K^+n \to K^{*+}n \to$ no one process appears to dominate
   c. $K^+n \to K^{*0}p \to$ dominated by π-exchange
   d. $(KN \to K^*N)_{I=0} \to$ dominated by π-exchange
   e. $(KN \to K^*N)_{I=1} \to$ same as 2(a), i.e., dominated by ω-exchange

We now attempt to get a consistent, though qualitative, description of the above experimental observations in terms of s- and t-channel isospin amplitudes A_I^s and a_I^t. A particle exchanged in the t channel contributes to both isospin states in the s channel. The $KN \to K^*N$ charge state scattering amplitudes, written alternatively in terms of s- and t-channel isospin amplitudes are:

$$A(K^+p \to K^{*+}p) = A_1 = (a_1 - a_0)/2, \tag{65a}$$

$$A(K^+n \to K^{*+}n) = (A_1 + A_0)/2 = -(a_1 + a_0)/2, \tag{65b}$$

$$A(K^+n \to K^{*0}p) = (A_1 - A_0)/2 = a_1. \tag{65c}$$

Solving for the s-channel isospin amplitudes, we get

$$A_0 = -(a_0 + 3a_1)/2, \tag{66a}$$

$$A_1 = -(a_0 - a_1)/2. \tag{66b}$$

If the main processes are the exchanges of low-mass mesons, then

$$A_0 \approx -[(\eta + \omega) + 3(\pi + \rho)]/2, \tag{67a}$$

$$A_1 \approx -[(\eta + \omega) - (\pi + \rho)]/2, \tag{67b}$$

where the particle symbols stand for the amplitudes for the exchange of these particles.

The angular distributions indicate that at least one pseudoscalar and one vector meson are exchanged. If only one of each is exchanged, the possible pairs are $\eta\omega$, $\pi\rho$, $\eta\rho$, and $\pi\omega$. Simple predictions follow from Eqs. 67a and 67b: For $\eta\omega$ or $\pi\rho$, A_0 and A_1 differ at most by a multiplicative constant, and thus the shapes of angular distributions in the two pure-isospin channels differ not at all. For $\eta\rho$, there is much more vector exchange in A_0 than in A_1; and for $\pi\omega$, there is much more pseudoscalar exchange in A_0 than in A_1. The last is what is seen, and thus in this simple picture the main processes are π- and ω-exchange. If these were the only processes, there would be the same amount of vector exchange in A_0 and A_1, and only pseudoscalar exchange in a_1, the amplitude for $K^+n \to K^{*0}p$. In neither case is this what we see, but the addition of relatively small amounts of other exchanges, such as ρ-exchange, can at least qualitatively resolve the discrepancies. Therefore a possible minimal set of exchanges might be $\pi\omega\rho$, so that

$$\begin{aligned} A_0 &\approx -[\omega + 3(\pi + \rho)]/2 & a_0 &\approx \omega, \\ A_1 &\approx -[\omega - (\pi + \rho)]/2 & a_1 &\approx (\pi + \rho). \end{aligned} \tag{68}$$

Recall the isospin-0 K^*N final state appears to exhibit more pure pion exchange than the $K^{*0}p$ final state produced by K^+n; this suggests that the ρ-exchange is present by an amount such that the combination $(\omega + 3\rho)$ in A_0 must practically vanish, i.e., $\rho \approx -\omega/3$.

We next see if the presence of a significant ρ-exchange amplitude, opposite in phase to the ω-exchange amplitude, can also explain the fact that $\sigma(K^+p \to K^{*+}p) \approx 2\,\sigma(K^+n \to K^{*+}n)$, [experimental observation 1(a)].

$$\frac{\sigma(K^+p \to K^{*+}p)}{\sigma\,(K^+n \to K^{*+}n)} = \frac{\int|A(K^+p \to K^{*+}p)|^2dt}{\int|A(K^+n \to K^{*+}n)|^2dt} = \frac{\int|(a_1 - a_0)/2|^2dt}{\int|-(a_1 + a_0)/2|^2dt}$$

$$\simeq\frac{\int|\pi + \rho - \omega|^2dt}{\int|\pi + \rho + \omega|^2dt}\approx \frac{\int|\pi - 4/3\,\omega|^2dt}{\int|\pi + 2/3\,\omega|^2dt}.$$

If one assumes no interference between pseudoscalar and vector exchanges, e.g., no absorption, then

$$\frac{\sigma(K^+p \to K^{*+}p)}{\sigma(K^+n \to K^{*+}n)} \approx \frac{\int\left[\pi^2 + \frac{16}{9}\,\omega^2\right]dt}{\int\left[\pi^2 + 4/9\,\omega^2\right]dt} \approx \frac{2}{1}\,,$$

which implies

$$\int\omega^2dt \approx (9/8)\int\pi^2dt \approx \int\pi^2dt.$$

Therefore the observed experimental result, $\sigma(K^+p \to K^{*+}p) \approx 2\sigma(K^+n \to K^{*+}n)$, can be explained in terms of our $\pi\omega\rho$ exchange model provided $\rho \approx -\omega/3$ and $\int\omega^2dt \approx \int\pi^2dt$. The problem is to show that the remaining experimental observations 1(b), 1(c), 2(a), 2(b), 2(c) are compatible with this picture.

Experimentally, at 1210 and 1365 MeV/c, we observe that $\sigma\,(K^+n \to K^{*0}p) \approx (1.5)\;\sigma(K^+p \to K^{*+}p)$. In terms of the model described above, we expect

$$\frac{\sigma(K^+n \to K^{*0}p)}{\sigma(K^+p \to K^{*+}p)} = \frac{\int|A(K^+n \to K^{*0}p)|^2dt}{\int|A(K^+p \to K^{*+}p)|^2dt} = \frac{\int|a_1|^2dt}{\int|(a_1 - a_0)/2|^2dt}$$

$$\approx \frac{\int|\pi + \rho|^2dt}{\int|(\pi + \rho - \omega)/2|^2dt} \approx \frac{\int|\pi - \omega/3|^2dt}{\int|(\pi - 4/3\,\omega)/2|^2dt}\approx\frac{\int\left[\pi^2 + \omega^2/9\right]dt}{\int\left[\frac{1}{4}(\pi^2+\frac{16}{9}\omega^2)\right]dt} \approx 3/2,$$

which implies

$$\frac{\sigma(K^+n \to K^{*0}p)}{\sigma(K^+p \to K^{*+}p)} \approx 1.5\,.$$

Experimentally, at 1210 and 1365 MeV/c, we observe that $\sigma_0(KN \to K^*N) \approx (2.5 - 2.7)\ \sigma_1(KN \to K^*N)$. In terms of our model we expect

$$\frac{\sigma_0(KN \to K^*N)}{\sigma_1(KN \to K^*N)} = \frac{\int |A_0|^2 dt}{\int |A_1|^2 dt} = \frac{\int |-(a_0 + 3a_1)/2|^2 dt}{\int |-(a_0 - a_1)/2|^2 dt} \approx \frac{\int |\omega + 3(\pi + \rho)|^2 dt}{\int |\omega - (\pi + \rho)|^2 dt}$$

$$\approx \frac{\int |3\pi|^2 dt}{\int |4/3\,\omega - \pi|^2 dt} \approx \frac{\int 9\pi^2 dt}{\int \left[\frac{16}{9}\omega^2 + \pi^2\right] dt} \approx \frac{3}{1},$$

which implies

$$\frac{\sigma_0(KN \to K^*N)}{\sigma_1(KN \to K^*N)} \approx \frac{3}{1}.$$

Experimentally, at 1210 and 1365 MeV/c, we observe that K^* production in the channel $(K^+p \to K^{*+}p) = (KN \to K^*N)_{I=1}$ is dominated by ω-exchange. In terms of our model we expect

$$|A(K^+p \to K^{*+}p)|^2 = |A_1|^2 = |(a_1 - a_0)/2|^2 \approx |1/2(\pi + \rho - \omega)|^2$$

$$\approx \frac{1}{4}\,|\pi - 4/3\,\omega|^2$$

$$\approx \frac{1}{4}\left[\pi^2 + \frac{16}{9}\omega^2\right],$$

which implies ~ 2/3 vector-exchange and ~ 1/3 pion-exchange.

Experimentally, at 1210 and 1365 MeV/c, we observe that K^* production in the channel $K^+n \to K^{*+}n$ does not appear to be dominated by any one process. In terms of our model we expect

$$|A(K^+n \to K^{*+}n)|^2 = |-(a_1 + a_0)/2|^2 \approx |(\pi + \rho + \omega)/2|^2$$

$$\approx \frac{1}{4}\,|\pi + 2/3\,\omega|^2$$

$$\approx \frac{1}{4}\left[\pi^2 + 4/9\ \omega^2\right],$$

which implies ~ 1/3 vector-exchange and ~ 2/3 pion-exchange.

Experimentally, at 1210 and 1365 MeV/c, we observe that K^* production in the channel $K^+n \rightarrow K^{*0}p$ is dominated π-exchange. In terms of our model we expect

$$|A(K^+n \rightarrow K^{*0}p)|^2 = |a_1|^2 \approx |\pi + \rho|^2$$
$$\approx \pi^2 + \rho^2 .$$

But $\rho^2 \approx (-\omega/3)^2 = \frac{1}{9}\omega^2$,

which implies ~ 1/9 vector-exchange and ~ 8/9 pion-exchange.

We therefore find qualitative agreement between our experimental observations for $KN \rightarrow K^*N$ and a $\pi\omega\rho$ exchange model subject to the constraints $\rho \approx -\omega/3$ and $\int\omega^2 dt \approx \int\pi^2 dt$. Note that our arguments still hold if we expand $\pi\omega\rho$ to mean the exchange-degenerate pairs (π, B), (ω, f), (ρ, A_2) provided we invoke strong exchange degeneracy.

VI. SUMMARY AND CONCLUSIONS

We have measured some of the K^+d partial cross sections around 1 GeV/c and have calculated most of the others by using relations derived from isospin conservation and data from other experiments. The $K^+d \rightarrow K^0pp$ cross section falls smoothly with increasing momentum (see Fig. 7). The single-pion production cross sections rise rapidly until about 1.2 GeV/c and then level off; they all have about the same shape though they differ in size. The double-pion production cross sections are extremely small until 1.2 GeV/c, after which they begin to rise. The most striking feature of the K^+d partial cross sections is the abrupt rise of the total single-pion production cross section to 15 mb at 1.2 GeV/c. As this is accompanied by a less precipitous fall of the KNN cross section, the total K^+d cross section increases by only 10 mb. The onset of double-pion production, by which time the single-pion production has leveled off, causes no marked change of the total cross section.

We have also extracted isospin-0 KN partial cross sections. The striking feature of these cross sections is the rapid rise of $\sigma_0(KN\pi)$ at the threshold for the quasi-two-body reaction $KN \rightarrow K^*N$ (see Fig. 8). It appears to come at a slightly higher momentum than does the increase of $\sigma_1(KN\pi)$. This is reasonable, because the reaction $KN \rightarrow K\Delta$, for which the threshold is slightly lower and which is known to be the major part of $\sigma_1(KN\pi)$ in this region, is forbidden to the isospin-0 channel. It is surprising then how similar in magnitude $\sigma_0(KN\pi)$ and $\sigma_1(KN\pi)$ quickly become. The rapid increase of $\sigma_0(KN\pi)$ is accompanied by a turn-over of $\sigma_0(KN)$. The latter then falls off quite rapidly, much more so than does $\sigma_1(KN)$. As in the case of the isospin-1 K^+N system, it appears that the structure around 1.2 GeV/c in the total cross section for the isospin-0 K^+N system is well reconstructed by the sum of three smoothly varying channel cross sections $\sigma_0(KN)$, $\sigma_0(KN\pi)$, and $\sigma_0(KN\pi\pi)$. The broad peak in $\sigma_0(KN)$ near 0.8 GeV/c is intriguing, but the answer to the question as to whether this is due to a Z_0^* resonance will have to wait until a reliable phase shift analysis is performed in the isospin-0 K^+N system.

We have studied the charge-exchange reaction $K^+d \rightarrow K^0p(p)$ and find that the cross section rises rapidly from threshold to about 7 mb at

0.6 GeV/c, remains constant until about 0.9 GeV/c, at which point it turns over and falls smoothly as P_K^{-2} from 1.2 GeV/c to 12.0 GeV/c. We have extended the Regge model of Rarita and Schwarzschild[43] down to momenta spanning this experiment and find reasonable agreement between the predictions of this model and the experimental differential cross sections, $(d\sigma/dt)_d$. Using this model we have extracted differential cross sections for $K^+n \to K^0p$, $(d\sigma/d\Omega)_n$, and have performed a Legendre polynomial fit to the data. We find that the expansion coefficients appear to vary smoothly in the region of this experiment. Finally we have compared the forward scattering cross section with that derived from the optical theorem and find that the K^+n charge exchange amplitude is predominantly real.

We have measured partial cross sections for several single-pion production reactions and find that above 1 GeV/c the quasi-two-body processes $KN \to K^*N$ and $KN \to K\Delta$ dominate. For K^* production near threshold we find $\sigma(K^+n \to K^{*0}p) \approx 1.5\,\sigma(K^+p \to K^{*+}p)$ and $\sigma(K^+p \to K^{*+}p) \approx 2\,\sigma(K^+n \to K^{*+}n)$ and $\sigma_0(KN \to K^*N) \approx (2.5 - 2.7) \times \sigma_1(KN \to K^*N)$. As already observed at 2.3 and 3.0 GeV/c,[46, 47] the isospin-1 K^*N production goes predominantly via ω-exchange, whereas the $K^+n \to K^{*0}p$ process goes largely via pion-exchange. It is striking that this behavior remains unchanged practically down to K^*N threshold. Unexpectedly the isospin-0 K^*N final state appears to exhibit more pure pion-exchange than the $K^{*0}p$ final state produced by K^+n. In terms of a simple particle-exchange model, in which $\pi\omega\rho$ are allowed to be exchanged, this suggest that the combination $(\omega + 3\rho)$ in Eq. 68 for A_0 must practically vanish, that is $\rho \approx -\omega/3$. The presence of a significant ρ-exchange amplitude, opposite in phase to the ω-exchange amplitude, also explains the fact that $\sigma(K^+p \to K^{*+}p) \approx 2\,\sigma(K^+N \to K^{*+}n)$, provided that $\int\omega^2 dt \approx (9/8)\int\pi^2 dt$. A $\pi\omega\rho$-exchange model subject to these two constraints on the amplitudes can qualitatively explain the gross features of the experimentally observed angular distributions and ratios of cross sections for the various charge states of $KN \to K^*N$. The processes dominated by pion-exchange have about the same energy dependence as the processes dominated by vector meson-exchange, at variance with theoretical

expectations from either Reggeized or absorptive exchange models.

We now summarize the results relevant to the important question of whether the peak in the isospin-0 total cross section at 1200 MeV/c is a resonance or not. The peak is undoubtedly associated with the K^*N threshold, since peak and threshold occur at the same place and the $KN \rightarrow K^*N$ cross section rises sharply there, while the only other important partial cross section (elastic scattering) undergoes a less marked variation. Close above threshold, the K^* angular distirubitons strongly indicate pion-exchange. There is no corresponding simple single-process interpretation from the s-channel point of view. If K^* production took place through a single s-channel partial wave, the production angular distributions would be symmetric about $\cos\theta = 0$, whereas the observed forward peak requires the constructive interference of several partial waves.

According to the theoretical concept of duality,[50] an amplitude can represent simultaneously both of what were once thought of as exclusively either s- or t-channel processes. Therefore, although the simple and economical description of K^* production is in terms of t-channel processes, we cannot rule out that some part of the t-channel amplitude is also an s-channel resonance. More mundanely, neither can we definitely exclude that besides the exchange amplitudes there is another small and possibly resonant amplitude. The way to finally resolve the question is to partial-wave analyze the isospin-0 $KN \rightarrow KN$ and $KN \rightarrow K^*N$ reactions, but this has not been done and will be difficult. The difficulties in finding unique solutions in such analyses, even when there are polarization data are well known. Here there are to be added the problems of correcting for effects of the deuteron and, in the case of the $KN \rightarrow K^*N$ reaction, of extracting K^* events from background and analyzing a final state in which both particles have spin.

ACKNOWLEDGMENTS

I wish to express my gratitude to Professor Gerson Goldhaber for his guidance, encouragement, and patience during the years I have studied under him. I am also grateful to the late Dr. Sulamith Goldhaber for her interest and encouragement. Special thanks are due Professor George H. Trilling for his advice and continued interest in this experiment.

I wish to particularly express my appreciation to Dr. Charles G. Wohl for his close collaboration and indispensible guidance in the analysis of this experiment. Special thanks are also due Dr. Roger W. Bland and Mr. Victor H. Seeger for many helpful discussions relating to this experiment. I also thank Drs. John A. Kadyk, John L. Brown, and Michael G. Bowler for their participation in the earlier phases of this experiment.

To the scanning and measuring staff of the Trilling-Goldhaber group, my thanks. The accuracy of the results is in large part due to their considerable efforts. To the computing staff attached to the Trilling-Goldhaber group, my special gratitude.

This work was done under the auspices of the U. S. Atomic Energy Commission.

APPENDIX

The K^+d reactions that occur at the energies spanned by this experiment are:

$$K^+d \rightarrow KNN \rightarrow K^+pn$$
$$K^0pp$$

$$K^+d \rightarrow KNN\pi \rightarrow \left.\begin{array}{l} K^+nn\pi^+ \\ K^0pn\pi^+ \\ K^+pp\pi^- \end{array}\right\} \sigma_c$$
$$\left.\begin{array}{l} K^+pn\pi^0 \\ K^0pp\pi^0 \end{array}\right\} \sigma_o$$

$$K^+d \rightarrow KNN\pi\pi \rightarrow \left.\begin{array}{l} K^0nn\pi^+\pi^+ \\ K^+pn\pi^+\pi^- \\ K^0pp\pi^+\pi^- \end{array}\right\} \sigma_{cc}$$
$$\left.\begin{array}{l} K^+nn\pi^+\pi^0 \\ K^0pn\pi^+\pi^0 \\ K^+pp\pi^-\pi^0 \end{array}\right\} \sigma_{co}$$
$$\left.\begin{array}{l} K^+pn\pi^0\pi^0 \\ K^0pp\pi^0\pi^0 \end{array}\right\} \sigma_{oo} \quad .$$

The reactions listed above are arranged according to the charge states of the pions. The symbol σ_{co}, for example, represents the sum of all cross sections leading to one charged and one neutral pion.

There is a simple way to find the linear relations between cross sections or decay rates that follow from isospin conservation. The method, due to Shmushkevich,[51-54] avoids using Clebsch-Gordon coefficients or expanding reaction amplitudes in terms of isospin amplitudes. In fact it says nothing about amplitudes.

Shmushkevich observed that if an initial state that is unpolarized in isospin space undergoes an interaction or decay that conserves isospin, then the final state reached is also unpolarized in isospin space. Unpolarized in isospin space means that within each particle multiplet, all the charge states (the I_z states) are equally populated. For example, the π multiplet is unpolarized if there are equal numbers of π^+'s, π^-'s, and π^0's. The procedure is to write down all the reactions that conserve

charge and then to constrain the rates or cross sections so that each particle multiplet is unpolarized.

Isospin Conservation and K^+d Reactions

Kd → KNNπ reactions. First we write down all the reactions that conserve charge.

1. $K^+d \to K^+nn\pi^+$
   $K^0d \to K^0pp\pi^-$
2. $K^+d \to K^0pn\pi^+$
   $K^0d \to K^+np\pi^-$
3. $K^+d \to K^+pp\pi^-$
   $K^0d \to K^0nn\pi^+$
4. $K^+d \to K^+pn\pi^0$
   $K^0d \to K^0np\pi^0$
5. $K^+d \to K^0pp\pi^0$
   $K^0d \to K^+nn\pi^0$

	π^+	π^-	π^0
σ_1	1	1	0
σ_2	1	1	0
σ_3	1	1	0
σ_4	0	0	2
σ_5	0	0	2

Note that the K^0d reactions are related to the K^+d reactions by charge symmetry, so that one need only consider the K^+d reactions provided one remembers that there are twice as many charged π's as π^0's. Therefore the constraint that there be equal numbers of π^+'s and π^0's leads to

$$\underbrace{(\sigma_1 + \sigma_2 + \sigma_3)}_{\sigma_c} = 2\,\underbrace{(\sigma_4 + \sigma_5)}_{\sigma_o}$$

so that

$$\sigma_c = 2\sigma_o.$$

This leads to the following relations between single pion production cross sections:

$$\begin{aligned}\sigma(\mathrm{KNN}\pi) &= \sigma_c + \sigma_o \\ &= 3\sigma_o \\ &= 3/2\,\sigma_c\,.\end{aligned}$$

In a similar manner, one can derive relations for the $Kd \to KNN\pi\pi$, $KN \to KN\pi$, and $KN \to KN\pi\pi$ reactions. We shall only sketch their derivation below.

The $Kd \to KNN\pi\pi$ reactions are:

1. $K^+d \to K^0nn\pi^+\pi^+$
   $K^0d \to K^+pp\pi^-\pi^-$
2. $K^+d \to K^+pn\pi^+\pi^-$
   $K^0d \to K^0np\pi^-\pi^+$
3. $K^+d \to K^0pp\pi^+\pi^-$
   $K^0d \to K^+nn\pi^-\pi^+$
4. $K^+d \to K^+nn\pi^+\pi^0$
   $K^0d \to K^0pp\pi^-\pi^0$
5. $K^+d \to K^0pn\pi^+\pi^0$
   $K^0d \to K^+np\pi^-\pi^0$
6. $K^+d \to K^+pp\pi^-\pi^0$
   $K^0d \to K^0nn\pi^+\pi^0$
7. $K^+d \to K^+pn\pi^0\pi^0$
   $K^+d \to K^0np\pi^0\pi^0$
8. $K^+d \to K^0pp\pi^0\pi^0$
   $K^0d \to K^+nn\pi^0\pi^0$

	π^+	π^-	π^0
σ_1	2	2	0
σ_2	2	2	0
σ_3	2	2	0
σ_4	1	1	2
σ_5	1	1	2
σ_6	1	1	2
σ_7	0	0	4
σ_8	0	0	4

Equating the number of π^+'s to the number of the π^0's leads to

$$2(\sigma_1 + \sigma_2 + \sigma_3) + (\sigma_4 + \sigma_5 + \sigma_6)$$

$$= 2\ [(\sigma_4 + \sigma_5 + \sigma_6) + 2(\sigma_7 + \sigma_8)\ ].$$

This can be rewritten in terms of the charge states of the pions as

$$2\sigma_{cc} + \sigma_{co} = 2\sigma_{co} + 4\sigma_{oo}$$

or

$$2\sigma_{cc} = 4\sigma_{oo} + \sigma_{co}$$

Therefore

$$\begin{aligned}\sigma(KNN\pi\pi) &= \sigma_{cc} + \sigma_{co} + \sigma_{oo} \\ &= 3(\sigma_{cc} - \sigma_{oo}) \\ &= 3/2\ (\sigma_{co} + 2\sigma_{oo}) \\ &= 3/4\ (\sigma_{co} + 2\sigma_{cc}).\end{aligned}$$

Isospin Conservation and K^+N Reactions

There are seven different charge states for single-pion production in K^+N interactions:

$$\left.\begin{aligned} K^+p &\to K^0\pi^+p \\ &\quad K^+\pi^+n \\ &\quad K^+\pi^0p \end{aligned}\right\} \quad \sigma_p$$

$$\left.\begin{aligned} K^+n &\to K^0\pi^+n \\ &\quad K^0\pi^0p \\ &\quad K^+\pi^0n \\ &\quad K^+\pi^-p \end{aligned}\right\} \quad \sigma_n \ .$$

Again using the method of Shmushkevich:

		π^+	π^-	π^0
1. $K^+p \to K^0\pi^+p$ $K^0n \to K^+\pi^-n$	σ_1	1	1	0
2. $K^+p \to K^+\pi^+n$ $K^0n \to K^0\pi^-p$	σ_2	1	1	0
3. $K^+p \to K^+\pi^0p$ $K^0n \to K^0\pi^0n$	σ_3	0	0	2
4. $K^+n \to K^0\pi^+n$ $K^0p \to K^+\pi^-p$	σ_4	1	1	0
5. $K^+n \to K^0\pi^0p$ $K^0p \to K^+\pi^0n$	σ_5	0	0	2
6. $K^+n \to K^+\pi^0n$ $K^0p \to K^0\pi^0p$	σ_6	0	0	2
7. $K^+n \to K^+\pi^-p$ $K^0p \to K^0\pi^+n$	σ_7	1	1	0

Again equating the number of π^+'s and π^0's, we get

$$(\sigma_1 + \sigma_2 + \sigma_4 + \sigma_7) = 2\,(\sigma_3 + \sigma_5 + \sigma_6)$$

or expressed in terms of the charge states of the pions we get as before

$$\sigma_c = 2\,\sigma_o\,.$$

Now note

$$\sigma_p = \sigma_1 + \sigma_2 + \sigma_3 = \sigma(I = 1)$$

$$\sigma_n = \sigma_4 + \sigma_5 + \sigma_6 + \sigma_7 = 1/2\ \ [\sigma(I=1) + \sigma(I=0)]\,.$$

Hence

$$\sigma(I=0) = 2\sigma_n - \sigma_p$$

$$= 2(\sigma_4 + \sigma_5 + \sigma_6 + \sigma_7) - (\sigma_1 + \sigma_2 + \sigma_3)\,.$$

Using the relation $\sigma_c = 2\sigma_o$ we finally obtain a relation for the isospin-0 single pion production reaction:

$$\sigma(I=0) = 3(\sigma_4 + \sigma_7 - \sigma_3)\,.$$

Therefore

$$\sigma_{I=0}(KN\pi) = 3\,[\sigma(K^+n \rightarrow K^0\,\pi^+n) + \sigma(K^+n \rightarrow K^+\pi^-p)$$

$$- \sigma(K^+p \rightarrow K^+\pi^0\,p)]\,.$$

According to Shmushkevich this relation should hold also for differential cross sections.

There are eleven charge states for double-pion production:

$K^+p \rightarrow K^0n\pi^+\pi^+$

$K^+p\pi^+\pi^-$

$K^+n\pi^+\pi^0$

$K^0p\pi^+\pi^0$

$K^+p\pi^0\pi^0$

$K^+n \rightarrow K^+n\pi^+\pi^-$

$K^0p\pi^+\pi^-$

$K^0n\pi^+\pi^0$

$K^+p\pi^-\pi^0$

$K^+n\pi^0\pi^0$

$K^0p\pi^0\pi^0$

Now applying Shmushkevich's method:

		π^+	π^-	π^0
1.	$K^+p \to K^0n\pi^+\pi^+$ $K^0n \to K^+p\pi^-\pi^-$	σ_1 2	2	0
2.	$K^+p \to K^+p\pi^+\pi^-$ $K^0n \to K^0n\pi^-\pi^+$	σ_2 2	2	0
3.	$K^+p \to K^+n\pi^+\pi^0$ $K^0n \to K^0p\pi^-\pi^0$	σ_3 1	1	2
4.	$K^+p \to K^0p\pi^+\pi^0$ $K^0n \to K^+n\pi^-\pi^0$	σ_4 1	1	2
5.	$K^+p \to K^+p\pi^0\pi^0$ $K^0n \to K^0n\pi^0\pi^0$	σ_5 0	0	4
6.	$K^+n \to K^+n\pi^+\pi^-$ $K^0p \to K^0p\pi^-\pi^+$	σ_6 2	2	0
7.	$K^+n \to K^0p\pi^+\pi^-$ $K^0p \to K^+n\pi^-\pi^+$	σ_7 2	2	0
8.	$K^+n \to K^0n\pi^+\pi^0$ $K^0p \to K^+p\pi^-\pi^0$	σ_8 1	1	2
9.	$K^+n \to K^+p\pi^-\pi^0$ $K^0p \to K^0n\pi^+\pi^0$	σ_9 1	1	2
10.	$K^+n \to K^+n\pi^0\pi^0$ $K^0p \to K^0p\pi^0\pi^0$	σ_{10} 0	0	4
11.	$K^+n \to K^0p\pi^0\pi^0$ $K^0p \to K^+n\pi^0\pi^0$	σ_{11} 0	0	4

Again equating the number of π^+'s and π^0's we get

$$2(\sigma_1 + \sigma_2 + \sigma_6 + \sigma_7) + (\sigma_3 + \sigma_4 + \sigma_8 + \sigma_9)$$

$$= 4(\sigma_5 + \sigma_{10} + \sigma_{11}) + 2(\sigma_3 + \sigma_4 + \sigma_8 + \sigma_9) ,$$

which expressed in terms of the charge states of the pions reduces to

$$2\sigma_{cc} = 4\sigma_{oo} + \sigma_{co}.$$

REFERENCES

1. J. Brown, R. W. Bland, M. Bowler, G. Goldhaber, S. Goldhaber, A. Hirata, J. Kadyk, V. Seeger and G. Trilling, in Proc. of the XII Int. Conf. on High Energy Physics, Dubna (Atomizdat, Moscow, 1966) p. 715.

2. M. Bowler, R. W. Bland, J. Brown, G. Goldhaber, J. Kadyk, V. Seeger and G. Trilling, Lecture presented at the Oxford Int. Conf. on Elementary Particles, Oxford, England, September 19-25, 1965 (UCRL-16370, Dec. 1965, unpublished).

3. R. Bland, M. Bowler, J. Brown, G. Goldhaber, S. Goldhaber, J. Kadyk and G. Trilling, Phys. Rev. Letters 17, 939 (1966).

4. R. Bland, M. Bowler, J. Brown, G. Goldhaber, S. Goldhaber, V. Seeger and G. Trilling, Phys. Rev. Letters 18, 1077 (1967).

5. R. W. Bland, G. Goldhaber and G. H. Trilling, Physics Letters 29B, 1466 (1968).

6. R. W. Bland (thesis), Lawrence Radiation Laboratory Report UCRL-18131, March 1968.

7. R. W. Bland, M. G. Bowler, J. L. Brown, J. A. Kadyk, G. Goldhaber, S. Goldhaber, V. H. Seeger, and G. H. Trilling, Nucl. Physics B13, 595 (1969).

8. R. W. Bland, M. G. Bowler, J. L. Brown, G. Goldhaber, S. Goldhaber, J. A. Kadyk, V. H. Seeger, and G. H. Trilling, Nucl. Physics B18, 537 (1970).

9. R. L. Cool, G. Giacomelli, T. F. Kycia, B. A. Leontic, K. K. Li, A. Lundby and J. Teiger, Phys. Rev. Letters, 17, 102 (1966).
R. L. Cool, G. Giacomelli, T. F. Kycia, B. A. Leontic, K. K. Li, A. Lundby, J. Teiger and C. Wilkin, Phys. Rev. D1, 1887 (1970).

10. D. V. Bugg, R. S. Gilmore, K. M. Knight, D. C. Slater, G. H. Stafford, E. J. N. Wilson, J. D. Davis, J. D. Dowell, P. M. Hattersley, R. J. Homer, A. W. O'Dell, A. A. Carter, R. J. Tapper, and K. F. Riley, Phys. Rev. 168, 1466 (1968).

11. T. Bowen, P. K. Caldwell, F. Ned Dikmen, E. W. Jenkins, R. M. Kalbach, D. V. Peterson, and A. E. Pifer, in Hyperon Resonances-70, Earle C. Fowler, editor, Moore Publishing Company, Durham, North Carolina, p. 3 (1970).

12. R. Glauber, Phys. Rev. 100, 242 (1955).

13. C. Wilkin, Phys. Rev. Letters 17, 561 (1966).

14. V. Franco and R. J. Glauber, Phys. Rev. 142, 1195 (1966).

15. G. Alexander, G. Goldhaber, and B. H. Hall, Reexamination of Deuteron Cross Sections and the I=0 K^+N Enhancement at 1.15 BeV/c, Lawrence Radiation Laboratory Report UCRL-18365, July 1968 (unpublished).

16. The latest K^+p phase shift analyses are listed below. Those references listed as (Duke p. ____) can be found in the Proceedings of the Duke Conference on Hyperon Resonances, Hyperon Resonances-70, Earle C. Fowler, editor, Moore Publishing Company, Durham, North Carolina, (1970).

a) S. Anderson, C. Daum, F. C. Erne, J. P. Lagnaux, J. C. Sens, F. Udo and F. Wagner, Physics Letters 30B, 56 (1969).

b) R. Ayed, P. Bareyre, J. Feltesse, and G. Villet, to be published in Physics Letters.

c) P. C. Barber, T. A. Broome, B. G. Duff, F. F. Heymann, D. C. Imrie, G. J. Lush, B. R. Martin, K. M. Potter, D. M. Ritson, L. A. Robbins, R. A. Rosner, S. J. Sharrock, A. D. Smith, R. C. Hanna, A. T. Lea and E. J. Sacharides, (Duke p. 453).

d) B. Barnett, J. Goldman, A. Laasanen and P. H. Steinberg, (Duke p. 443).

e) Bologna-Glasgow-Roma-Trieste Collaboration, (Duke p. 457).

f) B. Carreras, A. Donnachie and R. G. Kirsopp, (Duke p. 447).

g) F. C. Erne, J. C. Sens and F. Wagner, (Duke p. 375).

h) B. H. Hall, R. W. Bland, G. Goldhaber and G. H. Trilling (Duke p. 435).

i) S. Kato, P. Koehler, T. Novey, A. Yokosawa, G. Burleson, Phys. Rev. Letters 24, 615 (1970).

j) G. Giacomelli, P. Lugaresi-Serra, G. Mandrioli, F. Griffiths, I. S. Hughes, D. A. Jacobs, R. Jennings, B. C. Wilson, G. Ciapetti, V. Costantini, G. Martellotti, D. Zanello, E. Castelli and M. Sessa, Nucl. Physics B20, 301 (1970).

k) G. A. Rebka, Jr., J. Rothberg, A. Etkin, P. Glodis, J. Greenberg, V. W. Hughes, K. Kondo, D. C. Lu, S. Mori, and P. A. Thompson, Phys. Rev. Letters 24, 160 (1970).

17. Allan A. Hirata, Charles G. Wohl, Roger W. Bland, Gerson Goldhaber, Browyn H. Hall, John A. Kadyk, Victor H. Seeger, and George H. Trilling, Contribution of the XIVth International Conference on High-Energy Physics, Vienna, August 28-September 5, 1968, Lawrence Radiation Laboratory Report UCRL-18322 (unpublished).
18. A. A. Hirata, C. G. Wohl, G. Goldhaber, and G. H. Trilling, Phys. Rev. Letters 21, 1485 (1968); Errata, Phys. Rev. Letters 21, 1728 (1968).
19. A. A. Hirata, G. Goldhaber, V. H. Seeger, G. H. Trilling, and C. G. Wohl, Contribution to the Conference on Hyperon Resonances, in Hyperon Resonances-70, Earle C. Fowler, editor, Moore Publishing Company, Durham, North Carolina, p. 429, 1970.
20. R. B. Bell, R. W. Bland, M. G. Bowler, J. L. Brown, R. P. Ely, S. Y. Fung, G. Goldhaber, A. A. Hirata, J. A. Kadyk, J. Louie, C. T. Murphy, J. S. Sahouria, V. H. Seeger, W. M. Smart, and G. H. Trilling, A Variable Momentum Separated $K^{\pm}$ Beam at the Bevatron, Lawrence Radiation Laboratory Report UCRL-11527, 1964, (unpublished).
21. H. S. White, T. Aronstein, C. Osborne, N. Webre and W. G. Moorhead, Nucl. Instr. 20, 393 (1963).
22. Sioux and Arrow references: F. T. Solmitz, A. D. Johnson, and T. B. Day, Three View Geometry Program, Alvarez Group Programming Note P-117, June 1966. O. I. Dahl, T. B. Day, and F. T. Solmitz, SQUAW-Kinematic Fitting Program, Alvarez Group Programming Note P-126, August 1965. Orin I. Dahl, Frank T. Solmitz, Event Type Primer for TVGP and SQUAW (SIOUX), Alvarez Group Programming Note P-139, October 1966.
23. J. L. Brown, Trilling-Goldhaber Internal Report TN-29 (1964), Lawrence Radiation Laboratory, Berkeley, California, (unpublished).
24. The conditions of the applicability of the Impulse Approximation have been discussed by several authors: G. F. Chew, Phys. Rev. 80, 196 (1950). G. F. Chew and G. C. Wick, Phys. Rev. 85, 636 (1952). J. Askin and G. C. Wick, Phys. Rev. 85, 686 (1952). G. F. Chew and M. L. Goldberger, Phys. Rev. 87, 778 (1952). S. Fernbach, T. A. Green and K. M. Watson, Phys. Rev. 84, 1084 (1951). R. M. Rockmore, Phys. Rev. 105, 256 (1957). K. C. Rogers and L. M. Lederman, Phys. Rev.

105, 247 (1957). M. Gourdin and A. Martin, Nuovo Cimento 11, 670 (1959). E. M. Ferreira, Phys. Rev. 115, 1727 (1959). M. Gourdin and A. Martin, Nuovo Cimento 14, 722 (1959).

25. W. Slater, D. H. Stork, H. K. Ticho, W. Lee, W. Chinowsky, G. Goldhaber, S. Goldhaber, and T. O'Halloran, Phys. Rev. Letters 7, 378 (1961).

26. I. Butterworth, J. L. Brown, G. Goldhaber, S. Goldhaber, A. A. Hirata, J. A. Kadyk, B. M. Schwarzschild, and G. H. Trilling, Phys. Rev. Letters 15, 734 (1965), and unpublished data of the same authors.

27. A. A. Carter, The Argand Diagrams of the KN and $\bar{K}N$ Forward Scattering Amplitudes, Cavendish Laboratory Report HEP 68-10 (March 1968). This uses data from both Refs. 9 and 10. A. A. Carter, Phys. Rev. Letters 18, 801 (1967).

28. Several new unfoldings of the isospin-0 KN total cross section were presented at the Duke Conference on Hyperon Resonances and are reported in Hyperon Resonances-70, Earle C. Fowler, editor, Moore Publishing Company, Durham, North Carolina, (1970):

a) Rodney L. Cool, (Duke p. 47).

b) J. D. Dowell, (Duke p. 53).

c) Gerald Lynch, (Duke p. 9).

29. V. J. Stenger, W. E. Slater, D. H. Stork, H. K. Ticho, G. Goldhaber, and S. Goldhaber, Phys. Rev. 134, B1111 (1964).

30. S. Goldhaber, W. Chinowsky, G. Goldhaber, W. Lee, T. O'Halloran, T. F. Stubbs, G. M. Pjerrou, D. H. Stork, and H. K. Ticho, Phys. Rev. Letters 9, 135 (1962).

31. R. J. Abrams, R. L. Cool, G. Giacomelli, T. F. Kycia, K. K. Li, and D. N. Michael, Phys. Rev. Letters 30B, 564 (1969). Also see Reference 9.

32. L. Hulthén and A. Sugawara, Handbuch der Physik, Vol. XXXIV, Springer-Verlag, Berlin, 1957.

33. G. H. Trilling (private communication).

34. A. A. Carter, K. F. Riley, R. J. Tapper, D. V. Bugg, R. S. Gilmore, K. M. Knight, D. C. Slater, G. H. Stafford, J. D. Davies, J. D. Dowell, P. M. Hattersley, R. J. Homer, and A. W. O'Dell, Phys. Rev. 168, 1457 (1968).

35. B. M. Schwarzschild (thesis), Lawrence Radiation Laboratory Report UCRL-17572, June 1967.

36. J. Danberg (thesis), Lawrence Radiation Laboratory Report UCRL-19275, July 1969.

37. V. H. Seeger (thesis), Lawrence Radiation Laboratory Report (in preparation).

38. Y. Goldschmidt-Clermont, V. P. Henri, B. Jonejans, U. Kundt, F. Muller, R. L. Sekuln, M. Shafi, G. Wolf, J. M. Crispeels, J. Debaisieux, M. Delabaye, P. Dufour, F. Grard, J. Heughebaert, J. Naisse, G. Thill, R. Windmolders, K. Buchner, G. Dehm, G. Goebel, H. Hupe, T. Joldersma, I. S. Mittra, W. Wittek, Physics Letters 27B, 602 (1968).

39. A. Firestone, G. Goldhaber, D. Lissaurer, A. Hirata, and G. H. Trilling, Phys. Rev. Letters 25, 958 (1970).

40. D. R. O. Morrison, CERN/TC/Physics, 66-20.

41. R. D. Mathews, Evidence for the Exchange of the ρ and A_2 Regge Trajectories in the Reactions $\pi^+ p \rightarrow \pi^0 \Delta^{++}$, $\pi^+ p \rightarrow \eta^0 \Delta^{++}$ and $K^+ p \rightarrow K^0 \Delta^{++}$, Lawrence Radiation Laboratory Report UCRL-18611, Nov. 1968 (unpublished).

42. The cross sections for the reaction $K^+ p \rightarrow K^0 \Delta^{++}$ were taken from the compilations of L. R. Price, N. Barash-Schmidt, O. Benary, R. W. Bland, A. H. Rosenfeld, and C. G. Wohl, Lawrence Radiation Laboratory Report UCRL-2000 $K^+ N$, September 1969; also from V. Gordon Lind, G. Alexander, A. Firestone, C. Fu, and G. Goldhaber, Nucl. Phys. B14, 1 (1969).

43. W. Rarita and B. M. Schwarzschild, Phys. Rev. 162, 1378 (1967). See also Reference 35.

44. D. Cline, J. Matos, and D. D. Reeder, Phys. Rev. Letters 23, 1318 (1969).

45. R. J. N. Phillips and W. Rarita, Phys. Rev. 139, B1336 (1965).

46. S. Goldhaber, J. L. Brown, I. Butterworth, G. Goldhaber A. A. Hirata, J. A. Kadyk, and G. H. Trilling, Phys. Rev. Letters 15, 737 (1965).

47. G. Bassompierre, Y. Goldschmidt-Clermont, A. Grant, V. P. Henri, B. Jonejans, U. Kundt, F. Muller, J. M. Perreau, H. Piotrowska, R. Sekulin, J. K. Touminiemi, J. M. Crispeels, J. Debaisieux, J. De Jongh, M. Delabaye, P. Dufour, F. Grard, J. Heughebaert, J. Naisse, S. Tarernier, G. Thill, K. Buchner, G. Dehm, G. Goebel, H. Hupe, T. Joldersma, I. S. Mittra, W. Wittek, and G. Wolf, Nucl. Physics B16, 125 (1970).

48. A. Firestone (private communication).

49. The value of $\sigma_0(KN \rightarrow K\pi N)$ at 1365 MeV/c quoted here is larger than that given in Reference 18 by 2/3 standard deviation. This due to the fact that the normalization employed in Eq. 62 differs slightly from that used in Reference 18 (i.e., Eq. 16). The difference arises because at this momentum the fraction of events observed with spectator momentum greater than 150 MeV/c for $K^+d \rightarrow K^0\pi^+pn$ is 7 per cent greater than for $K^+d \rightarrow K^+\pi^-pp$, (see Table IV).

50. R. Dolen, D. Horn, and C. Schmid, Phys. Rev. 166, 1768 (1968). For further references and a review see H. Harari, XXIV International Conference on High Energy Physics, Vienna 1968, (CERN, Geneva, Switzerland), p. 195.

51. I. Shmushkevich, Dokl. Akad. Nauk. SSSR 103, 235 (1955), (translated by M. Hammermesh, AEC-tr-2270).

52. N. Duskin and I. Shmushkevich, Sov. Phys.-Doklady 1, 94 (1956).

53. G. Pinski, A. J. Macfarlane, and E. C. G. Sudarshan, Phys. Rev. 140, B1045 (1965).

54. Charles G. Wohl, Isospin Analysis of Single Pion Production in K^+N Interactions, Trilling-Goldhaber Group Physics Note TG-160 (unpublished). Charles G. Wohl, Linear Relations Between Cross Sections or Decay Rates From Isospin Conservation, Trilling-Goldhaber Group Physics Note TG-165 (unpublished).

FIGURE CAPTIONS

Fig. 1. K^+d and K^+p total cross sections from Cool et al.,[9] Bugg et al.[10] and Bowen et al.[11]

Fig. 2. Isospin-0 and isospin-1 total K^+N cross sections.

Fig. 3. K^+p elastic, single-pion production, and double-pion production cross sections from Bland et al.[7]

Fig. 4. The physical layout of the beam used in this experiment at the Bevatron.

Fig. 5. The event topologies scanned in this experiment.

Fig. 6. (a) Cross sections directly measured. (b) Components of $K^+d \rightarrow K^0pn\pi^+$.

Fig. 7. Derived K^+d cross sections. Also shown are the total K^+d cross-section data of Cool et al.,[9] Bugg et al.,[10] and Bowen et al.[11] and some partial cross section data from Slater et al.[25] and Butterworth et al.[26]

Fig. 8. Isospin-0 KN scattering cross sections. Also shown are the total cross sections from Carter[27] and isospin-1 partial cross sections from a compilation made by Bland et al.[7]

Fig. 9. Spectator nucleon momentum and angular distributions for the reaction $K^+d \rightarrow K^0p(p)$. The shaded events correspond to visible proton spectators. The curve is the prediction of the Hulthén wave function.

Fig. 10. Spectator nucleon momentum and angular distributions for the reaction $K^+d \rightarrow K^+\pi^-p(p)$. The shaded events correspond to visible proton spectators. The curve is the prediction of the Hulthén wave function.

Fig. 11. Spectator nucleon momentum and angular distributions for the reaction $K^+d \rightarrow K^0\pi^0p(p)$. The shaded events correspond to visible proton spectators. The curve is the prediction of the Hulthén wave function.

Fig. 12. Spectator nucleon momentum and angular distributions for the reaction $K^+d \rightarrow K^0\pi^+pn$. The shaded events correspond to events in which the proton is the spectator, i.e., $K^+d \rightarrow K^0\pi^+n(p)$. The curve is the prediction of the Hulthén wave function.

Fig. 13. Scatter plot of the proton momentum as a function of the neutron momentum for the reaction $K^+d \rightarrow K^0\pi^+pn$ at 1210 MeV/c.

Fig. 14. Total cross sections for the reaction $K^+d \rightarrow K^0p(p)$.

Fig. 15. Total cross sections for the reaction $K^+d \rightarrow K^0p(p)$.

Fig. 16. Total cross sections for the reactions $K^+d \rightarrow K^0p(p)$ and $K^+p \rightarrow K^0\Delta^{++}$.

Fig. 17. Differential cross sections as a function of the momentum transfer for the reaction $K^+d \rightarrow K^0p(p)$ at 865, 970, 1210, and 1365 MeV/c.

Fig. 18. Differential cross sections as a function of the center-of-mass scattering angle for the reaction $K^+d \rightarrow K^0p(p)$ at 865, 970, 1210, and 1365 MeV/c.

Fig. 19. Legendre polynomial coefficients defined by

$$(d\sigma/d\Omega)_n = (\lambda^2/4) \sum_{n=0}^{n_{max}} A_n P_n(\cos\theta)$$ for the reaction $K^+d \rightarrow K^0p(p)$.

Fig. 20. A comparison of various distributions for the reaction $K^+p \rightarrow K^0\pi^+p$ and $K^+p(n) \rightarrow K^0\pi^+p(n)$ at 1210 MeV/c. Areas being compared are equal. The angles are defined in the text.

Fig. 21. Dalitz plots for the reaction $K^+d \rightarrow K^0\pi^+p(n)$ at 865, 970, 1210, and 1365 MeV/c.

Fig. 22. Dalitz plots for the reaction $K^+d \rightarrow K^0\pi^+n(p)$ at 865, 970, 1210, and 1365 MeV/c.

Fig. 23. Dalitz plots for the reaction $K^+d \rightarrow K^+\pi^-p(p)$ at 865, 970, 1210, and 1365 MeV/c.

Fig. 24. Dalitz plots for the reaction $K^+d \rightarrow K^0\pi^0p(p)$ at 865, 970, 1210, and 1365 MeV/c.

Fig. 25. Dalitz plot projections for the reaction $K^+d \rightarrow K^0\pi^+p(n)$ at 865, 970, 1210, and 1365 MeV/c.

Fig. 26. Dalitz plot projections for the reaction $K^+d \rightarrow K^0\pi^+n(p)$ at 865, 970, 1210, and 1365 MeV/c.

Fig. 27. Dalitz plot projections for the reaction $K^+d \rightarrow K^+\pi^-p(p)$ at 865, 970, 1210, and 1365 MeV/c.

Fig. 28. Dalitz plot projections for the reaction $K^+d \rightarrow K^0\pi^0p(p)$ at 865, 970, 1210, and 1365 MeV/c.

Fig. 29. Cross sections for the reactions $K^+p \to K^{*+}p$, $K^+n \to K^{*+}n$, and $K^+n \to K^{*0}p$.

Fig. 30. Cross sections for the reactions $K^+p \to K^{*+}p$, $K^+n \to K^{*+}n$, and $K^+n \to K^{*0}p$.

Fig. 31. Invariant mass spectra for the isospin-0 $KN \to K\pi N$ channel at 1210 MeV/c together with the corresponding distributions for the three channels $K^+n \to K^0\pi^+n$, $K^+n \to K^+\pi^-p$, and $K^+p \to K^+\pi^0p$ which are the components of $\sigma_0(KN \to K\pi N)$.

Fig. 32. K^* angular distributions for the isospin-0 $KN \to K^*N$ channel at 1210 MeV/c together with the corresponding distributions for the three channels $K^+n \to (K^0\pi^+)^*n$, $K^+n \to (K^+\pi^-)^*p$, and $K^+p \to (K^+\pi^0)^*p$ which are the components of $\sigma_0(KN \to K^*N)$.

Fig. 33. Invariant mass spectra for the isospin-0 $KN \to K\pi N$ channel at 1365 MeV/c together with the corresponding distributions for the three channels $K^+n \to K^0\pi^+n$, $K^+n \to K^+\pi^-p$, and $K^+p \to K^+\pi^0p$ which are the components of $\sigma_0(KN \to K\pi N)$.

Fig. 34. K^* angular distributions for the isospin-0 $KN \to K^*N$ channel at 1365 MeV/c together with the corresponding distributions for the three channels $K^+n \to (K^0\pi^+)^*n$, $K^+n \to (K^+\pi^-)^*p$, and $K^+p \to (K^+\pi^0)^*p$ which are the components of $\sigma_0(KN \to K^*N)$.

Fig. 35. $K\pi$ and $N\pi$ invariant mass spectra for the isospin-0 $KN \to K\pi N$ channel for momenta at 970, 1210, and 1365 MeV/c.

Fig. 36. Isospin-0 and isospin-1 $KN \to K^*N$ cross sections.

Fig. 37. Production and decay angular distributions for the isospin-0 $KN \to K^*N$ reaction at 1210 and 1365 MeV/c.

Fig. 38. Differential cross sections and density matrix elements for the isospin-0 reaction $KN \to K^*N$ at 1210 and 1365 MeV/c.

Table I. Numbers of events found in directly measured channels.

Channel	Momentum (MeV/c) 865	970	1210	1365
$K^+ \rightarrow \pi^+\pi^-\pi^+$	570	956	827	377
$K^+d \rightarrow K^0pp$	559	996	832	311
$K^0pp\pi^0$	39	129	354	177
$K^0pn\pi^+$	89	369	1018	505
$K^0d\pi^+$	11	20	23	15
$K^0d\pi^+\pi^0$	0	0	1	1
$K^0NN\pi\pi$	0	0	3	22
$K^+d \rightarrow K^+pp\pi^-$	122	461	1583	894
$K^+pp\pi^-\pi^0$	0	0	11	14
$K^0pp\pi^-\pi^+$	0	0	12	23
$K^+pn\pi^-\pi^+$	0	2	22	53
$K^+d\pi^-\pi^+$	0	0	2	5

Table II. K^+d scattering cross sections (in mb).

	Channel	Momentum (MeV/c) 865	970	1210	1365
Cross sections directly measured	$K^+d \rightarrow K^0pp$	6.72±0.40	6.26±0.29	4.99±0.24	3.69±0.29
	$\rightarrow K^0pp\pi^0$	0.48±0.08	0.82±0.08	2.09±0.13	2.06±0.19
	$\rightarrow K^0pn\pi^+$	1.24±0.14	2.47±0.16	6.21±0.29	6.08±0.42
	$\rightarrow K^+pp\pi^-$	0.46±0.05	0.91±0.05	2.89±0.12	3.21±0.20
	$\rightarrow KNN\pi\pi$[a]	---	0.01±0.005	0.11±0.02	0.59±0.07
Components of $K^+d \rightarrow K^0pn\pi^+$	$K^+d \rightarrow K^0\pi^+d$	0.13±0.04	0.13±0.03	0.14±0.03	0.18±0.05
	$K^+p(n) \rightarrow K^0\pi^+p(n)$	0.98±0.13	1.99±0.15	4.76±0.26	4.78±0.38
	$K^+n(p) \rightarrow K^0\pi^+n(p)$	0.13±0.04	0.35±0.05	1.31±0.12	1.12±0.15
Derived cross sections[b]	$K^+d \rightarrow KNN$	27.59±0.32	27.17±0.35	22.73±0.63	20.97±0.99
	$\rightarrow K^+pn$	20.87±0.56	20.91±0.50	17.74±0.78	17.28±1.15
	$\rightarrow KNN\pi$	2.74±0.24	5.54±0.29	14.51±0.60	15.54±0.95
	$\rightarrow KNN\pi\pi$	---	0.01±0.005	0.17±0.05	0.76±0.18
	K^+d total[c]	30.33±0.21	32.72±0.19	37.41±0.20	37.27±0.15

[a] This is the sum over the six (of eight) charge channels observed.

[b] These include cross sections for the reactions in which NN is a deuteron.

[c] From Bugg et al.[10]

Table III. Isospin-zero KN scattering cross sections (in mb).

	Momentum (MeV/c)			
Channel[a]	865	970	1210	1365
KN → all[b]	22.5	24.0	24.1	21.9
KN → KN	21.5	21.5	16.1	13.0
KN → KNπ	1.0±0.4	2.5±0.6	8.0±1.0 8.0±0.9[c]	8.9±1.8 10.1±1.7[c]

[a] We were not able to extract KN → KNππ cross sections, but even at 1364 MeV/c it is much smaller than the errors on the other cross sections.

[b] From Carter. Errors are unknown but sizable.

[c] These cross sections were determined by using the normalization scheme of Eq. 62 (see Reference 49).

Table IV. Fraction of events with spectator momentum greater than 150 MeV/c and 300 MeV/c.

Channel $K^+d \rightarrow XNN$	P_K (MeV/c)	% p_{sp} > 150 MeV/c	% p_{sp} > 300 MeV/c
$K^+d \rightarrow K^0pp$	865	22.5±2.2	10.7±1.5
	970	24.7±1.8	12.5±1.2
	1210	26.7±2.0	15.7±1.5
	1365	26.7±3.3	15.3±2.4
$K^+d \rightarrow K^0\pi^0pp$	865	28.6±9.8	10.8±5.6
	970	18.8±4.2	9.5±2.9
	1210	16.5±2.3	6.5±1.4
	1365	15.8±3.2	7.8±2.2
$K^+d \rightarrow K^0\pi^+pn$	865	19.0±5.0	6.7±2.8
	970	16.9±2.3	5.0±1.2
	1210	16.7±1.4	7.4±0.9
	1365	24.0±2.4	10.9±1.6
$K^+d \rightarrow K^+\pi^-pp$	865	16.4±4.0	4.1±1.9
	970	18.7±2.2	4.8±1.0
	1210	17.1±1.1	6.9±0.7
	1365	16.7±1.5	6.6±0.9

Table V. Estimates of the Glauber-Wilkin screening correction to the total cross section. The total K^+d, K^+p, and K^+n cross sections were obtained by drawing a smooth curve through the points of Bugg et al.[10] and Cool et al.[9] (taken from UCRL-20 000 K^+N) and assigning errors commenserate with the errors on neighboring points.

P_K (MeV/c)	σ_{K^+d} (mb)	σ_{K^+p} (mb)	σ_{K^+n} (mb)	$\Delta = \sigma_{K^+p} + \sigma_{K^+n} - \sigma_{K^+d}$	σ_{GW}	$\sigma_{GW}/\sigma_{K^+d}$	R_c [a]
865	30.20±0.30	13.55±0.30	16.52±0.70	-0.13±0.82	0.53±0.19	0.018±0.006	1.14±0.14
970	32.80±0.25	15.70±0.25	18.18±0.50	1.08±0.61	0.69±0.24	0.021±0.007	1.28±0.11
1210	37.60±0.25	18.45±0.20	20.55±0.20	1.40±0.38	0.81±0.27	0.022±0.007	1.07±0.06
1365	37.05±0.20	18.33±0.20	19.30±0.20	0.58±0.35	0.72±0.24	0.020±0.007	1.12±0.10

[a] R_c is the experimentally observed ratio $\sigma(K^+p \rightarrow K^0\pi^+p)/\sigma[K^+d \rightarrow K^0\pi^+p\,(n)]$.

Table VI. K^+N partial cross sections determined from K^+d partial cross sections – a comparison of two methods.

Channel $K^+d \rightarrow XN(N)$	P_K (MeV/c)	$\sigma(K^+d \rightarrow XN(N))$ (mb)	Glauber-Wilkin corr. factor $C_{GW}=(\sigma^T_{GW}/\sigma^T_{Kd})$	Pauli principle corr. factor C_{PP}	$\sigma(KN \rightarrow XN) \equiv[1+C_{GW}+C_{PP}] \times\sigma(Kd \rightarrow XN(N))$	$\sigma(KN \rightarrow XN) \equiv R_c \times\sigma[K^+d \rightarrow XN(N)]$
$K^+d \rightarrow K^0pp$	865	6.72±0.40	0.018±0.006	0.028±0.087	7.03±0.72	
	970	6.26±0.29	0.021±0.007	0.025±0.067	6.55±0.52	
	1210	4.99±0.24	0.022±0.007	0.023±0.070	5.22±0.43	
	1365	3.69±0.29	0.020±0.007	0.027±0.114	3.86±0.52	
$K^+d \rightarrow K^0\pi^+p(n)$	865	0.98±0.13	0.018±0.006	———	1.00±0.13	1.12±0.20
	970	1.99±0.15	0.021±0.007	———	2.03±0.15	2.55±0.29
	1210	4.76±0.26	0.022±0.007	———	4.86±0.27	5.09±0.40
	1365	4.78±0.38	0.020±0.007	———	4.88±0.39	5.35±0.64
$K^+d \rightarrow K^0\pi^+n(p)$	865	0.13±0.04	0.018±0.006	———	0.13±0.04	0.15±0.05
	970	0.35±0.05	0.021±0.007	———	0.36±0.05	0.45±0.07
	1210	1.31±0.12	0.022±0.007	———	1.34±0.12	1.40±0.15
	1365	1.12±0.15	0.020±0.007	———	1.14±0.15	1.25±0.20
$K^+d \rightarrow K^+\pi^-p(p)$	865	0.46±0.05	0.018±0.006	0.03±0.13	0.48±0.08	0.52±0.09
	970	0.91±0.05	0.021±0.007	0.02±0.07	0.95±0.08	1.16±0.12
	1210	2.89±0.12	0.022±0.007	0.02±0.04	3.01±0.16	3.09±0.22
	1365	3.21±0.20	0.020±0.007	0.02±0.05	3.34±0.26	3.60±0.39
$K^+d \rightarrow K^0\pi^0p(p)$	865	0.48±0.08	0.018±0.006	0.02±0.23	0.50±0.14	0.55±0.11
	970	0.82±0.08	0.021±0.007	0.03±0.13	0.86±0.14	1.05±0.14
	1210	2.09±0.13	0.022±0.007	0.02±0.08	2.18±0.21	2.24±0.19
	1365	2.06±0.19	0.020±0.007	0.02±0.11	2.14±0.30	2.31±0.30

Table VII. $K^+d \rightarrow K^0pp$ total cross sections.

P_K (GeV/c)	σ (mb)	Reference
0.230	$1.0^{+0.4}_{-0.3}$	W. Slater, et al., Phys. Rev. Letters 7, 378 (1961)
0.330	2.7 ±0.4	
0.377	3.1 ±0.4	
0.530	6.5 ±0.6	
0.642	6.7 ±0.6	
0.812	6.6 ±0.7	
0.865	6.72±0.40	This experiment
0.970	6.26±0.29	
1.210	4.99±0.24	
1.365	3.69±0.29	
1.585	2.65±0.22	V. H. Seeger (thesis, unpublished)
2.260	1.50±0.15	I. Butterworth et al., Phys. Rev. Letters 15, 734 (1965)
3.000	0.75±0.08	Y. Goldschmidt-Clermont et al., Physics Letters 27B, 602 (1968)
12.000	0.031±0.005	A. Firestone et al., Phys. Rev. Letters 25, 958 (1970)

Table VIII. Differential cross sections for $K^+d \rightarrow K^0p(p)$; t is the square of the momentum transfer from the incident K^+ to the outgoing K^0.

$-t(GeV/c)^2$		$\frac{d\sigma}{dt}$ [mb/(GeV/c)^2]			
From	To	865 MeV/c	970 MeV/c	1210 MeV/c	1365 MeV/c
0.00	0.05	4.6±1.1	4.3±0.8	2.7±0.6	3.1±0.6
0.05	0.10	9.3±1.6	6.2±0.9	5.7±0.9	
0.10	0.15	11.5±1.7	7.8±1.0	6.7±1.0	3.8±0.7
0.15	0.20	10.6±1.7	10.3±1.2	6.5±0.9	
0.20	0.25	9.3±1.5	10.4±1.2	6.0±0.9	4.5±0.8
0.25	0.30	9.4±1.6	9.2±1.1	5.5±0.8	
0.30	0.35	11.8±1.8	7.6±1.0	6.3±0.9	4.0±0.7
0.35	0.40	8.6±1.5	6.6±0.9	6.1±0.9	
0.40	0.45	8.0±1.4	6.6±0.9	5.2±0.8	3.9±0.7
0.45	0.50	8.1±1.4	6.3±0.9	3.6±0.7	
0.50	0.55	8.7±1.5	5.3±0.8	5.0±0.8	2.9±0.6
0.55	0.60	6.1±1.2	5.6±0.9	4.6±0.8	
0.60	0.65	4.6±1.1	5.2±0.8	2.8±0.6	1.8±0.5
0.65	0.70	6.1±1.2	4.5±0.8	3.6±0.7	
0.70	0.75	6.4±1.3	4.4±0.8	3.2±0.6	2.0±0.5
0.75	0.80	3.5±0.9	5.1±0.8	3.1±0.6	
0.80	0.85	3.2±0.9	4.4±0.8	2.7±0.6	1.4±0.4
0.85	0.90	1.8±0.7	4.5±0.8	2.3±0.5	
0.90	0.95	1.3±0.6	2.8±0.6	2.6±0.6	1.2±0.4
0.95	1.00	1.2±0.6	3.0±0.6	2.4±0.5	
1.00	1.05	0.12±0.09	2.0±0.5	1.9±0.5	1.4±0.4
1.05	1.10		1.0±0.4	1.2±0.4	
1.10	1.15		0.64±0.29	1.3±0.4	1.8±0.5
1.15	1.20		0.51±0.25	1.6±0.4	
1.20	1.25		0.25±0.18	1.1±0.4	1.8±0.5
1.25	1.30		0.39±0.22	1.3±0.4	
1.30	1.35		0.14±0.10	1.2±0.4	
1.35	1.40			0.95±0.34	0.83±0.23
1.40	1.50			0.49±0.17	
1.50	1.60			0.30±0.14	0.64±0.20
1.60	1.70			0.05±0.02	
1.70	2.20				0.08±0.04
2.20	2.30				

Table IX. Input parameters to the Regge model of Rarita and Schwarzschild (Reference 43).

	Trajectories		KN residue parameters			
	α^0	α^1	C^0 (mb-GeV)	D^0 (mb)	C^1 (GeV^{-2})	D^1 (GeV^{-2})
ρ	0.58	0.92	1.30	22.7	2.92	0.26
ρ'	-0.48	1.44	5.02	-264.0 -135.0[a]	4.4	2.95 2.30[a]
A_2	0.37	0.41	5.50	-116.0	0.42	0.66

[a]Values used for predictions for data of this experiment.

Table X. Differential cross section for the reaction $K^+d \rightarrow K^0p(p)$.

Cos θ		$\frac{d\sigma}{d\Omega}$ (mb/sr)			
From	To	865 MeV/c	970 MeV/c	1210 MeV/c	1365 MeV/c
-1.0	-0.9	0.20±0.06	0.27±0.06	0.11±0.03	0.04±0.03
-0.9	-0.8	0.42±0.09	0.35±0.06	0.15±0.04	0.09±0.04
-0.8	-0.7	0.37±0.09	0.37±0.06	0.20±0.04	0.21±0.06
-0.7	-0.6	0.37±0.09	0.38±0.06	0.21±0.04	0.17±0.06
-0.6	-0.5	0.54±0.10	0.34±0.06	0.20±0.04	0.21±0.06
-0.5	-0.4	0.48±0.10	0.44±0.07	0.30±0.06	0.23±0.07
-0.4	-0.3	0.40±0.09	0.51±0.07	0.27±0.05	0.28±0.07
-0.3	-0.2	0.50±0.10	0.39±0.06	0.21±0.05	0.17±0.06
-0.2	-0.1	0.69±0.12	0.36±0.06	0.33±0.06	0.23±0.07
-0.1	0.0	0.52±0.12	0.37±0.06	0.35±0.06	0.19±0.06
0.0	0.1	0.57±0.11	0.63±0.08	0.46±0.07	0.20±0.06
0.1	0.2	0.65±0.11	0.52±0.07	0.38±0.06	0.18±0.06
0.2	0.3	0.57±0.11	0.63±0.08	0.47±0.07	0.22±0.06
0.3	0.4	0.93±0.14	0.51±0.07	0.54±0.08	0.41±0.09
0.4	0.5	0.59±0.11	0.63±0.08	0.64±0.08	0.57±0.11
0.5	0.6	0.57±0.11	0.97±0.10	0.67±0.08	0.69±0.12
0.6	0.7	0.86±0.13	0.72±0.09	0.66±0.08	0.32±0.08
0.7	0.8	0.55±0.11	0.64±0.08	0.74±0.09	0.65±0.12
0.8	0.9	0.72±0.12	0.54±0.08	0.66±0.09	0.54±0.11
0.9	1.0	0.21±0.06	0.38±0.06	0.39±0.06	0.31±0.08

Table XI. Coefficients A_n from the least-squares fit of the differential cross sections to the series $(d\sigma/d\Omega)_n = \frac{\lambda^2}{4} \sum_{n=0}^{n_{max}} A_n P_n(\cos\theta)$.

Momentum (MeV/c)	$\frac{\lambda^2}{4}$ (mb)	n_{max}	A_0	A_1	A_2	A_3	A_4	A_5	A_6	χ^2	Expected χ^2	CL (%)
865	0.4440	3	1.18±0.05	0.34±0.08	-0.49±0.10	-0.22±0.12				25.0	16	7.0
		[4]	1.20±0.05	0.36±0.08	-0.41±0.11	-0.27±0.12	-0.37±0.15			18.9	15	21.8
		5	1.20±0.05	0.36±0.09	-0.41±0.11	-0.26±0.13	-0.38±0.15	-0.07±0.18		18.7	14	17.5
		6	1.21±0.05	0.37±0.09	-0.39±0.11	-0.25±0.13	-0.36±0.15	-0.14±0.18	-0.36±0.21	15.8	13	26.0
970	0.3733	3	1.33±0.04	0.54±0.08	-0.08±0.10	-0.26±0.12				32.5	16	0.9
		[4]	1.34±0.04	0.56±0.08	-0.10±0.10	-0.33±0.12	-0.44±0.13			21.3	15	12.8
		5	1.34±0.04	0.56±0.08	-0.10±0.10	-0.34±0.12	-0.45±0.13	-0.05±0.15		21.2	14	9.7
		6	1.34±0.04	0.56±0.08	-0.10±0.10	-0.34±0.12	-0.44±0.14	-0.04±0.15	0.09±0.17	20.9	13	7.5
1210	0.2698	3	1.47±0.05	1.13±0.09	-0.08±0.11	-0.26±0.12				20.3	16	20.5
		[4]	1.48±0.05	1.17±0.09	-0.05±0.11	-0.47±0.14	-0.50±0.14			8.0	15	92.4
		5	1.49±0.05	1.18±0.09	-0.04±0.11	-0.46±0.14	-0.57±0.16	-0.17±0.17		7.0	14	93.5
		6	1.49±0.05	1.18±0.09	-0.03±0.12	-0.46±0.14	-0.58±0.16	-0.22±0.19	-0.14±0.20	6.5	13	92.4
1365	0.2286	3	1.21±0.08	0.98±0.15	0.22±0.16	0.30±0.18				33.2	15	0.4
		4	1.32±0.08	1.10±0.16	0.23±0.16	-0.18±0.22	-0.88±0.24			19.1	14	16.3
		[5]	1.39±0.09	1.23±0.16	0.22±0.16	-0.32±0.22	-1.27±0.28	-0.66±0.26		12.4	13	49.7
		6	1.39±0.09	1.23±0.16	0.21±0.16	-0.32±0.22	-1.27±0.28	-0.65±0.29	0.02±0.29	12.4	12	41.7

Table XII. Forward and backward differential cross sections for $K^+n \rightarrow K^0p$.

P_K (MeV/c)	$\left(\frac{d\sigma}{d\Omega}\right)^{a}_{\theta=0°}$ (mb/sr)	$\left(\frac{d\sigma}{d\Omega}\right)^{b}_{\theta=0°}$ (mb/sr)	$\left\{\left(\frac{k}{4\pi}\right)\left[\sigma^{tot}_{K^+p} - \sigma^{tot}_{K^+n}\right]\right\}^2$ (mb/sr)	$\left(\frac{d\sigma}{d\Omega}\right)^{b}_{\theta=180°}$ (mb/sr)
865	0.11	0.22±0.10	0.031±0.016	0.14±0.08
970	0.12	0.38±0.09	0.026±0.012	0.21±0.07
1210	0.14	0.44±0.08	0.026±0.007	0.06±0.04
1365	0.15	0.13±0.14	0.007±0.004	0.02±0.05

[a]From Regge model predictions described in text.

[b]From Legendre polynomial fits.

Table XIII(a). Results of fits to the single-pion production Dalitz plots at 865 and 970 MeV/c. The errors quoted are statistical only.

Momentum (MeV/c)	Reaction	No. of events[a]	Model[b]	χ^2/dof	d	A_Δ	A_{K^*}	%KΔ	% K^*N	%K^*-Δ interference	% Bkgd.	φ (deg)
865	$K^+d \to K^0\pi^+p(n)$	61	NI	12.9/8	--	--	--	69±23	--	--	31±23	--
	$K^+d \to K^0\pi^+n(p)$	15	NI	2.1/5	--	--	--	28±65	--	--	72±65	--
	$K^+d \to K^+\pi^-p(p)$	99	NI	11.8/8	--	--	--	10±22	--	--	90±22	--
	$K^+d \to K^0\pi^0p(p)$	28	NI	6.3/7	--	--	--	12±39	--	--	88±39	--
970	$K^+d \to K^0\pi^+p(n)$	258	NI	17.9/10	--	--	--	84±8	--	--	16±8	--
	$K^+d \to K^0\pi^+n(p)$	71	NI	12.2/10	--	--	--	23±20	--	--	77±20	--
	$K^+d \to K^+\pi^-p(p)$	370	NI	18.4/11	--	--	--	25±9	--	--	75±9	--
	$K^+d \to K^0\pi^0p(p)$	105	NI	25.8/11	--	--	--	46±14	--	--	54±14	--

[a] We limit ourselves to events with spectator momentum less than 150 MeV/c.

[b] NI — non-interference model.

Table XIII(b). Results of fits to the single-pion production Dalitz plots at 1210 MeV/c. The errors quoted are statistical only.

Momentum (MeV/c)	Reaction	No. of events[a]	Model[b]	χ^2/dof	d	A_Δ	A_{K^*}	% KΔ	% K^*N	% K^* - Δ interference	% Bkgd.	φ (deg)
1210	$K^+d \to K^0\pi^+p(n)$	666	NI	62/29	--	-0.53±0.11	$0.39^{+0.75}_{-0.50}$	78±4	28±4	--	-6±4	--
			NIC	62/30	--	-0.53±0.12	0.34±0.58	77	29±3	--	-6±3	--
			EI	34/27	0.57±0.17	-0.71±0.12	$-0.04^{+0.75}_{-0.46}$	72±5	20±3	4±7	4±4	45±13
			EIC	34/28	0.63±0.16	-0.70±0.13	$0.00^{+0.72}_{-0.49}$	68	19±3	7±5	6±4	37±9
	$K^+d \to K^0\pi^+n(p)$	181	NI	5.8/9	--	$-0.2^{+0.7}_{-0.5}$	$0.0^{+1.0}_{-0.6}$	40±18	57±8	--	3±19	--
			NIC	6.0/10	--	$-0.2^{+0.9}_{-0.5}$	$-0.2^{+0.7}_{-0.5}$	31	57±8	--	12±8	--
			EI	4.0/7	$0.7^{+1.6}_{-0.5}$	$0.4^{+2.1}_{-1.3}$	$0.1^{+1.5}_{-0.8}$	19±11	46±7	18±10	17±20	-22±22
			EIC	4.1/8	0.5±0.4	$0.3^{+1.4}_{-0.8}$	$0.2^{+1.1}_{-0.7}$	27	48±7	16±4	9±10	-27±22
	$K^+d \to K^+\pi^-p(p)$	1311	NI	115/26	--	-0.41±0.20	1.09±0.32	25±4	65±2	--	10±4	--
			NIC	123/27	--	-0.51±0.34	0.83±0.26	14	66±2	--	20±2	--
			EI	38/24	1.00±0.12	-0.67±0.24	1.24±0.48	16±2	49±3	15±4	20±4	25±6
			EIC	41/25	1.00±0.04	-0.71±0.26	1.06±0.39	12	52±2	13±4	23±4	25±7
	$K^+d \to K^0\pi^0p(p)$	294	NI	19.8/13	--	-0.8±0.2	$1.4^{+1.4}_{-0.8}$	56±11	53±5	--	-9±11	--
			NIC	21.3/14	--	-0.9±0.3	$0.9^{+0.9}_{-0.6}$	39	55±5	--	6±5	--
			EI	7.2/11	0.6±0.4	-1.0±0.2	$1.2^{+1.7}_{-1.0}$	43±10	40±5	8±13	9±9	42±20
			EIC	7.6/12	0.8±0.3	-1.0±0.2	$1.2^{+1.6}_{-0.9}$	34	37±4	13±10	16±10	31±15

[a] We limit ourselves to events with spectator momentum less than 150 MeV/c.

[b] NI – non-interference model
NIC – non-interference model with amount of Δ constrained
EI – empirical-interference model
EIC – empirical-interference model with amount of Δ constrained.

Table XIII(c). Results of fits to the single-pion production Dalitz plots at 1365 MeV/c. The errors quoted are statistical only.

Momentum (MeV/c)	Reaction	No. of events[a]	Model[b]	χ^2/dof	d	A_Δ	A_{K^*}	%KΔ	%K^*N	% K^* - Δ interference	% Bkgd.	φ (deg)
1365	$K^+d \to K^0\pi^+p(n)$	310	NI	32/21	--	-0.86 ± 0.14	$3.0^{+4.0}_{-1.6}$	69±7	30±5	--	1±7	--
			NIC	32/22	--	-0.88 ± 0.15	$2.8^{+3.3}_{-1.5}$	66	30±4	--	4±4	--
			EI	14/19	1.00 ± 0.35	-0.78 ± 0.23	$5.6^{+10.0}_{-3.3}$	51±6	20±4	19±7	10±10	5±10
			EIC	15/20	0.86 ± 0.24	-0.77 ± 0.22	$6.2^{+10.1}_{-3.4}$	57	20±3	17±7	6±9	4±12
	$K^+d \to K^0\pi^+n(p)$	74	NI	2.9/4	--	$0.8^{+7.6}_{-1.8}$	$-0.2^{+1.1}_{-0.7}$	42±30	64±12	--	-6±36	--
			NIC	3.0/5	--	$0.9^{+4.7}_{-1.8}$	$-0.2^{+1.1}_{-0.7}$	31	63±12	--	6±12	--
			EI	1.6/2	0.5 ± 0.3	-0.3 ± 1.3	-0.9 ± 0.9	56±32	72±15	-24±14	-4±26	136±27
			EIC	2.3/3	0.4 ± 0.4	-0.2 ± 3.8	-0.6 ± 0.9	27	64±14	-11±5	20±11	127±51
	$K^+d \to K^+\pi^-p(p)$	744	NI	50/26	--	$0.1^{+1.3}_{-0.6}$	0.9 ± 0.3	12±5	70±3	--	18±5	--
			NIC	50/27	--	$0.1^{+1.2}_{-0.6}$	0.9 ± 0.3	11	70±3	--	19±3	--
			EI	37/24	1.0 ± 0.4	-0.6 ± 1.2	0.9 ± 0.4	5±2	60±4	8±5	27±5	35±12
			EIC	38/25	0.7 ± 0.2	$-0.5^{+0.9}_{-0.5}$	0.9 ± 0.4	9	61±3	6±5	24±5	39±14
	$K^+d \to K^0\pi^0p(p)$	148	NI	11.9/8	--	-1.00 ± 0.14	$2.6^{+33.0}_{-2.4}$	47±13	31±8	--	22±16	--
			NI	12.6/9	--	-1.00 ± 0.15	$1.5^{+6.3}_{-1.6}$	34	32±8	--	34±8	--
			EI	10.6/6	$0.4^{+0.7}_{-0.3}$	-1.00 ± 0.14	$1.6^{+13.2}_{-2.0}$	38±13	27±7	4±16	31±18	51±56
			EIC	10.9/7	0.5 ± 0.4	-1.00 ± 0.16	$1.4^{+8.1}_{-2.0}$	29	25±7	6±14	40±16	42±41

[a] We limit ourselves to events with spectator momentum less than 150 MeV/c.

[b] NI – non-interference model
NIC – non-interference model with amount of Δ constrained
EI – empirical-interference model
EIC – empirical-interference model with amount of Δ constrained.

Table XIV. Resonance production cross sections for the single-pion production reactions. The errors quoted are $\sqrt{2}$ times the statistical error at 865 and 970 MeV/c and twice the statistical error at 1210 and 1365 MeV/c.

							Δ - constrained			
Momentum (MeV/c)	Reaction	$\sigma(KN \to K\pi N)$[a] (mb)	$\sigma(K\Delta)$	$\sigma(K^*N)$ (mb)	$\sigma(K^* - \Delta$ int.) (mb)	σ(bkgd.) (mb)	"Input" $\sigma(K\Delta)$ (mb)	$\sigma(K^*N)$ (mb)	$\sigma(K^* - \Delta$ int.) (mb)	σ(bkgd.) (mb)
865	$K^+p \to K^0\pi^+p$	1.12±0.20	0.77±0.41	--	--	0.35±0.37	--	--	--	--
	$K^+n \to K^0\pi^+n$	0.15±0.05	0.04±0.14	--	--	0.11±0.14	--	--	--	--
	$K^+n \to K^+\pi^-p$	0.52±0.09	0.05±0.17	--	--	0.47±0.20	--	--	--	--
	$K^+n \to K^0\pi^0p$	0.55±0.11	0.07±0.30	--	--	0.48±0.34	--	--	--	--
970	$K^+p \to K^0\pi^+p$	2.55±0.29	2.14±0.45	--	--	0.41±0.30	--	--	--	--
	$K^+n \to K^0\pi^+n$	0.45±0.07	0.11±0.13	--	--	0.35±0.16	--	--	--	--
	$K^+n \to K^+\pi^-p$	1.16±0.12	0.29±0.16	--	--	0.87±0.20	--	--	--	--
	$K^+n \to K^0\pi^0p$	1.05±0.14	0.48±0.23	--	--	0.57±0.23	--	--	--	--
1210	$K^+p \to K^0\pi^+p$	5.09±0.40	3.67±0.76	1.02±0.34	0.20±0.72	0.20±0.40	3.46	0.97±0.34	0.36±0.52	0.30±0.42
	$K^+n \to K^0\pi^+n$	1.40±0.15	0.27±0.32	0.64±0.24	0.25±0.28	0.24±0.56	0.38	0.67±0.24	0.22±0.12	0.13±0.28
	$K^+n \to K^+\pi^-p$	3.09±0.22	0.49±0.14	1.52±0.28	0.46±0.26	0.62±0.26	0.37	1.61±0.26	0.40±0.26	0.71±0.26
	$K^+n \to K^0\pi^0p$	2.24±0.19	0.96±0.48	0.89±0.28	0.18±0.58	0.21±0.40	0.76	0.83±0.22	0.29±0.46	0.36±0.46
1365	$K^+p \to K^0\pi^+p$	5.35±0.64	2.73±0.92	1.07±0.50	1.02±0.78	0.53±1.08	3.05	1.07±0.42	0.91±0.78	0.32±0.96
	$K^+n \to K^0\pi^+n$	1.25±0.20	0.70±0.84	0.90±0.48	-0.30±0.36	-0.05±0.66	0.34	0.80±0.44	-0.14±0.14	0.25±0.28
	$K^+n \to K^+\pi^-p$	3.60±0.39	0.18±0.16	2.16±0.56	0.29±0.36	0.97±0.42	0.33	2.19±0.52	0.22±0.36	0.86±0.40
	$K^+n \to K^0\pi^0p$	2.31±0.30	0.88±0.64	0.62±0.36	0.09±0.74	0.72±0.86	0.67	0.58±0.36	0.14±0.64	0.92±0.78

[a] $\sigma(KN \to K\pi N) = R_c\,\sigma[Kd \to K\pi N(N)]$ where $R_c = \sigma(K^+p \to K^0\pi^+p)/\sigma[K^+d \to K^0\pi^+p(n)]$. The errors are statistical only.

Table XV. Cross sections for the reaction $KN \rightarrow K^*N$ decaying into all decay modes. See text for references.

Momentum (GeV/c)	$\sigma(K^+p \rightarrow K^{*+}p)$ [a] (mb)	$\sigma(K^+n \rightarrow K^{*+}n)$ [b] (mb)	$\sigma(K^+n \rightarrow K^{*0}p)$ [c] (mb)
1.140	1.3 ±0.4		
1.210	1.6 ±0.2	1.0 ±0.4	2.4 ±0.4
1.365	2.6 ±0.4	1.2 ±0.7	3.3 ±0.8
1.585	3.2 ±0.5	1.4 ±0.4	4.8 ±0.6
1.960	1.8 ±0.3		
2.260	1.6 ±0.3		
2.300			2.1 ±0.3
2.650	2.2 ±0.4		
2.965	1.19±0.15		
2.970	1.39±0.16		
2.970	1.23±0.17	0.86±0.12	1.46±0.15
3.535	0.82±0.03		
4.6	0.54±0.06		
5.0	0.46±0.09		
8.25	0.20±0.04		
9.0	0.15±0.03		
10.0	0.13±0.03		
12.0			0.043±0.005
12.7	0.076±0.018		

[a] From Reference 42.

[b] We have used R(all K^{*+} charge states)/R($K^{*+} \rightarrow K^0\pi^+$) = 3/2.

[c] We have used R(all K^{*0} charge states)/R($K^{*0} \rightarrow K^+\pi^-$) = 3/2.

Table XVI. Isospin-0 and isospin-1 KN → K^*N cross sections from 1.0 to 3.0 GeV/c.

Momentum (GeV/c)	$\sigma_0^{tot}(K\pi N)$ (mb)	$\sigma_0(K^*N)$ (mb)	$\sigma_1^{tot}(K\pi N)$ (mb)	$\sigma_1(K^*N)$ (mb)
1.140				1.3 ±0.4
1.210	8.0±1.0[a] 8.0±0.9[b]	5.2±1.1[c] 6.0±1.1[d]	7.40±0.17	1.6 ±0.2
1.365	8.9±1.8[a] 10.1±1.7[b]	6.4±2.1[c] 8.6±2.2[d]		2.6 ±0.4
1.455			8.16±0.30	
1.585	11.7±1.9	7.5±1.4		3.2 ±0.5
1.960			7.4 ±0.5	1.8 ±0.3
2.260				1.6 ±0.3
2.300	10.3±1.4			
2.650				2.2 ±0.4
2.965				1.19±0.15
2.970			4.4 ±0.4	1.39±0.16
2.970	8.1±0.9	3.4±0.4		1.23±0.17

[a]Here we have used Eq. 16 to calculate $\sigma_0(K\pi N)$.

[b]Here we have used Eq. 62 to calculate $\sigma_0(K\pi N)$. See footnote 49.

[c]Here we have used the method of Eq. 63. Refer to the text for details.

[d]Here we have employed the normalization of Eq. 62 and have fitted the mass projection $d\sigma_0/dm_{K\pi}$ and quote errors that are $\sqrt{2}$ times the statistical error.

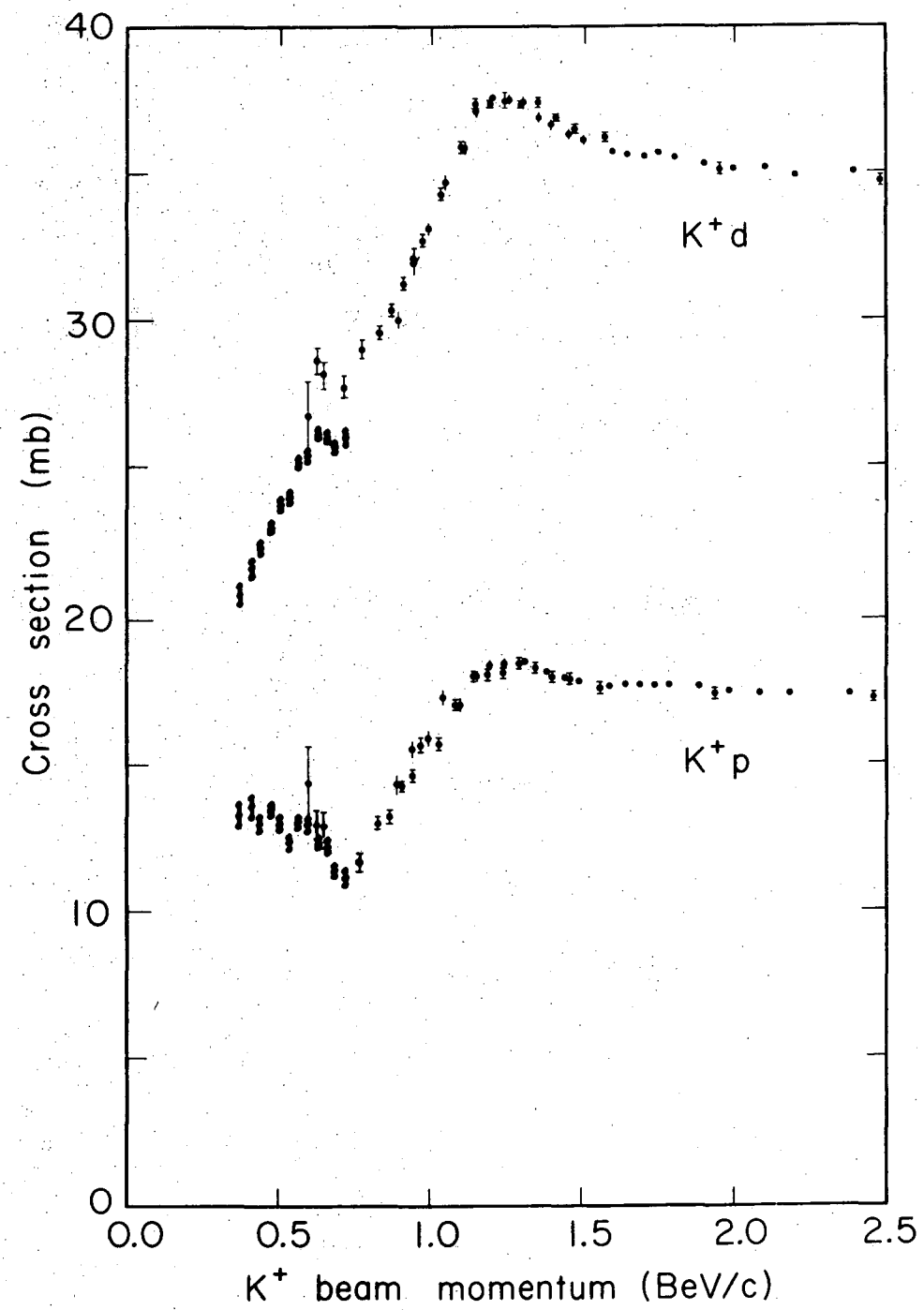

Fig. 1

XBL 6810-7090

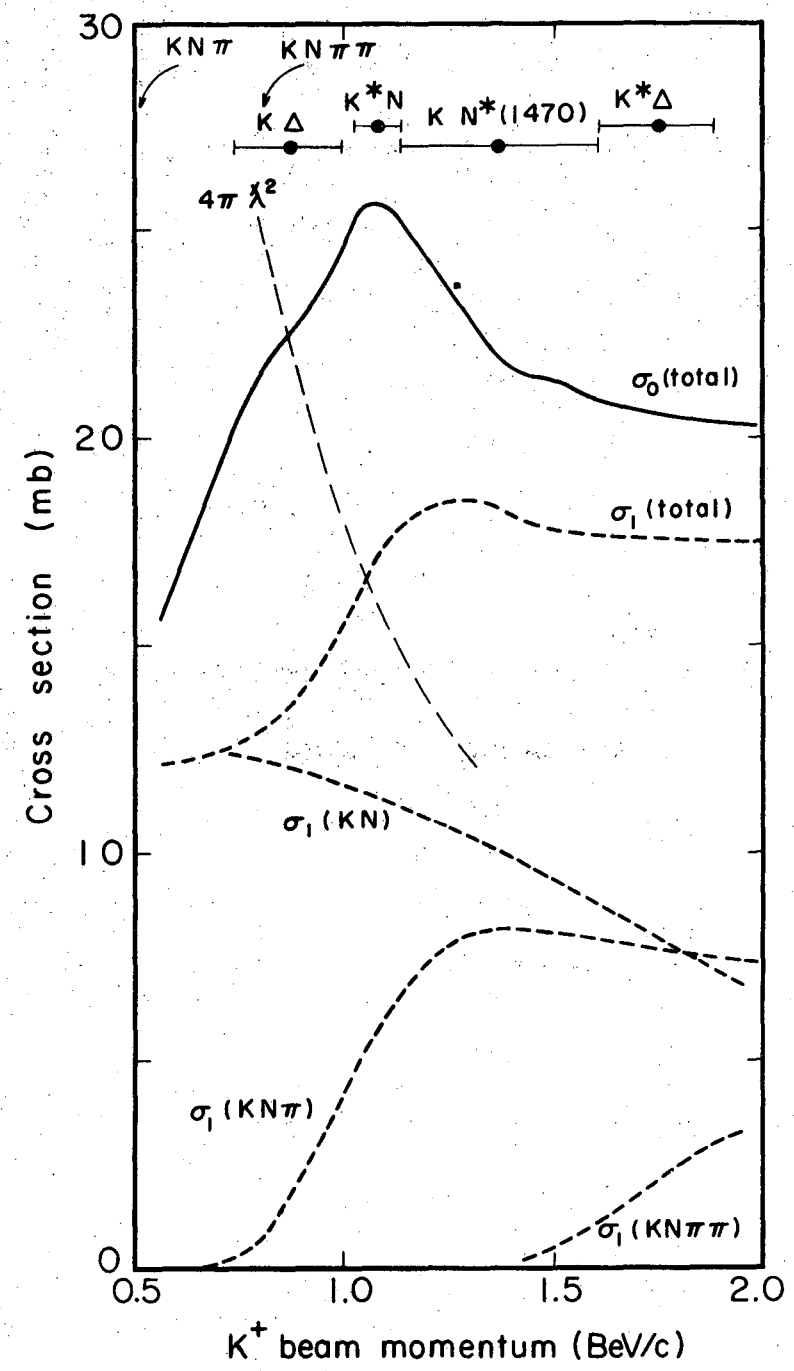

Fig. 2 XBL6810-7089

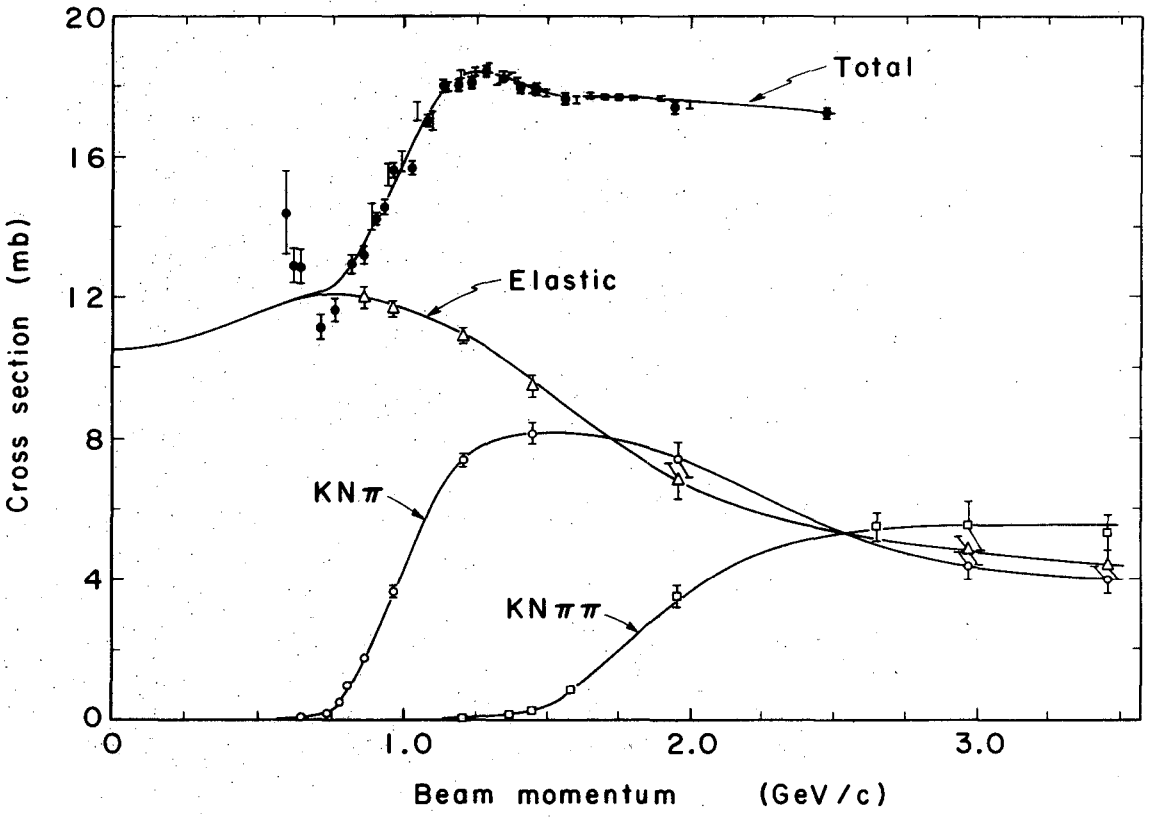

Fig. 3

XBL696-2973

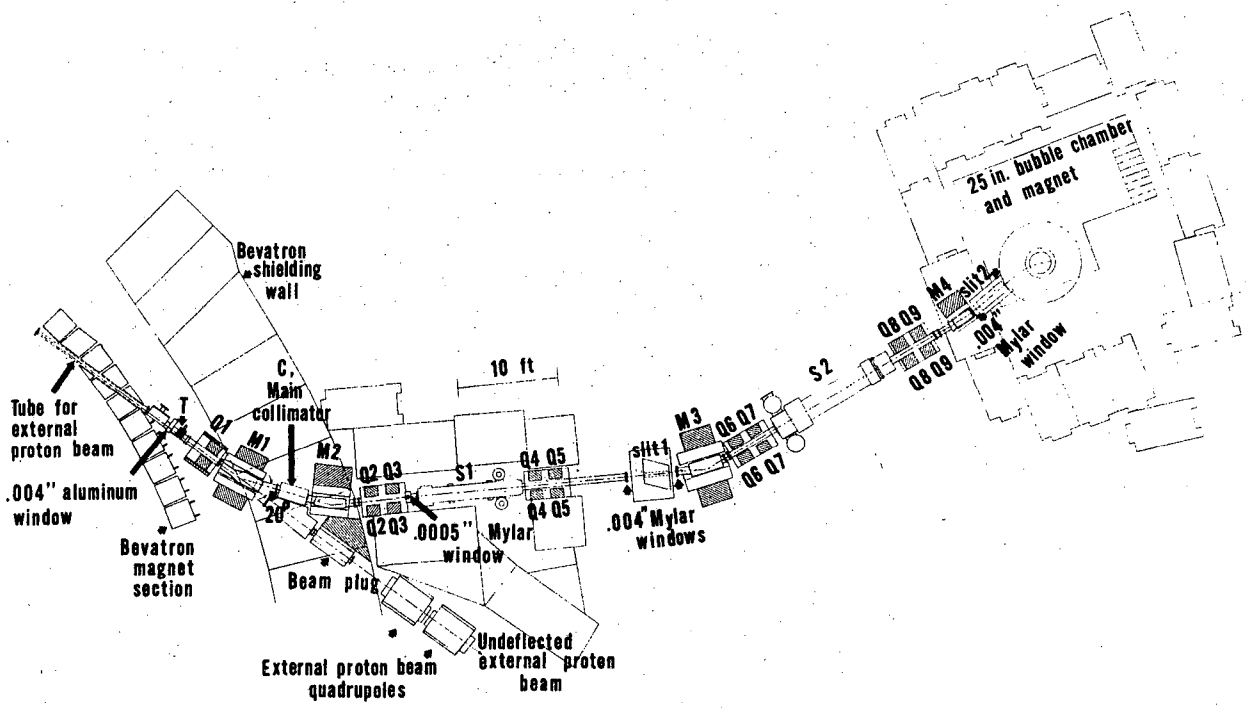

Fig. 4

MUB-3362

EVENT TOPOLOGIES

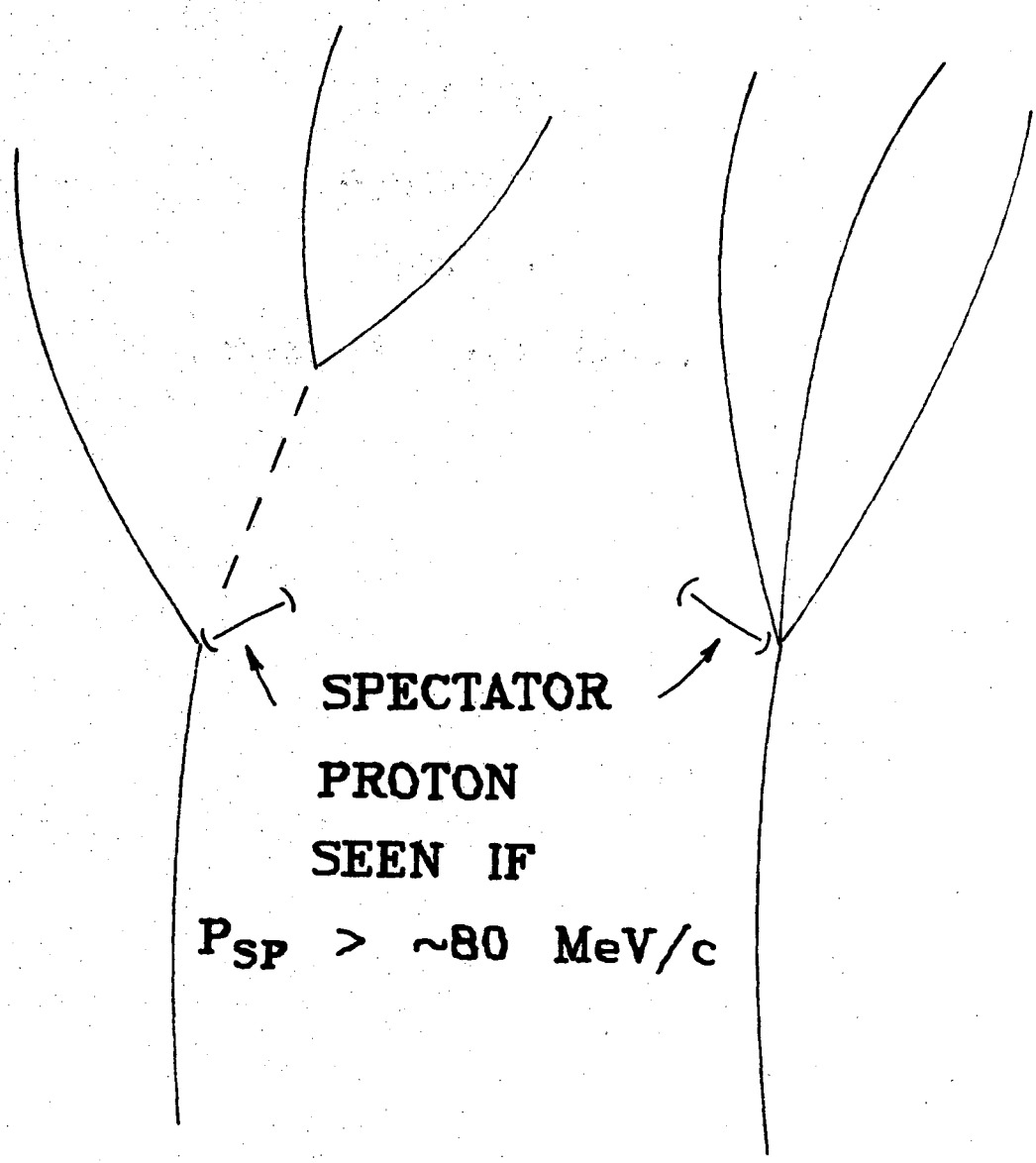

Fig. 5

XBL 708-1983

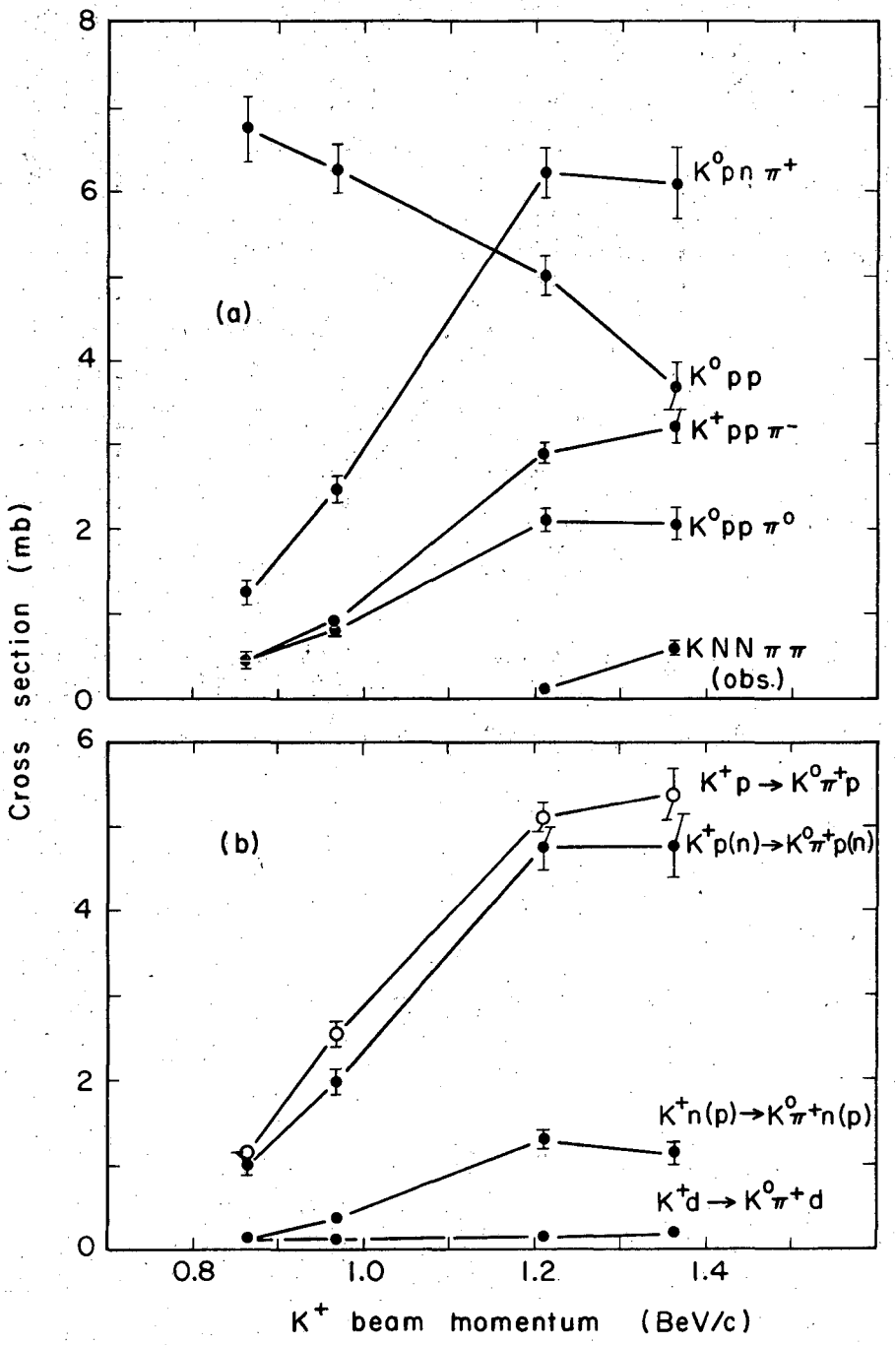

Fig. 6

XBL688-3494

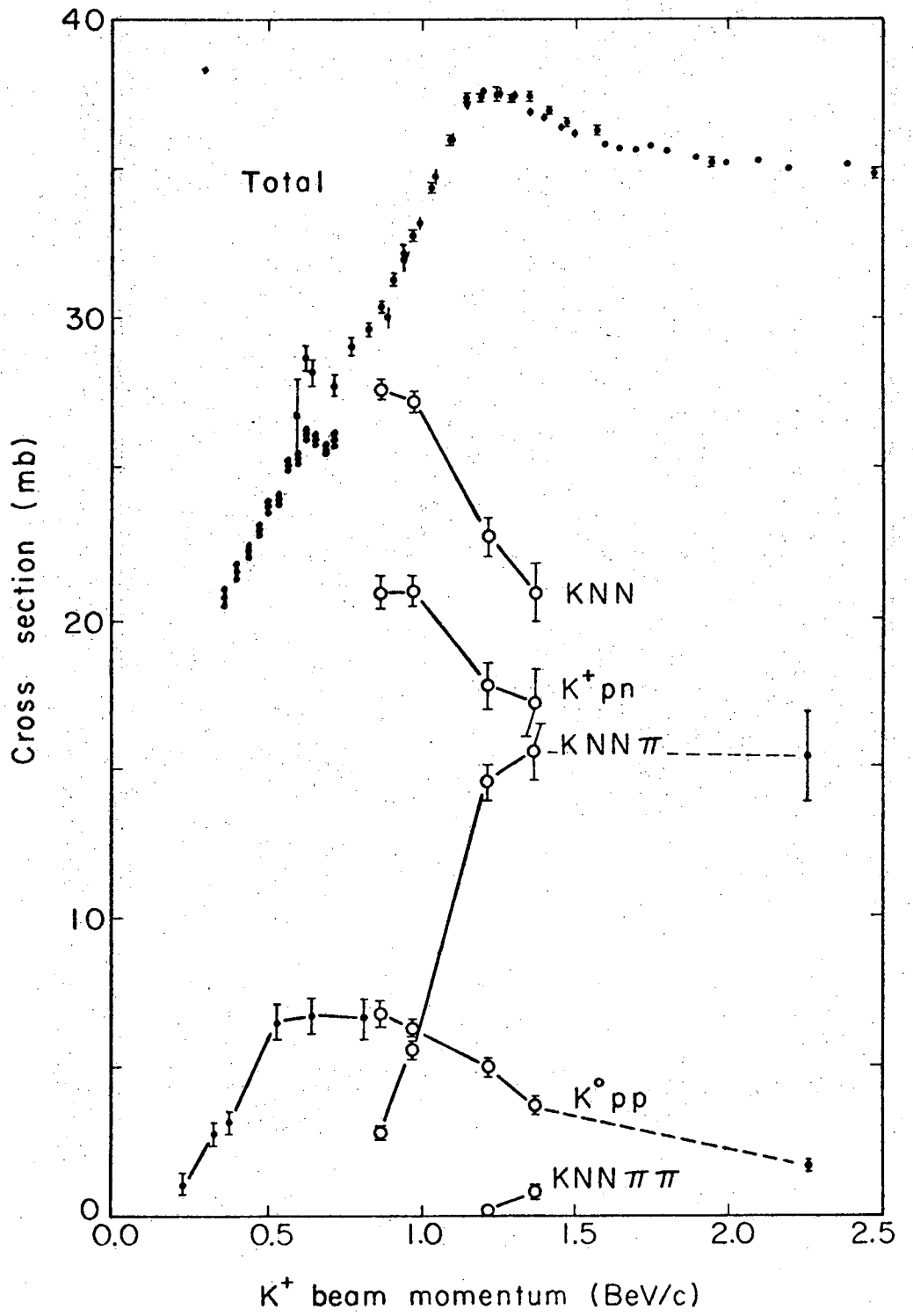

Fig. 7

XBL688-3495

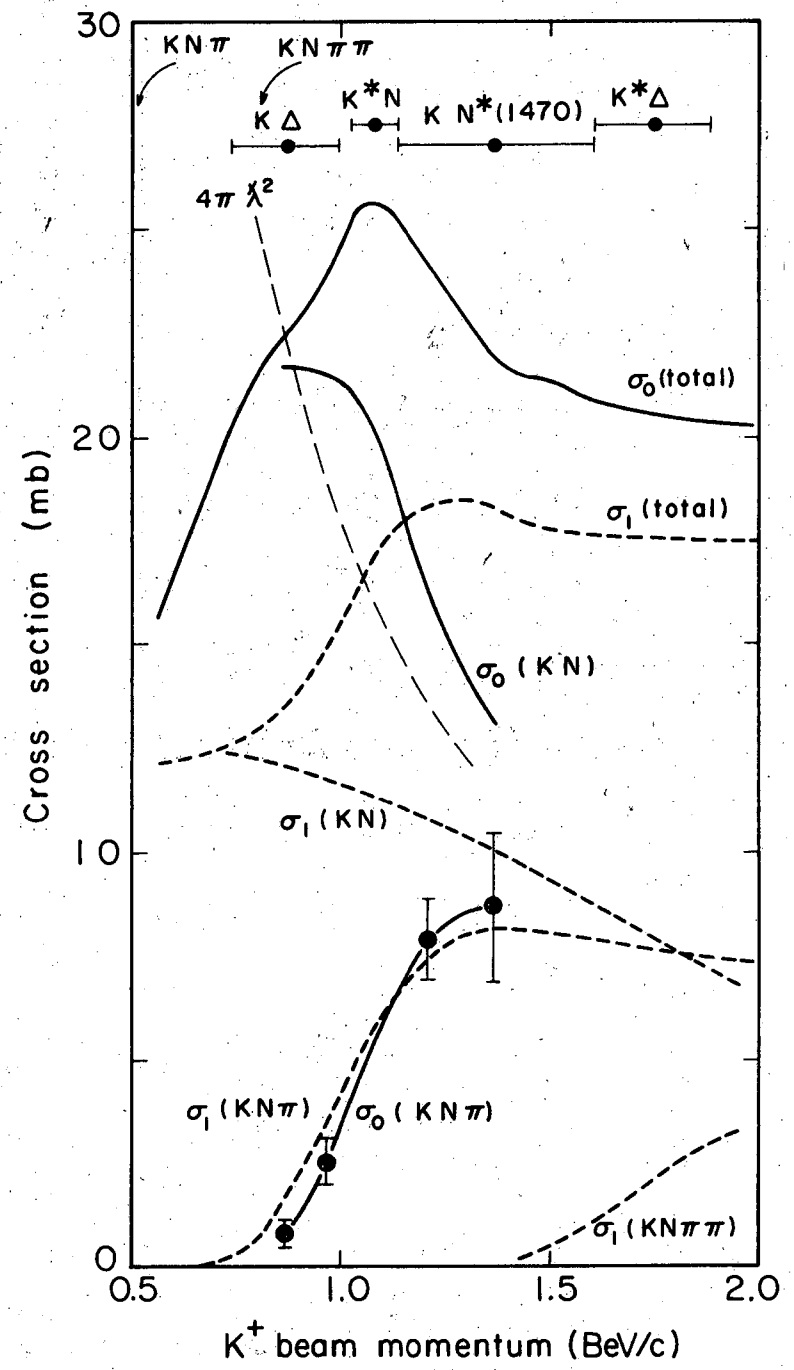

Fig. 8 XBL686-3493

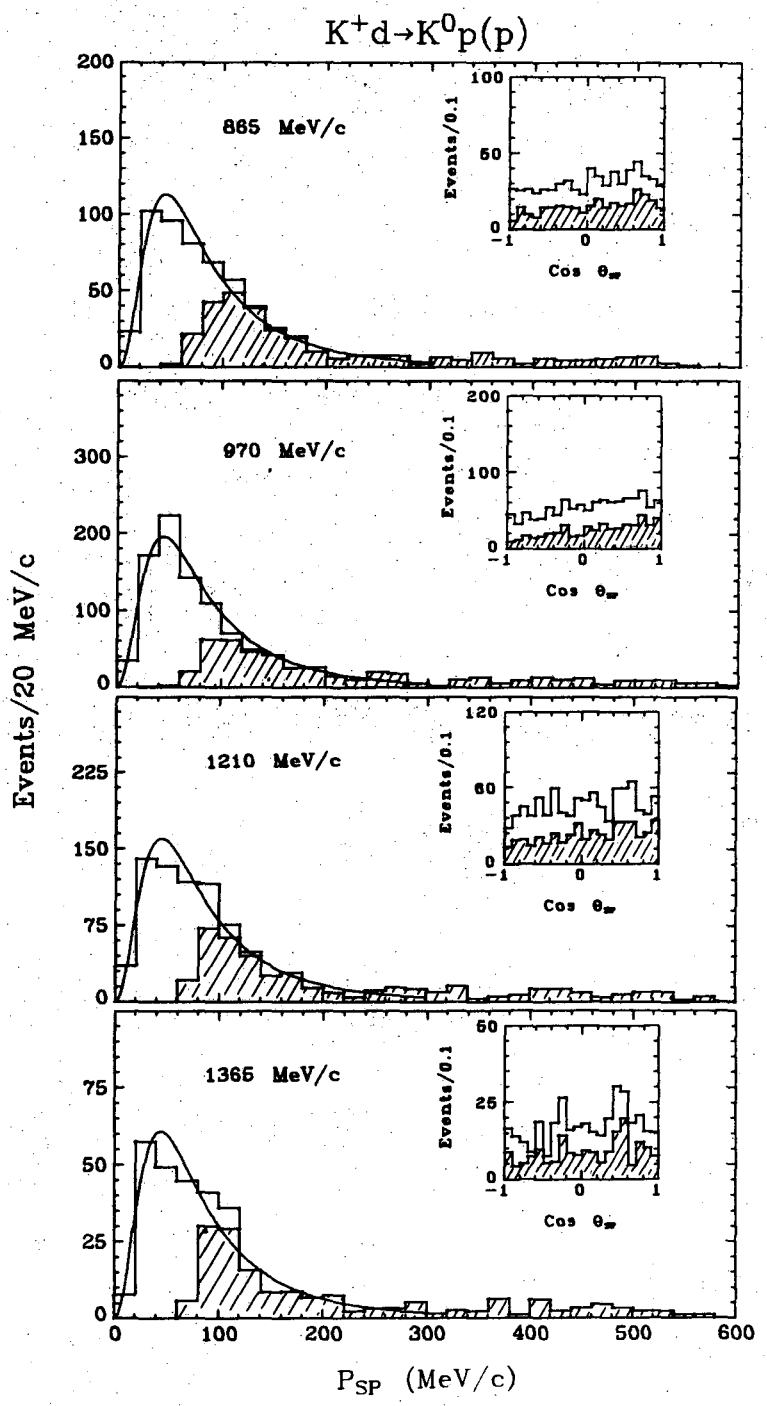

Fig. 9

XBL708-1989

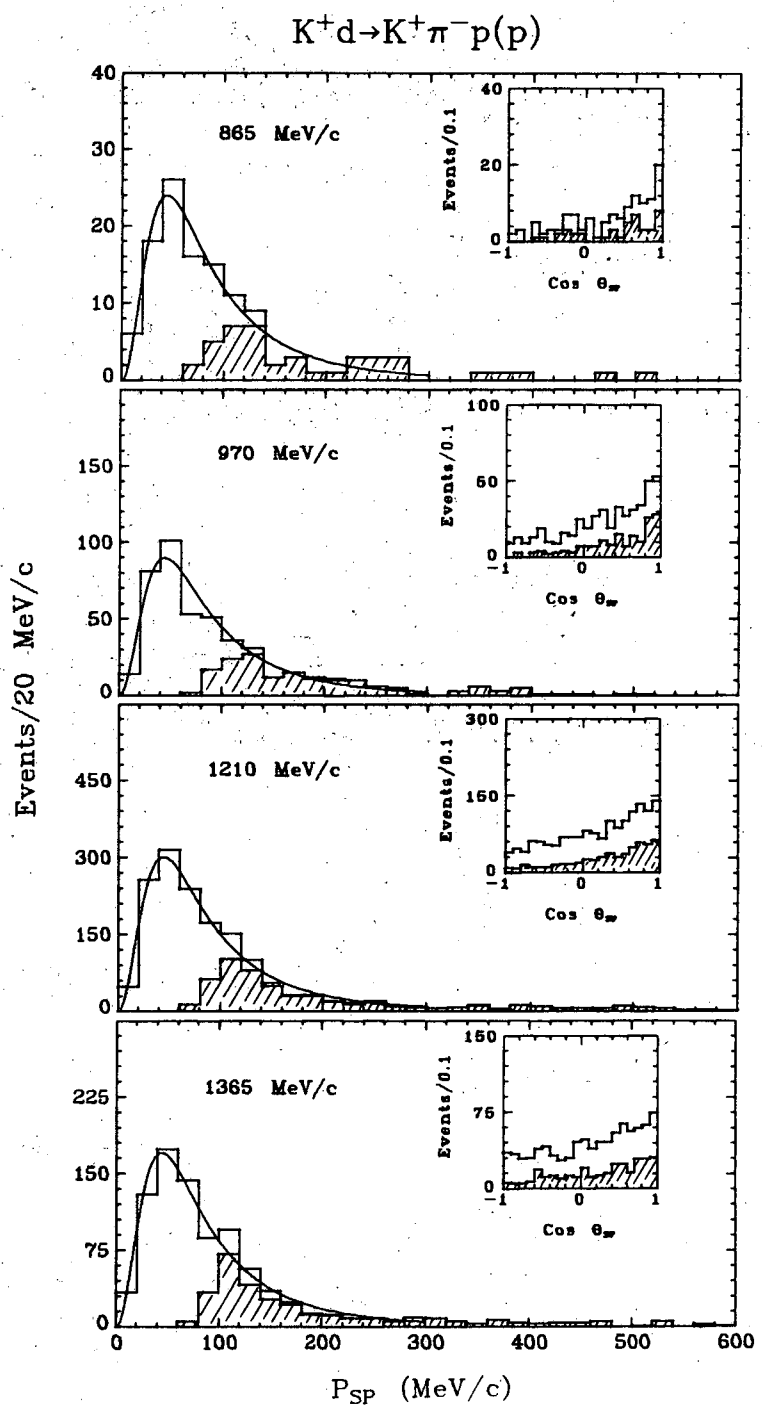

Fig. 10

XBL 708-1990

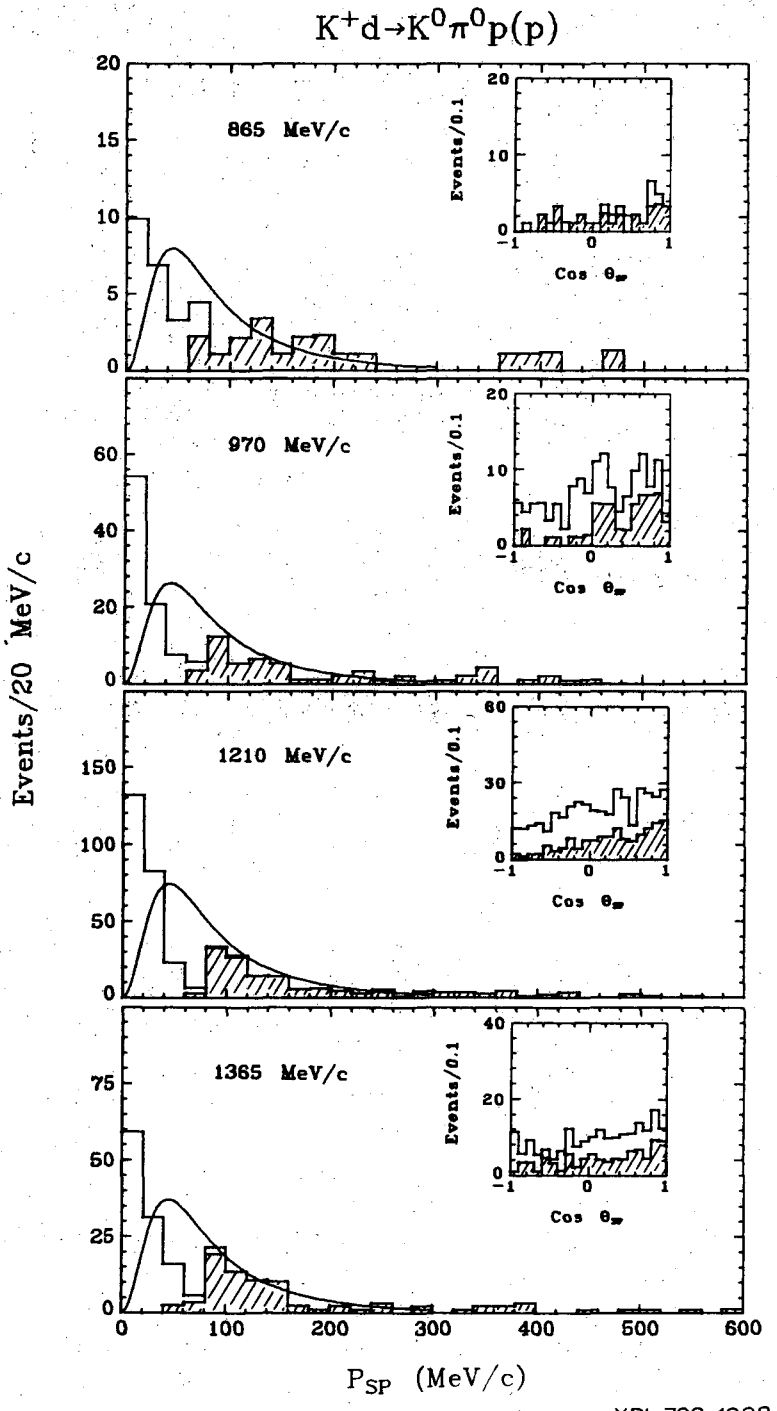

XBL 708-1988

Fig. 11

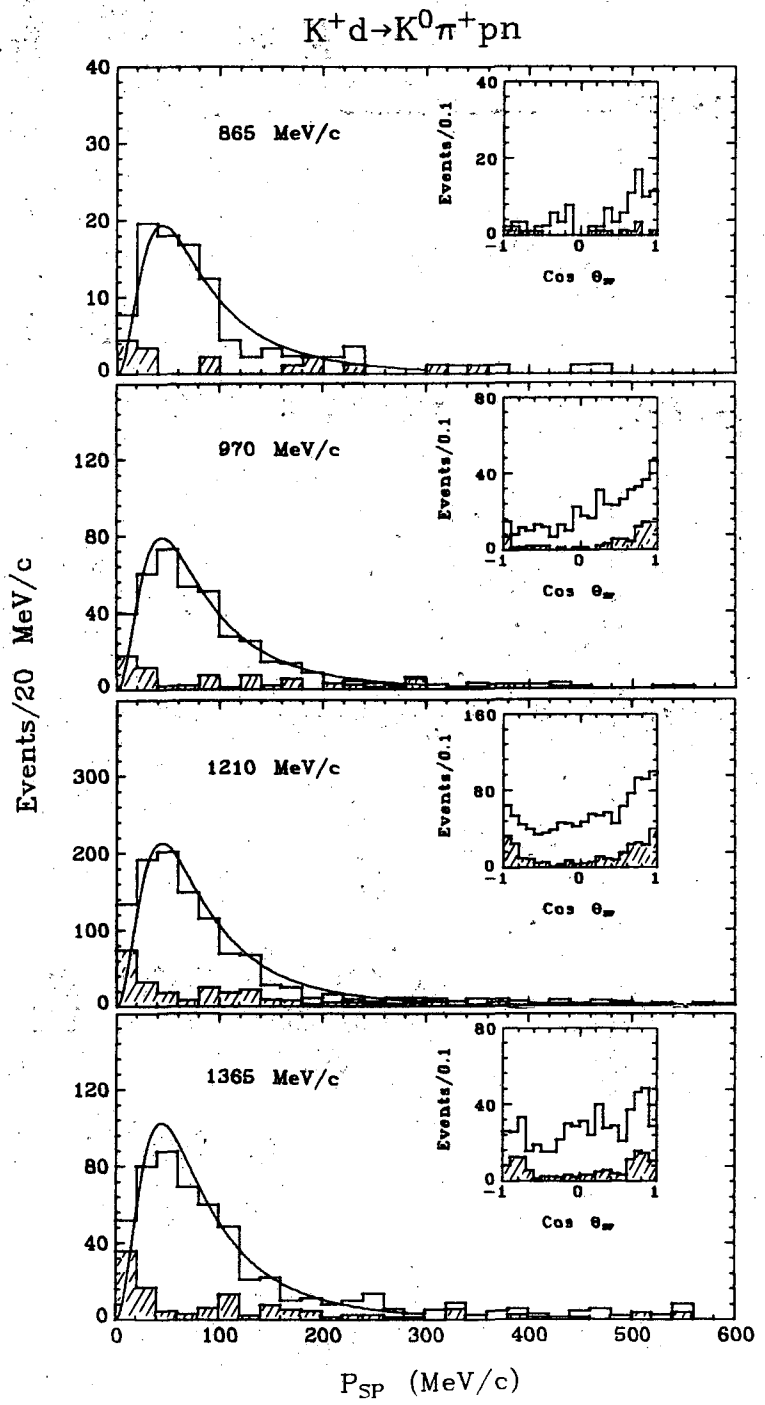

XBL 708-1991

Fig. 12

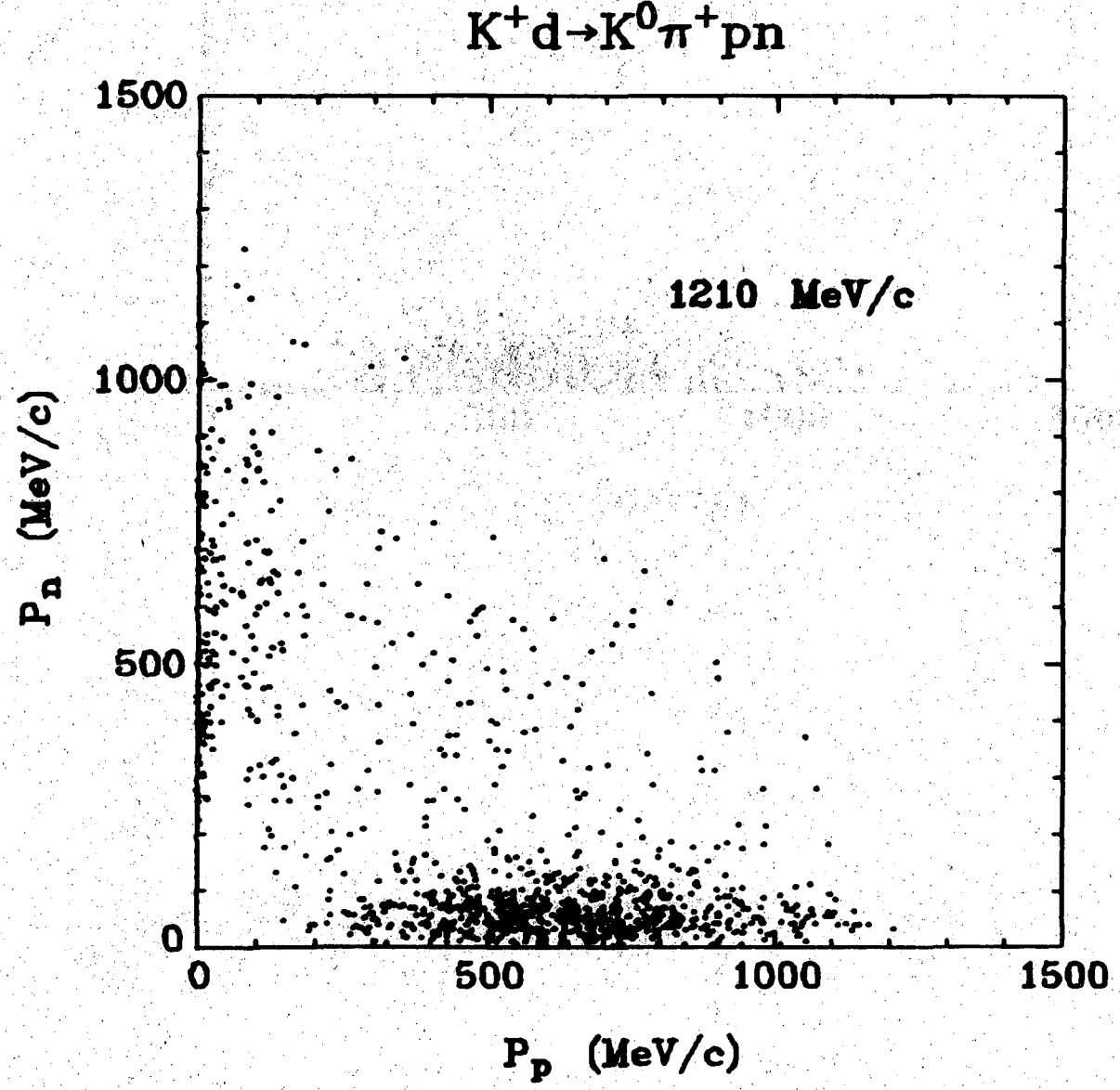

Fig. 13

XBL 708-1984

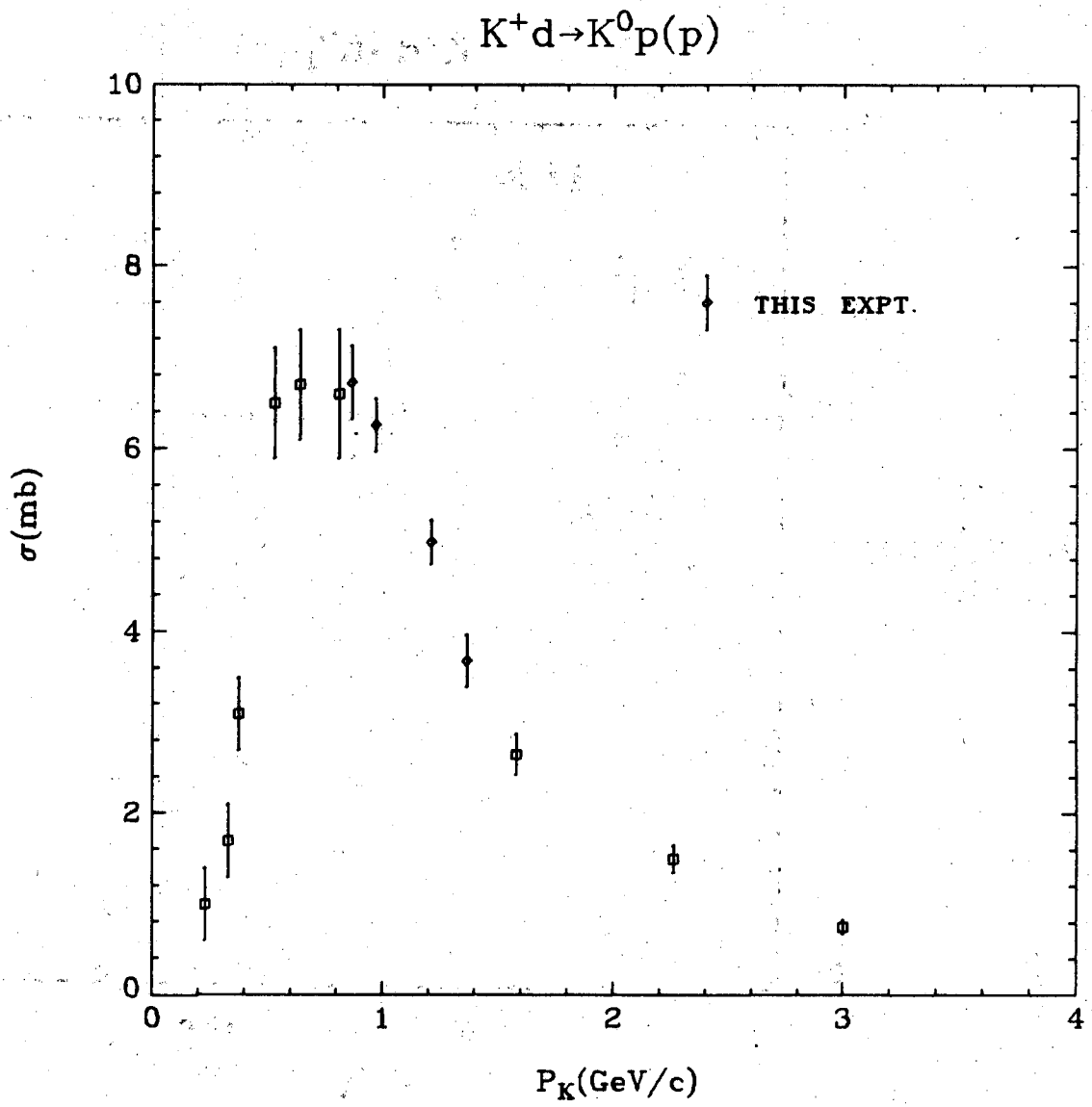

Fig. 14

XBL 708-1987

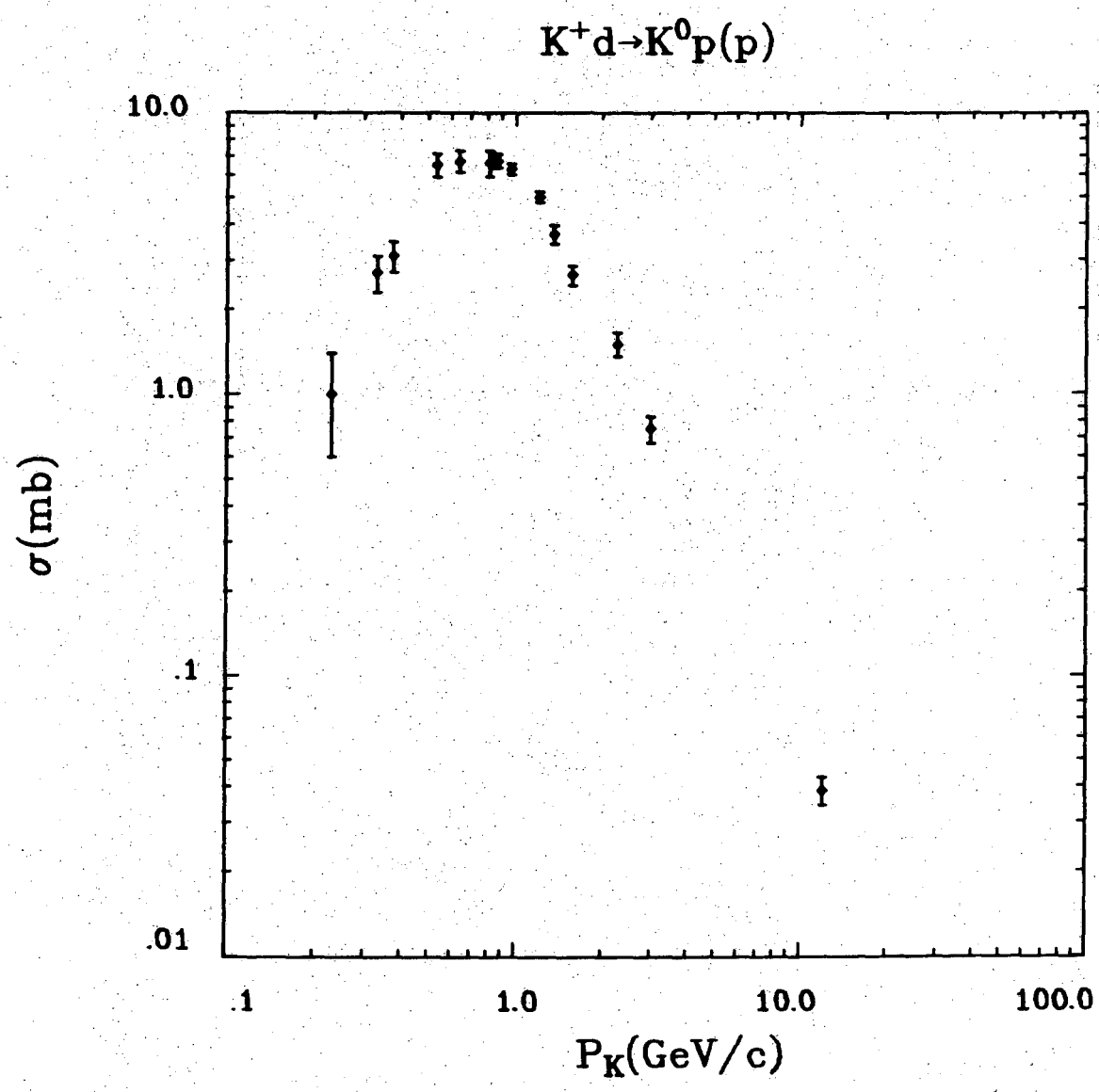

Fig. 15

XBL 708-1985

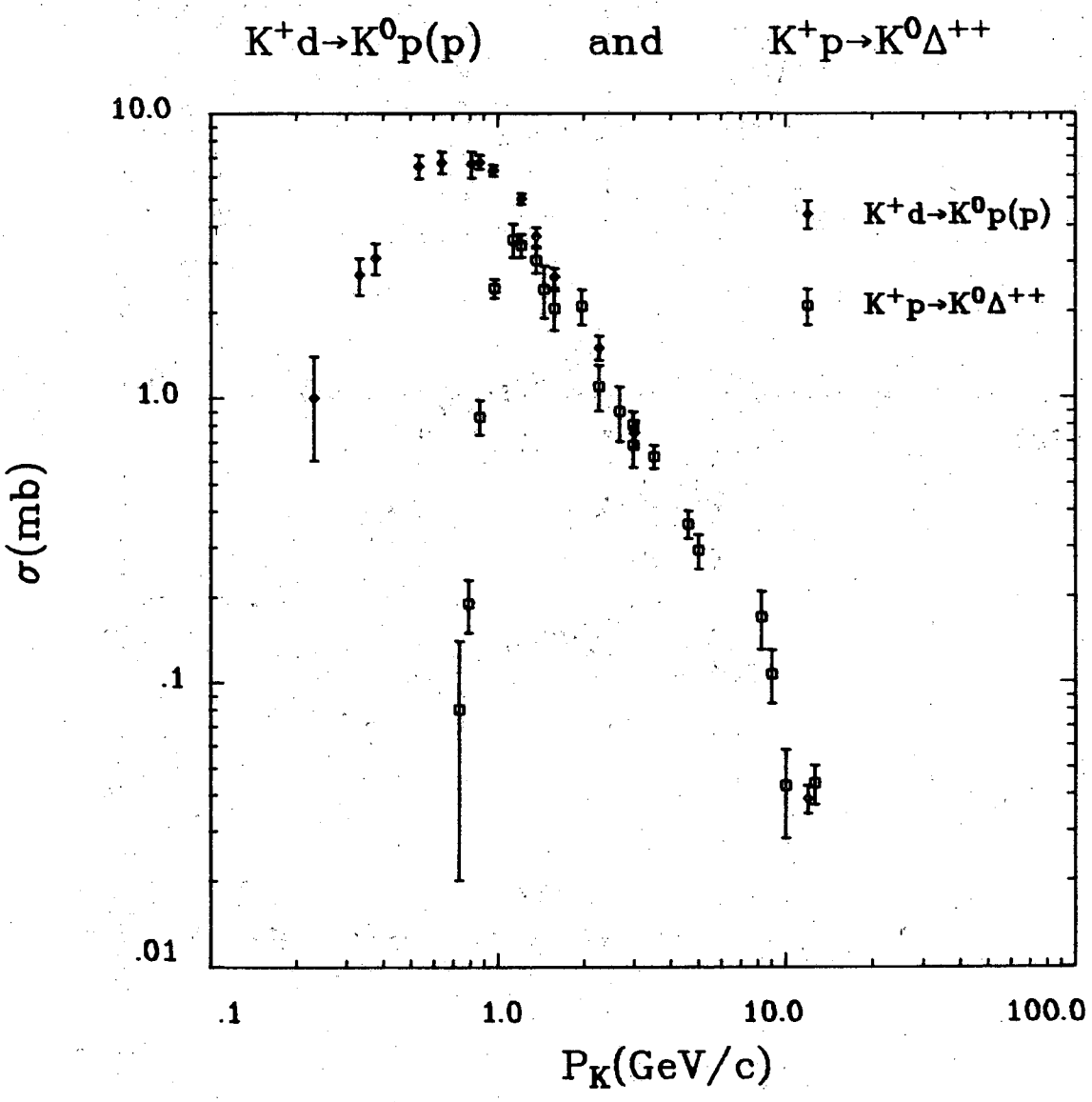

Fig. 16

XBL 708-1986

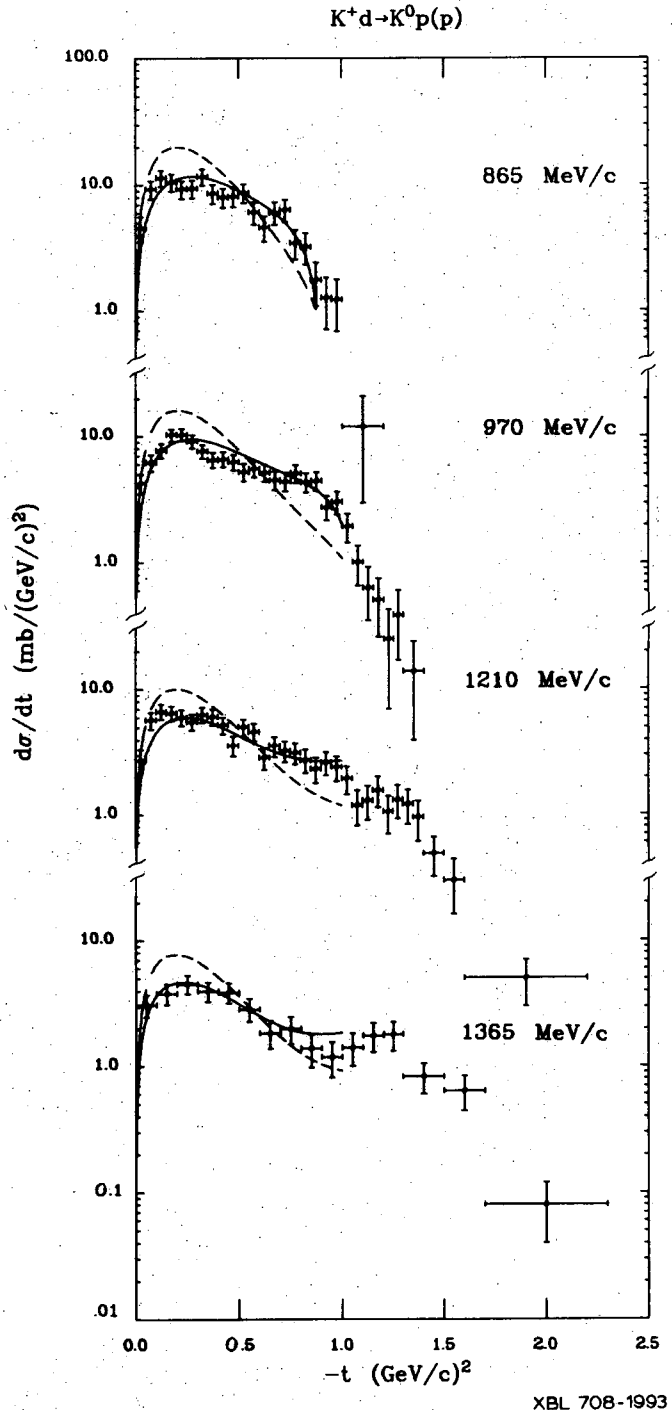
K+d→K0p(p)
100.0
10.0
1.0
865 MeV/c
10.0
1.0
970 MeV/c
10.0
1.0
1210 MeV/c
10.0
1.0
0.1
.01
1365 MeV/c
dσ/dt (mb/(GeV/c)2)
0.0
0.5
1.0
1.5
2.0
2.5
−t (GeV/c)2
XBL 708-1993

Fig. 17

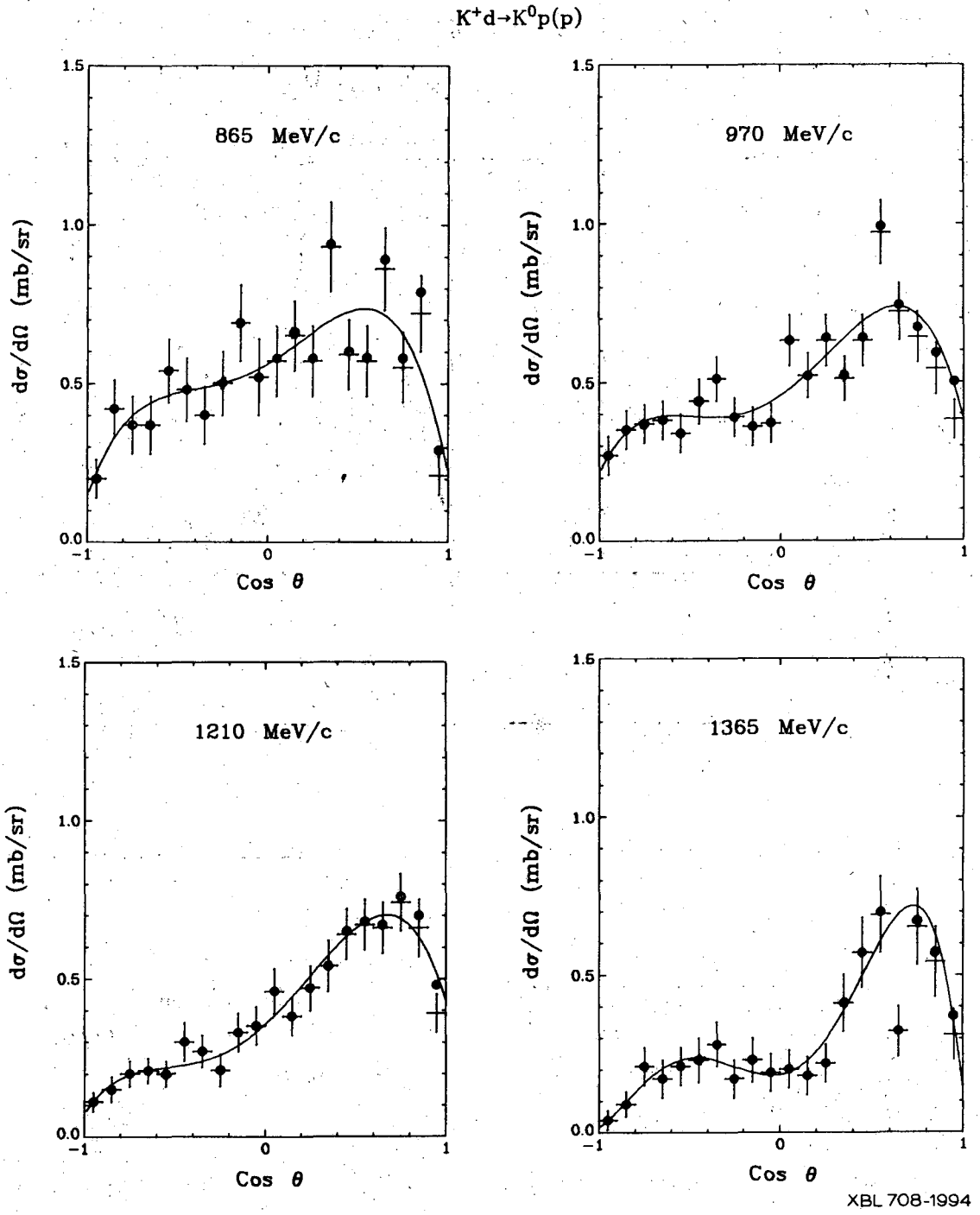
$K^+d \rightarrow K^0p(p)$
865 MeV/c
970 MeV/c
1210 MeV/c
1365 MeV/c
dσ/dΩ (mb/sr)
Cos θ
XBL 708-1994

Fig. 18

$K^+n \rightarrow K^0p$

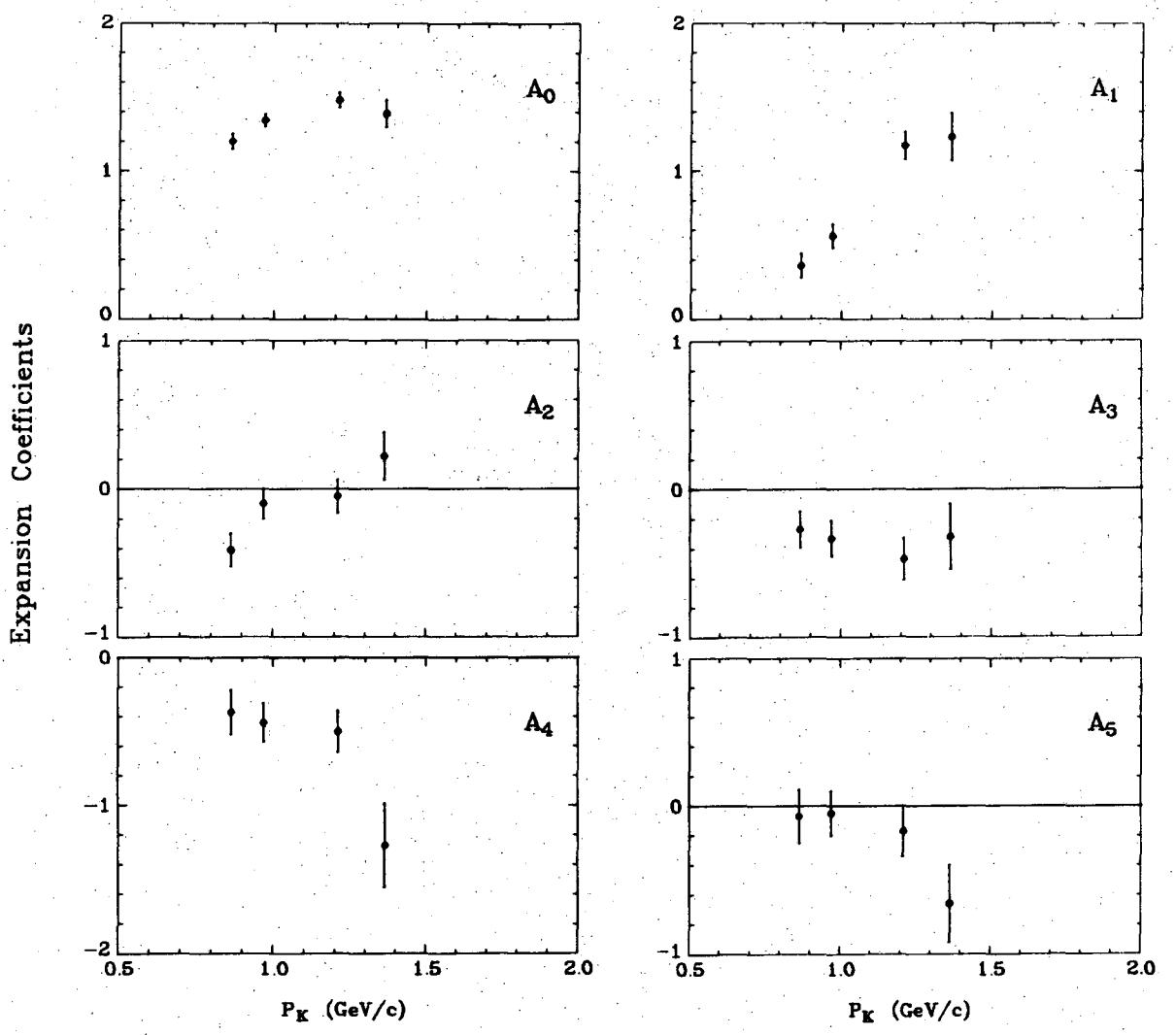

Fig. 19

XBL 708-1995

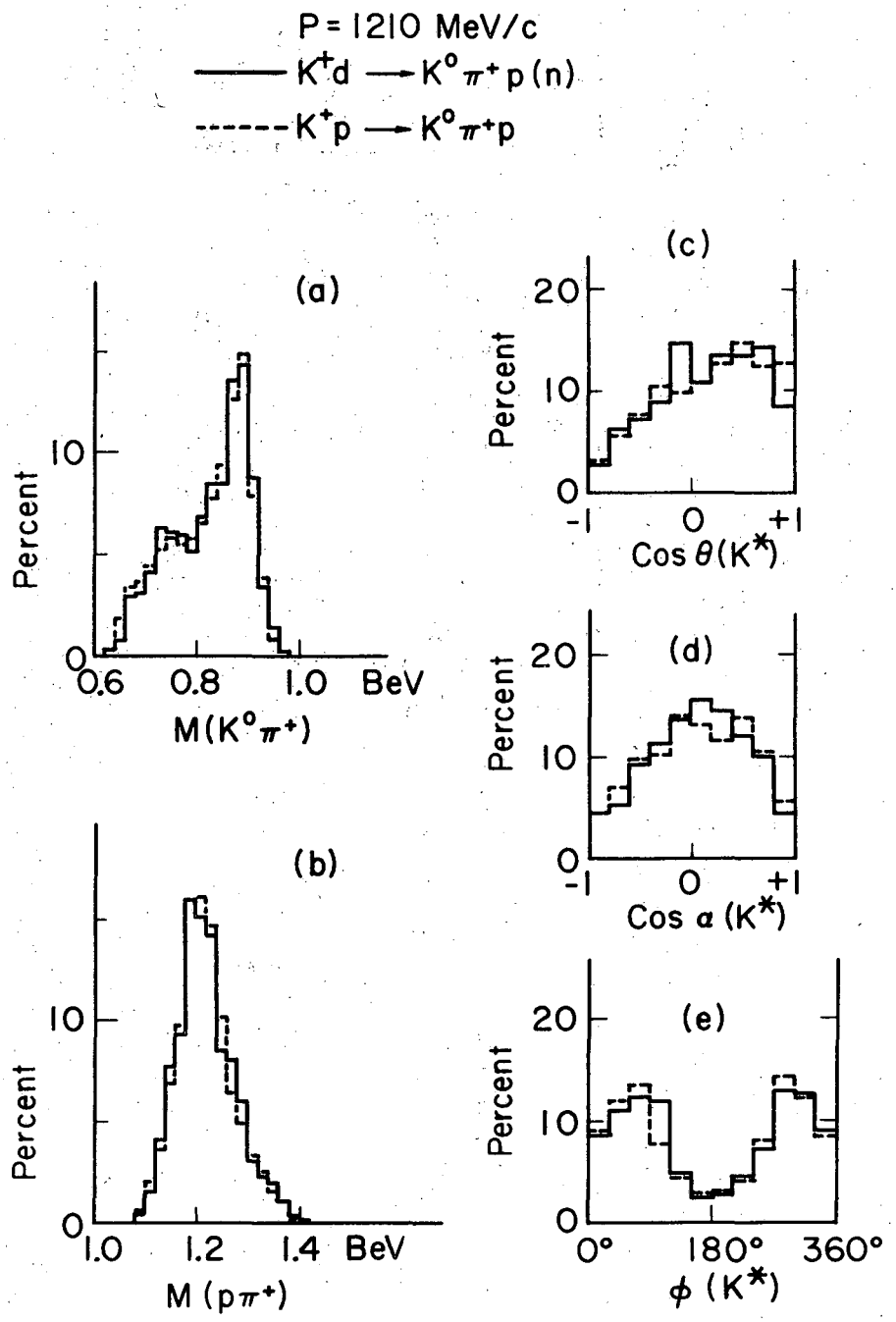

Fig. 20 XBL697-3211

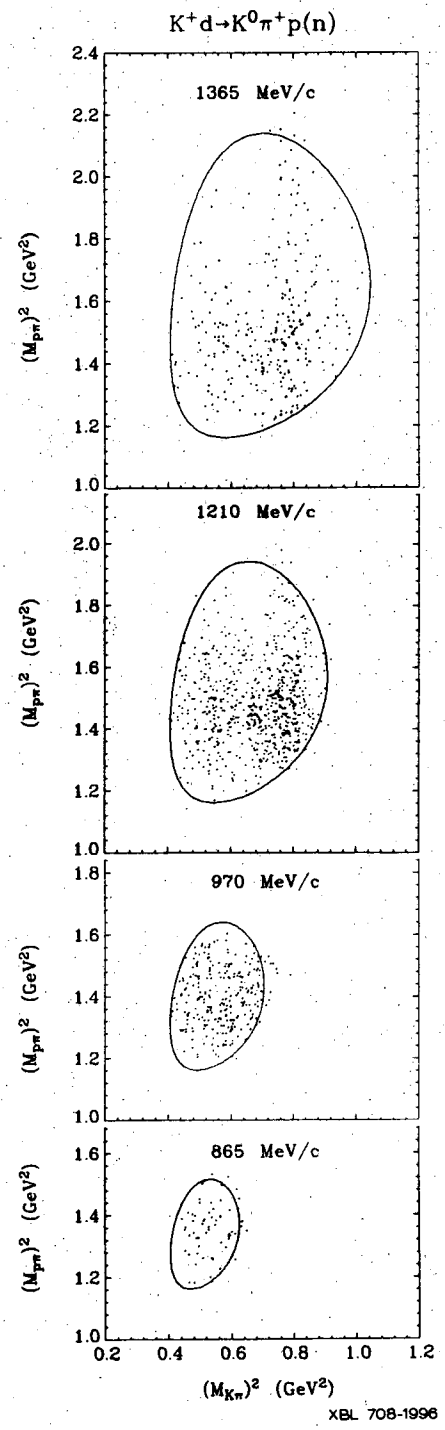
K+d→K0π+p(n)
1365 MeV/c
1210 MeV/c
970 MeV/c
865 MeV/c
(Mpπ)2 (GeV2)
(MKπ)2 (GeV2)
XBL 708-1996

Fig. 21

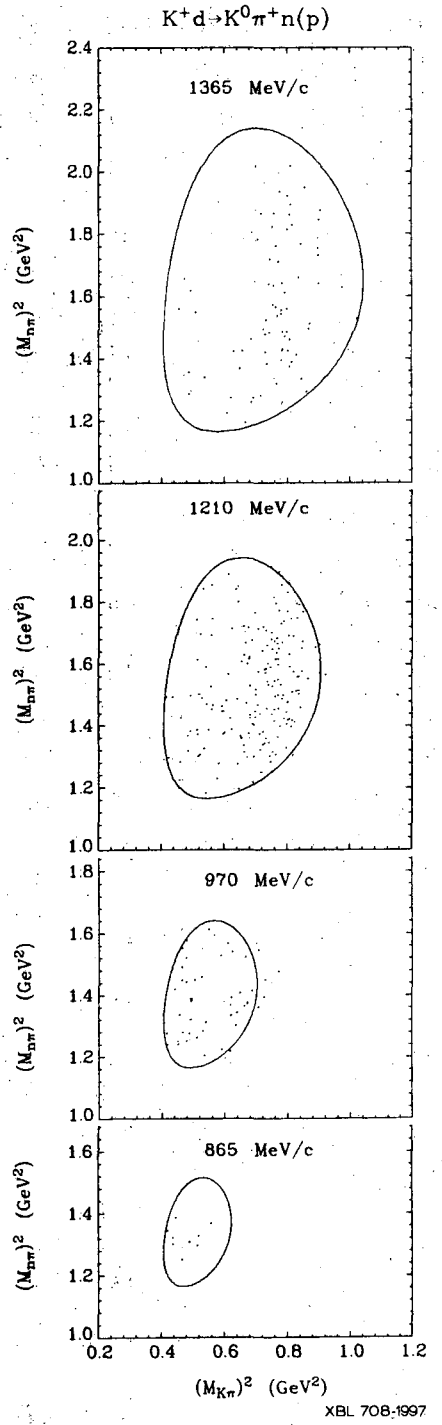
$K^+d \to K^0\pi^+n(p)$
1365 MeV/c
1210 MeV/c
970 MeV/c
865 MeV/c
$(M_{n\pi})^2$ (GeV^2)
$(M_{K\pi})^2$ (GeV^2)
XBL 708-1997

Fig. 22

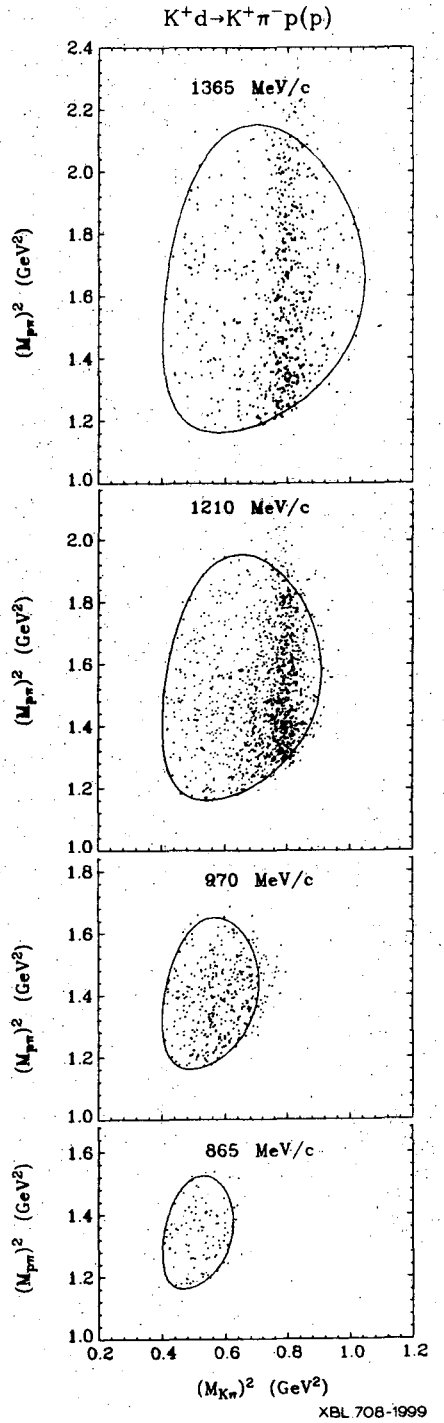
$K^+d \to K^+\pi^-p(p)$
1365 MeV/c
1210 MeV/c
970 MeV/c
865 MeV/c
$(M_{p\pi})^2$ (GeV^2)
$(M_{K\pi})^2$ (GeV^2)
XBL 708-1999

Fig. 23

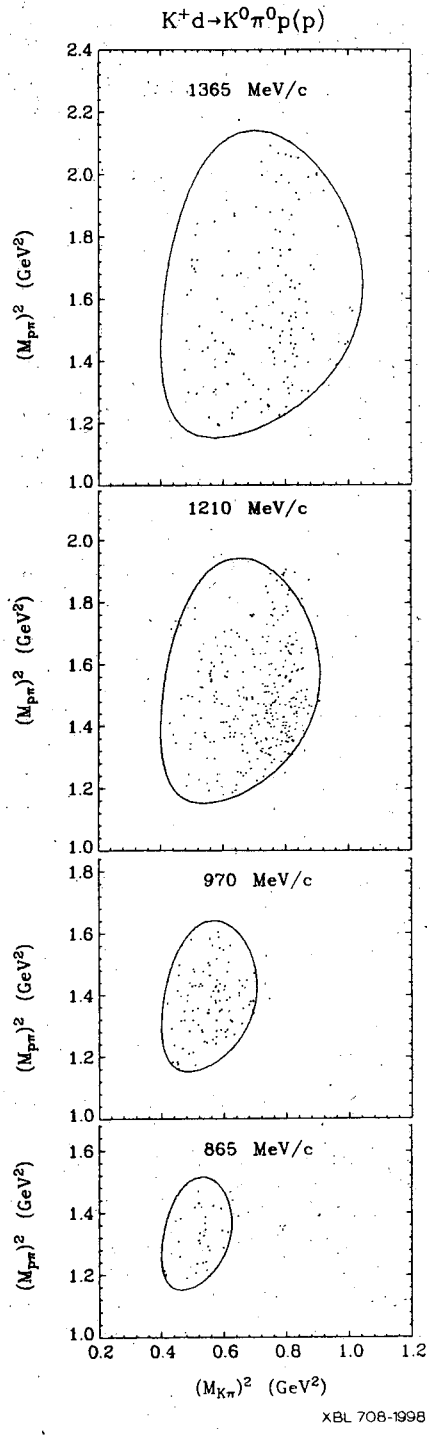
$K^+d \to K^0\pi^0p(p)$
1365 MeV/c
1210 MeV/c
970 MeV/c
865 MeV/c
$(M_{p\pi})^2$ (GeV^2)
$(M_{K\pi})^2$ (GeV^2)
XBL 708-1998

Fig. 24

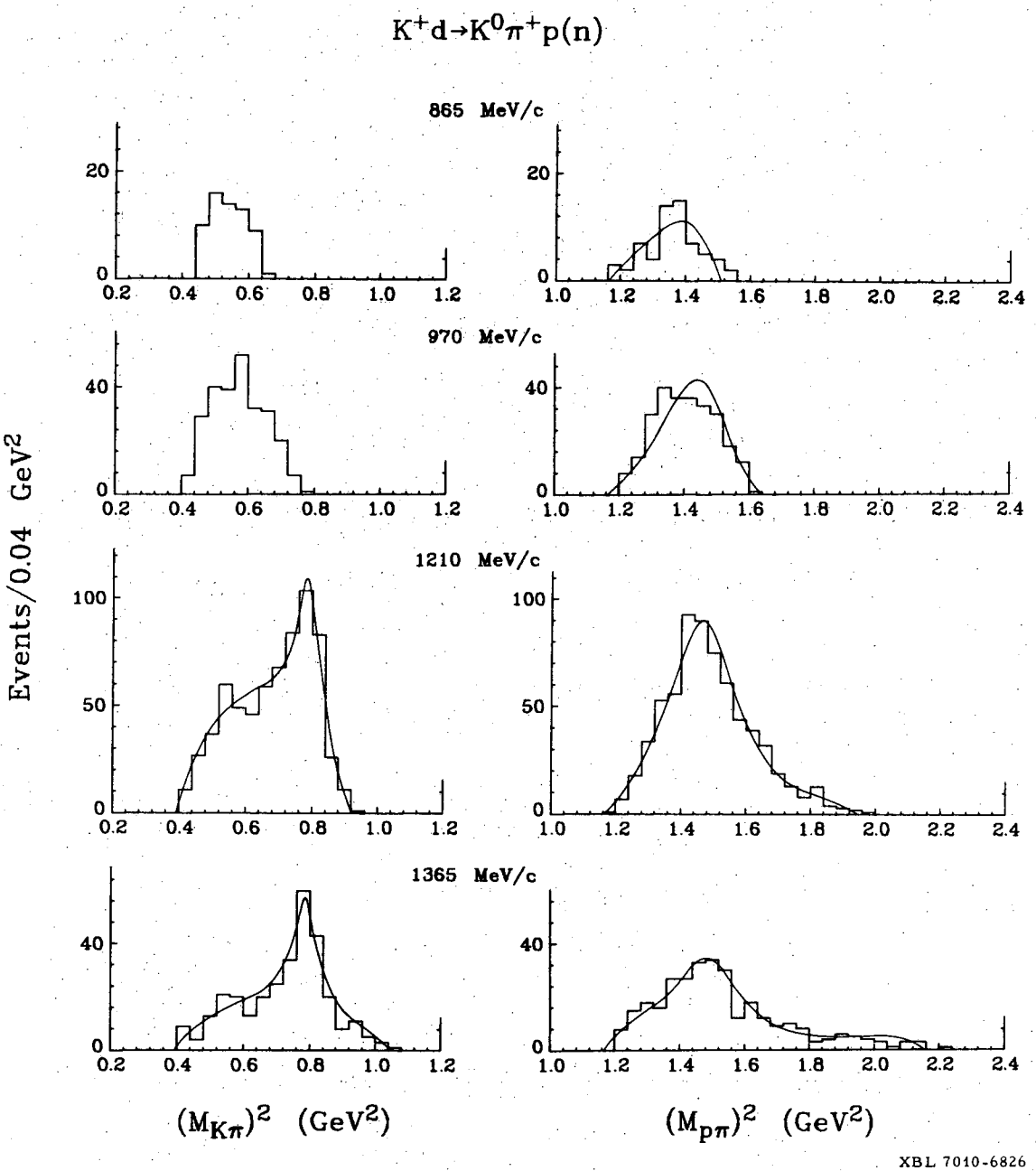
$K^+d \to K^0\pi^+p(n)$
865 MeV/c
970 MeV/c
1210 MeV/c
1365 MeV/c
Events/0.04 GeV^2
$(M_{K\pi})^2$ (GeV^2)
$(M_{p\pi})^2$ (GeV^2)
XBL 7010-6826

Fig. 25

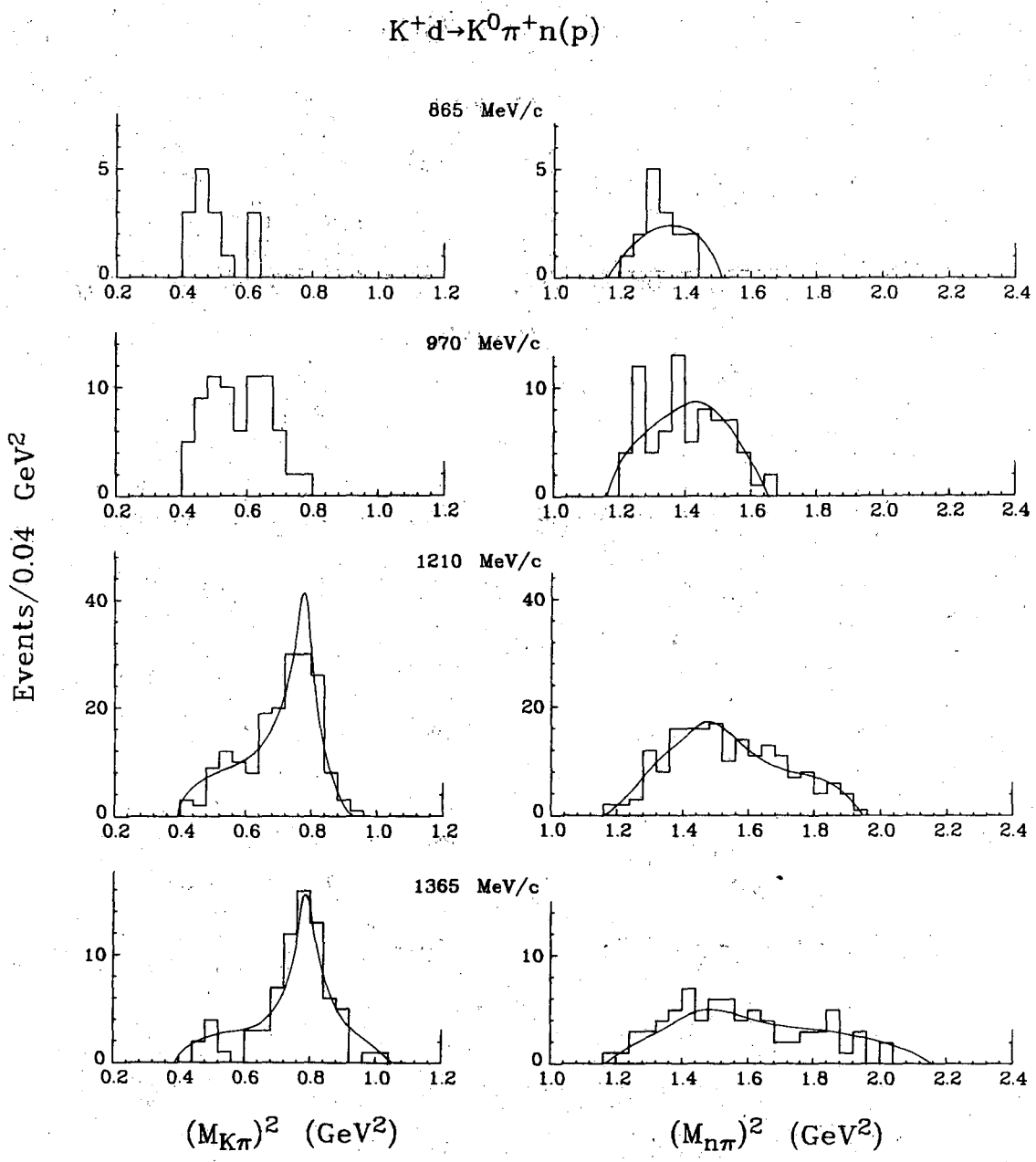
$K^+d \to K^0\pi^+n(p)$
865 MeV/c
970 MeV/c
1210 MeV/c
1365 MeV/c
Events/0.04 GeV^2
$(M_{K\pi})^2$ (GeV^2)
$(M_{n\pi})^2$ (GeV^2)
XBL 7010-6827

Fig. 26

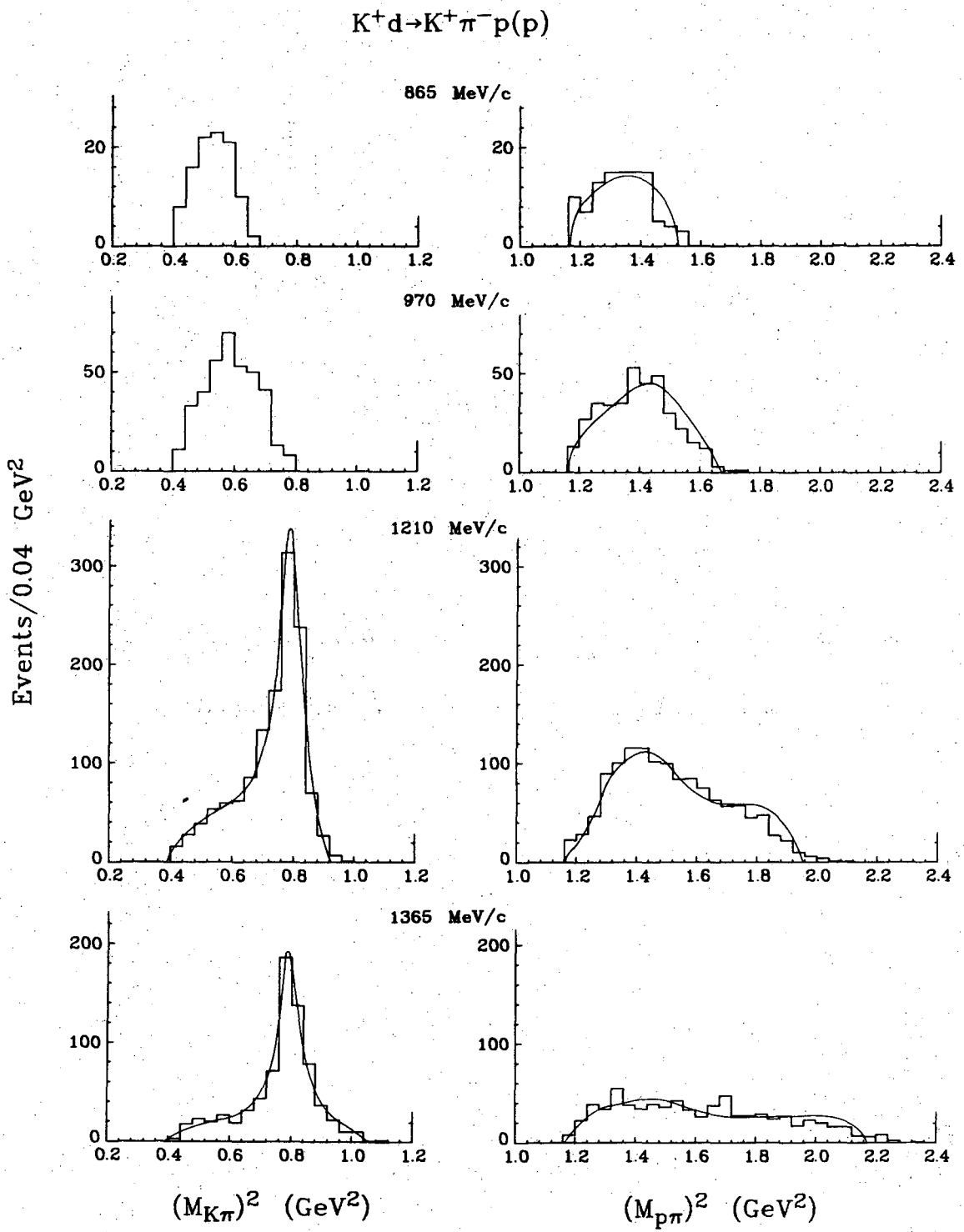

Fig. 27

XBL 7010-6828

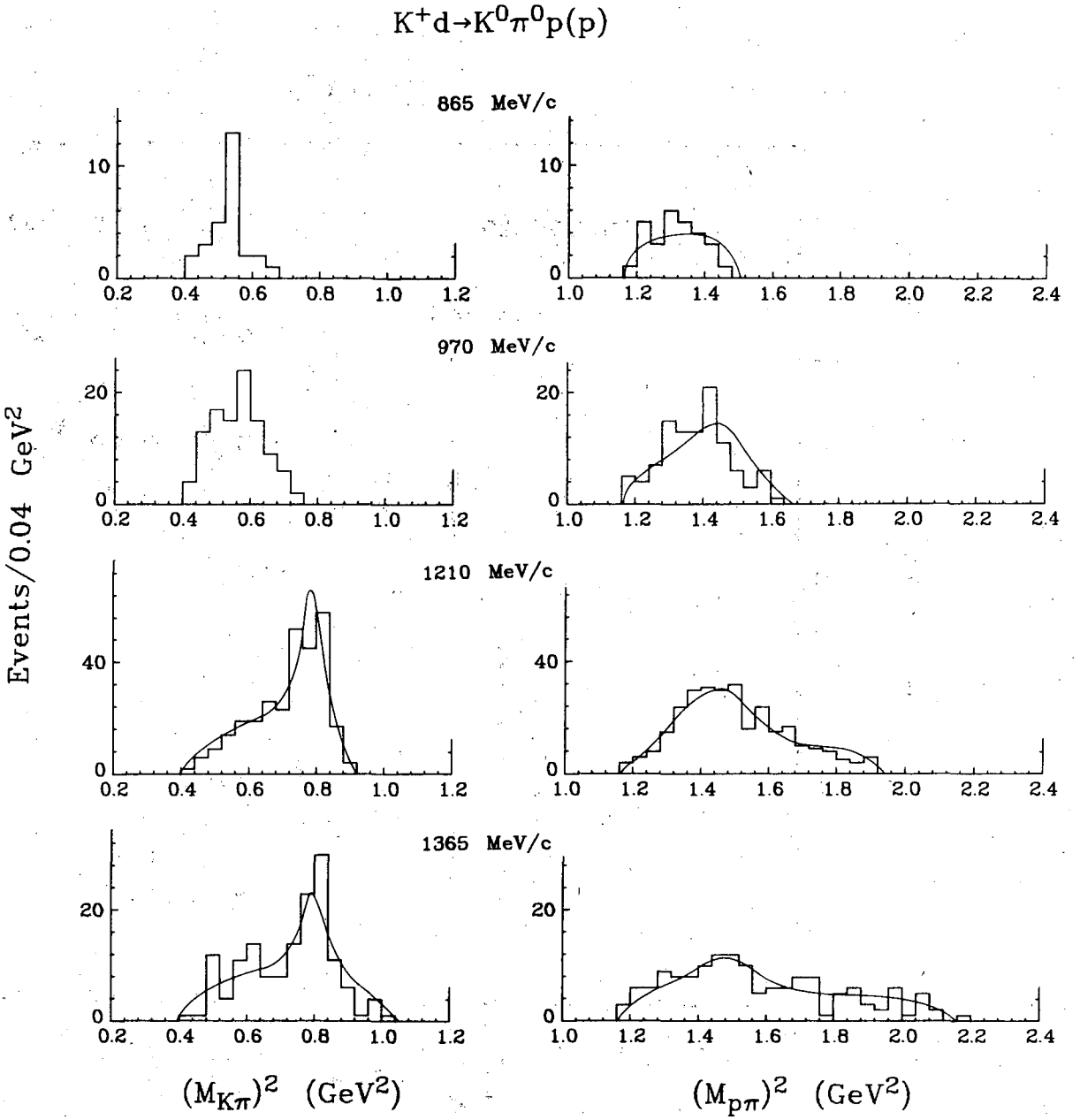

Fig. 28

XBL 7010-6829

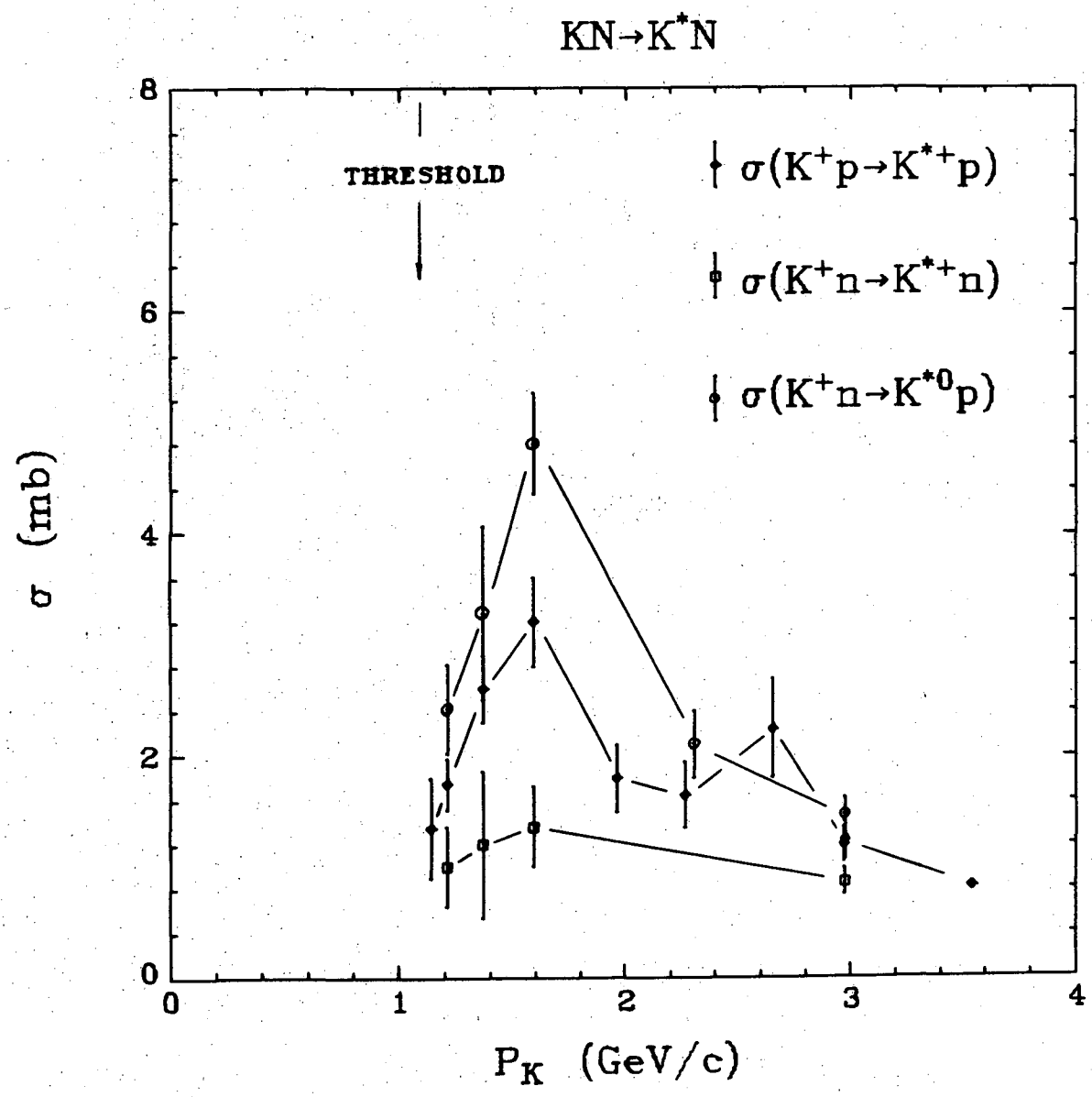

Fig. 29

XBL 7010-6681

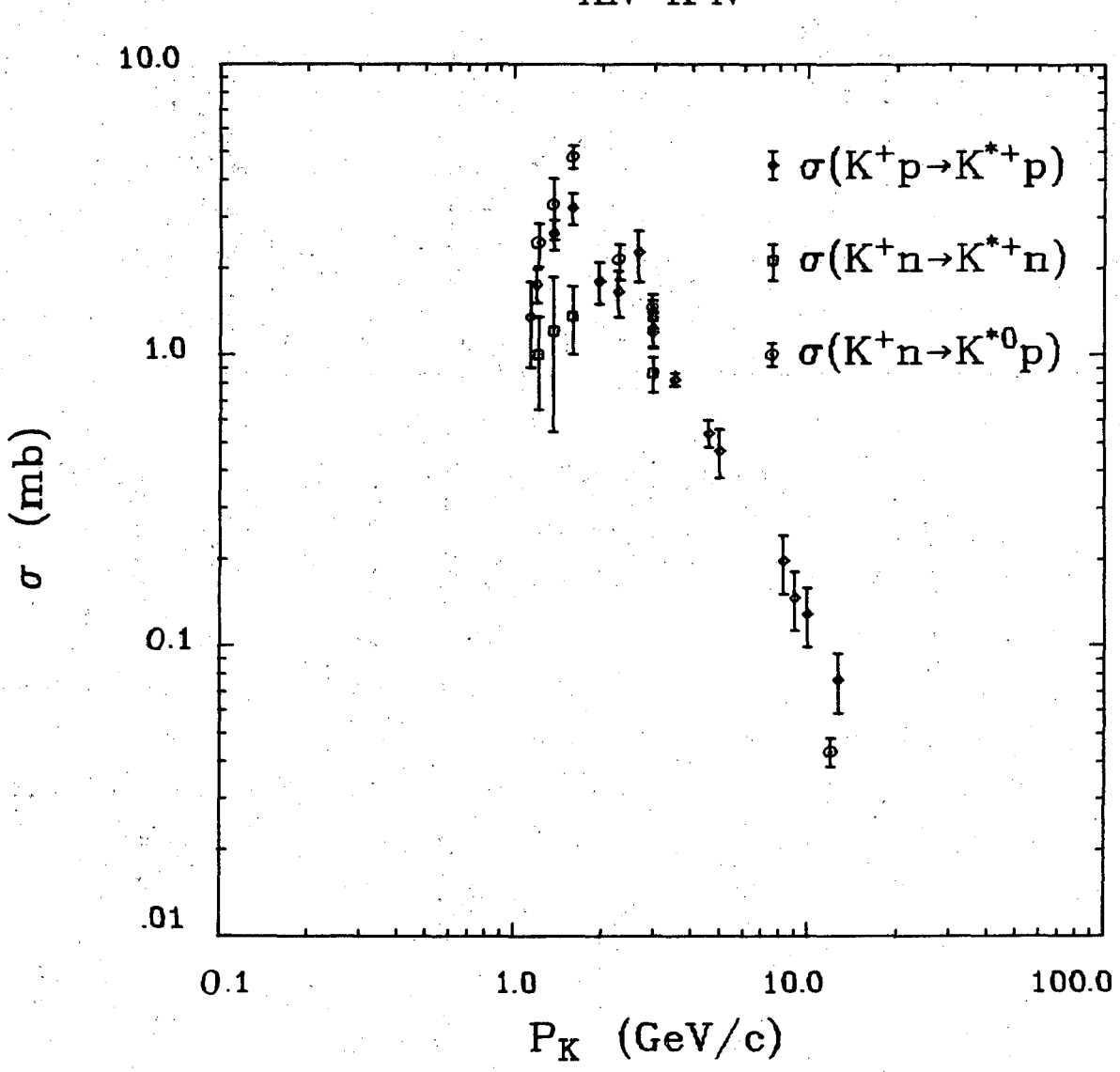

Fig. 30

XBL 7010-6680

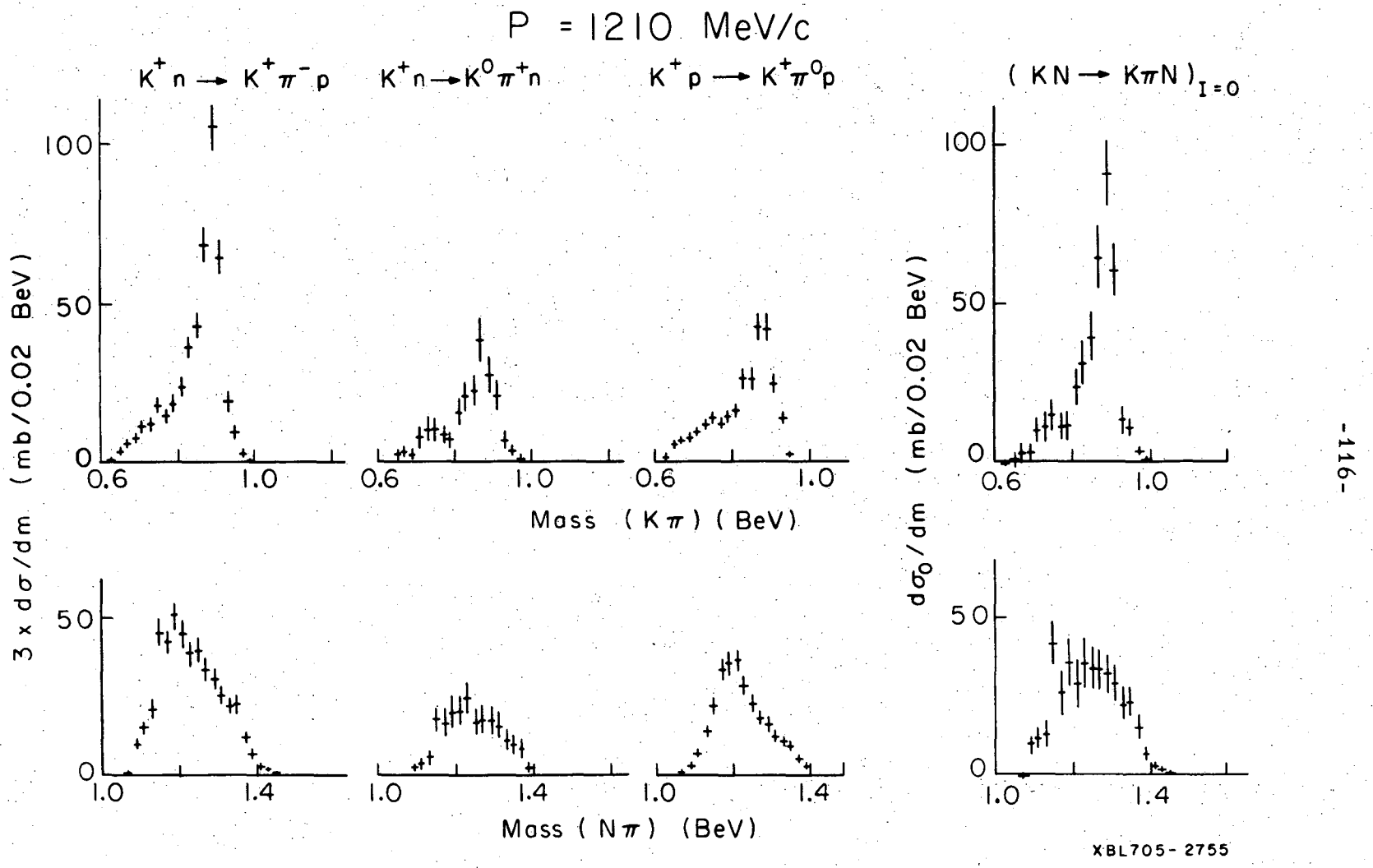
P = 1210 MeV/c
K+n → K+π−p
K+n → K0π+n
K+p → K+π0p
(KN → Kπ N)I=0
3 x dσ/dm (mb/0.02 BeV)
dσ0/dm (mb/0.02 BeV)
Mass (Kπ) (BeV)
Mass (Nπ) (BeV)
XBL705-2755

Fig. 31

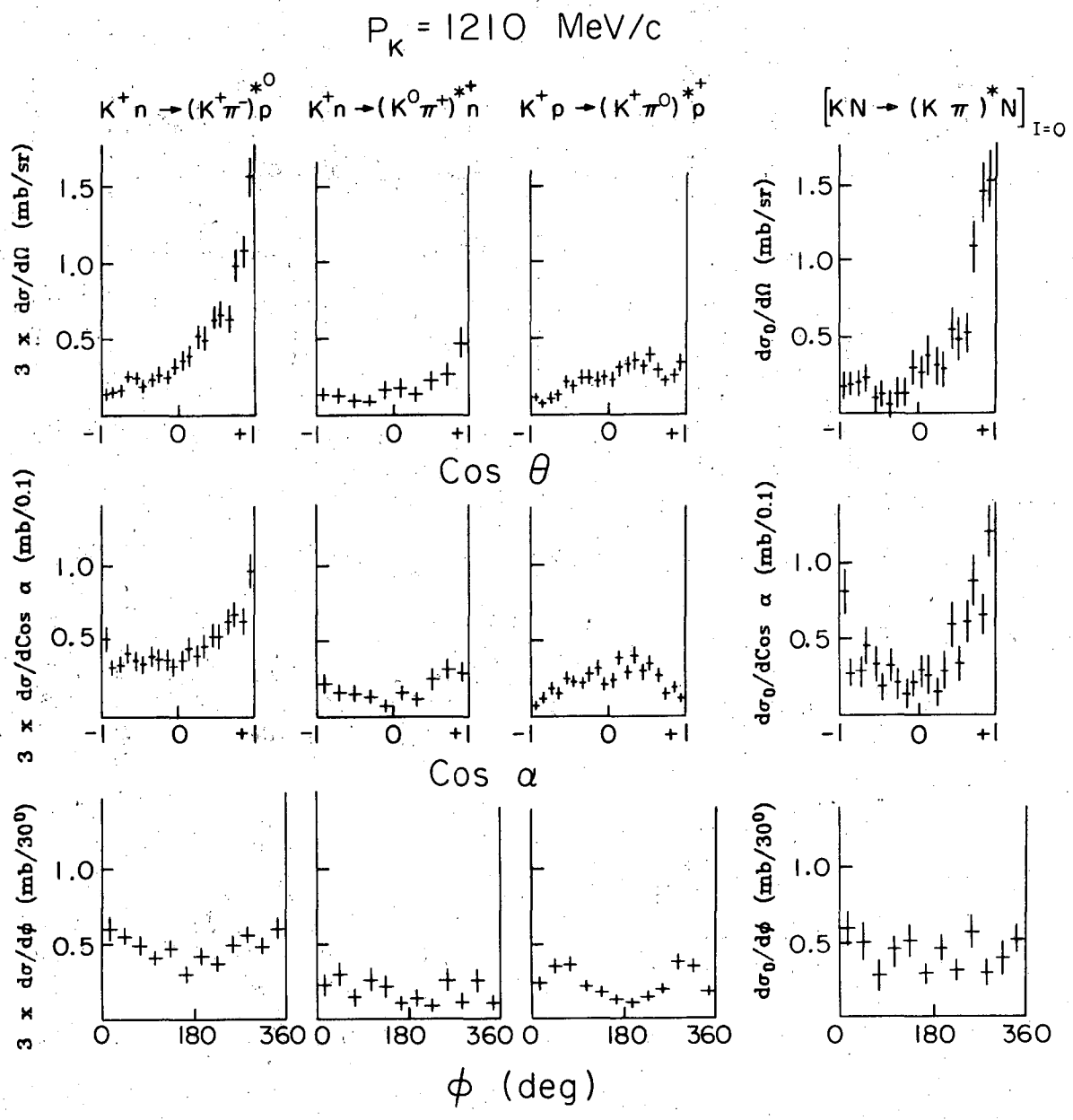

XBL705-2754

Fig. 32

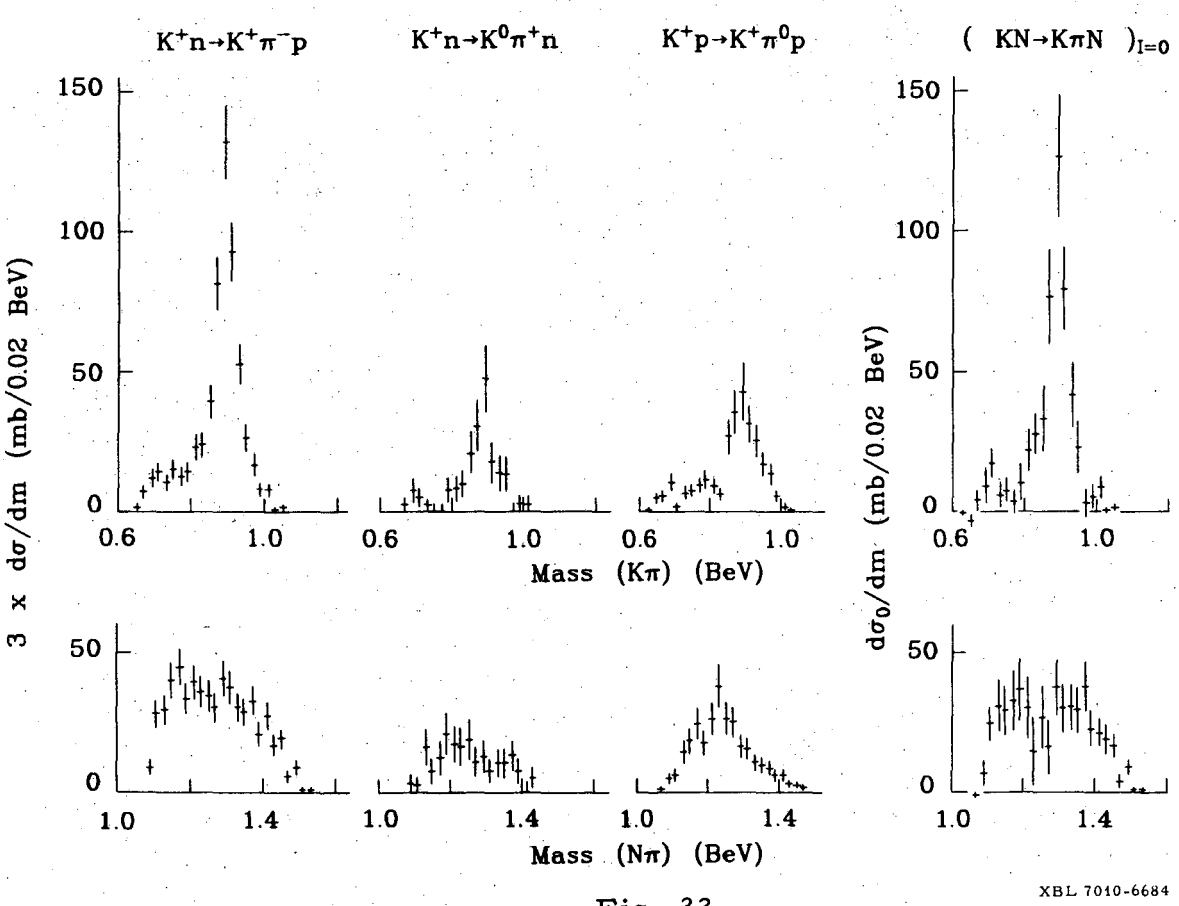
P = 1365 MeV/c
K⁺n→K⁺π⁻p
K⁺n→K⁰π⁺n
K⁺p→K⁺π⁰p
(KN→Kπ N)I=0
3 x dσ/dm (mb/0.02 BeV)
dσ0/dm (mb/0.02 BeV)
Mass (Kπ) (BeV)
Mass (Nπ) (BeV)
XBL 7010-6684

Fig. 33

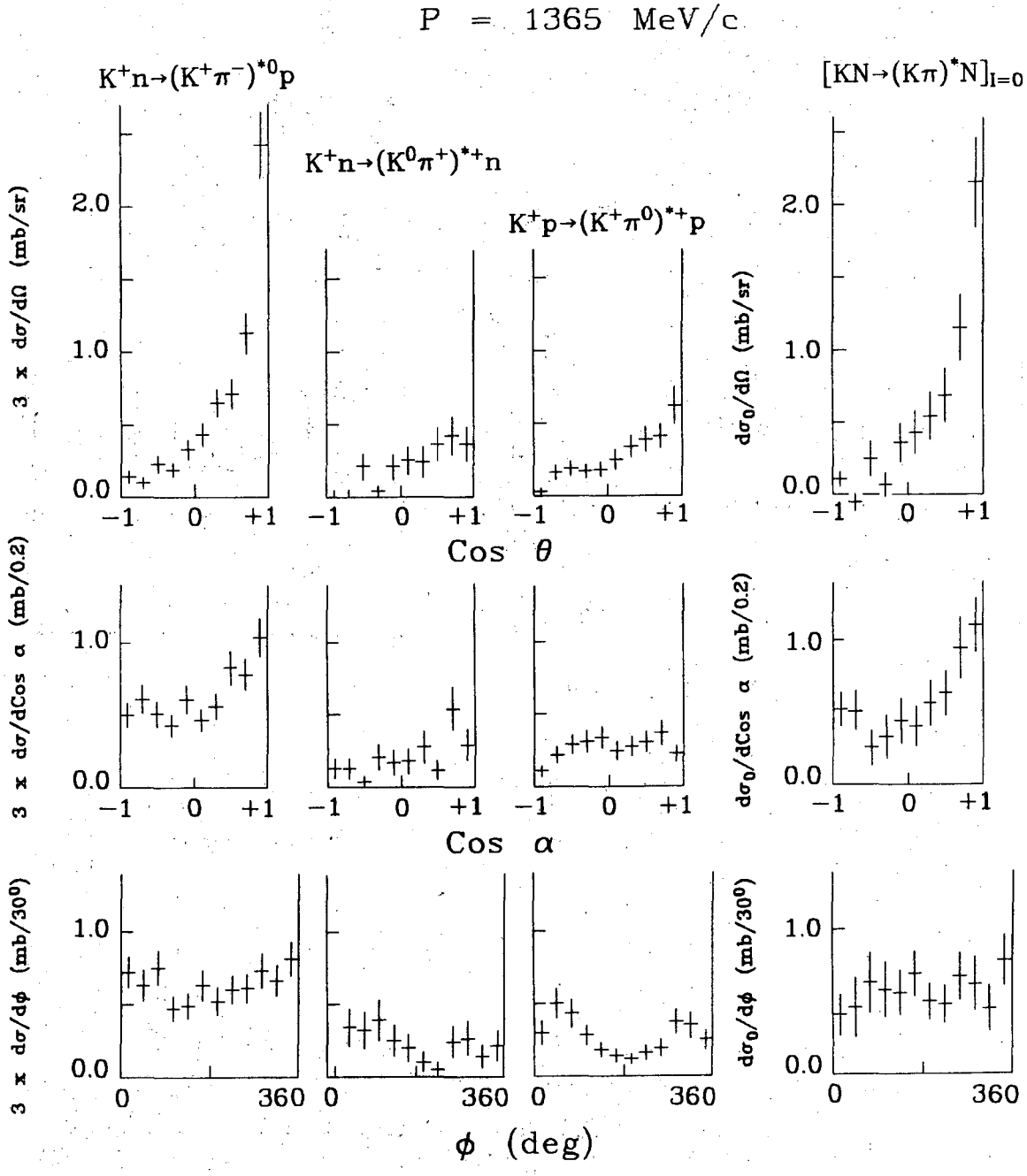

XBL 7010-6683

Fig. 34

$(KN \longrightarrow KN\pi)_{I=0}$

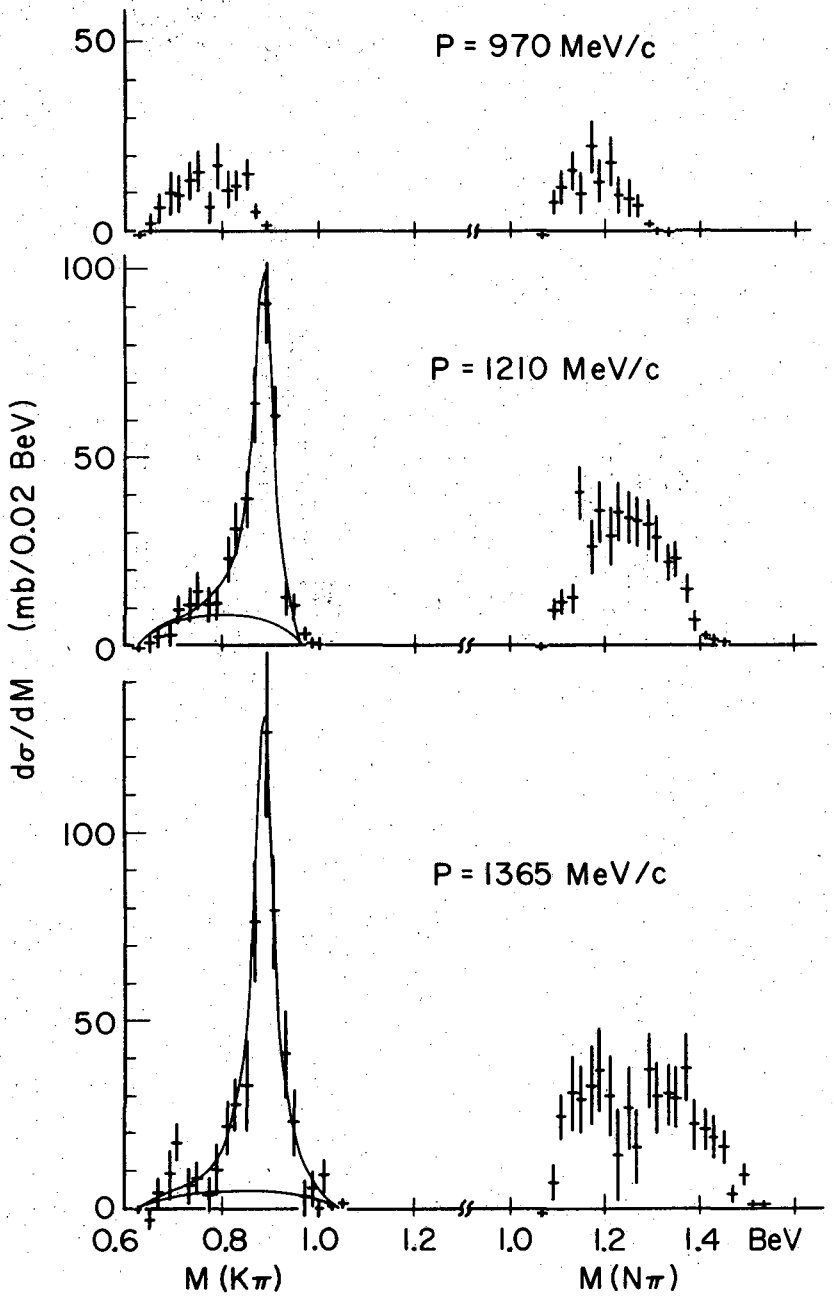

Fig. 35

XBL697-3212

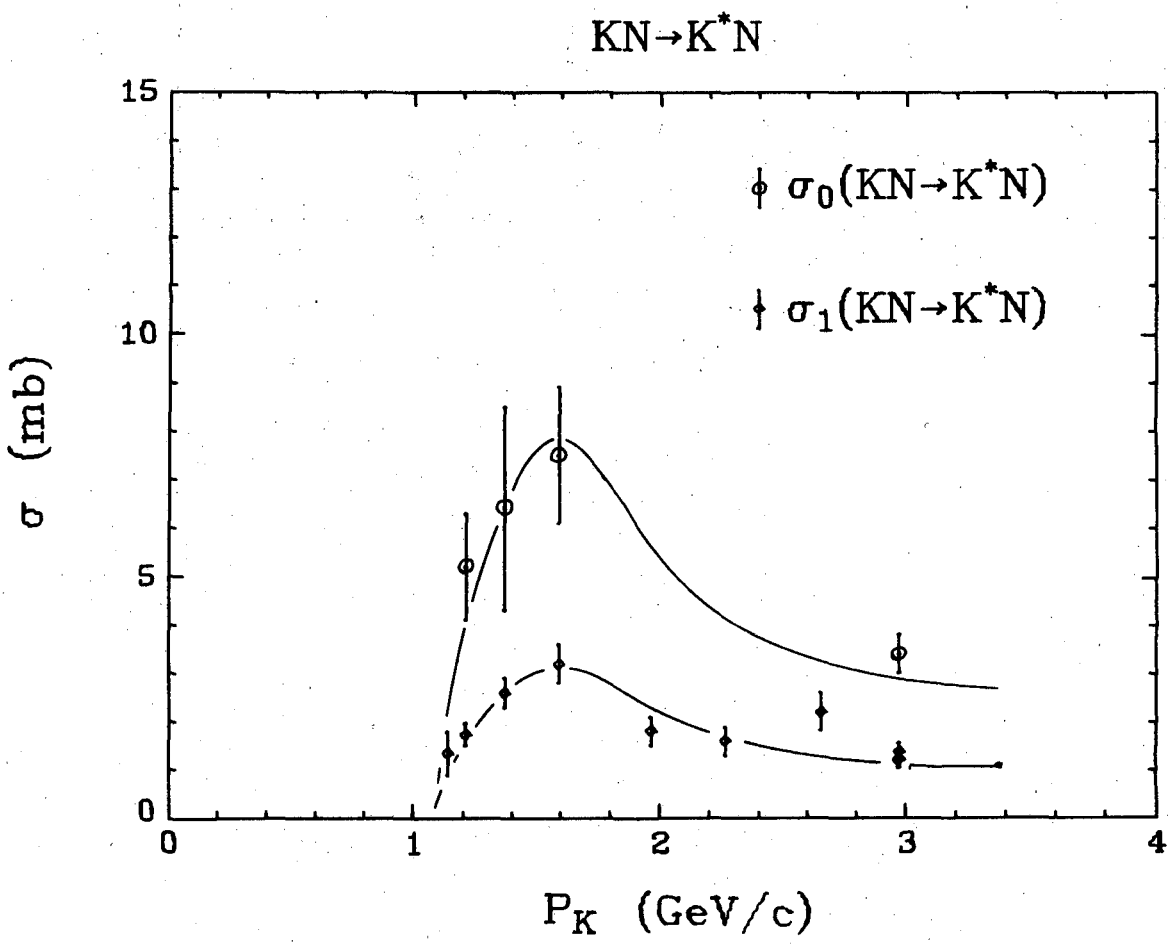

Fig. 36

XBL 7010-6679

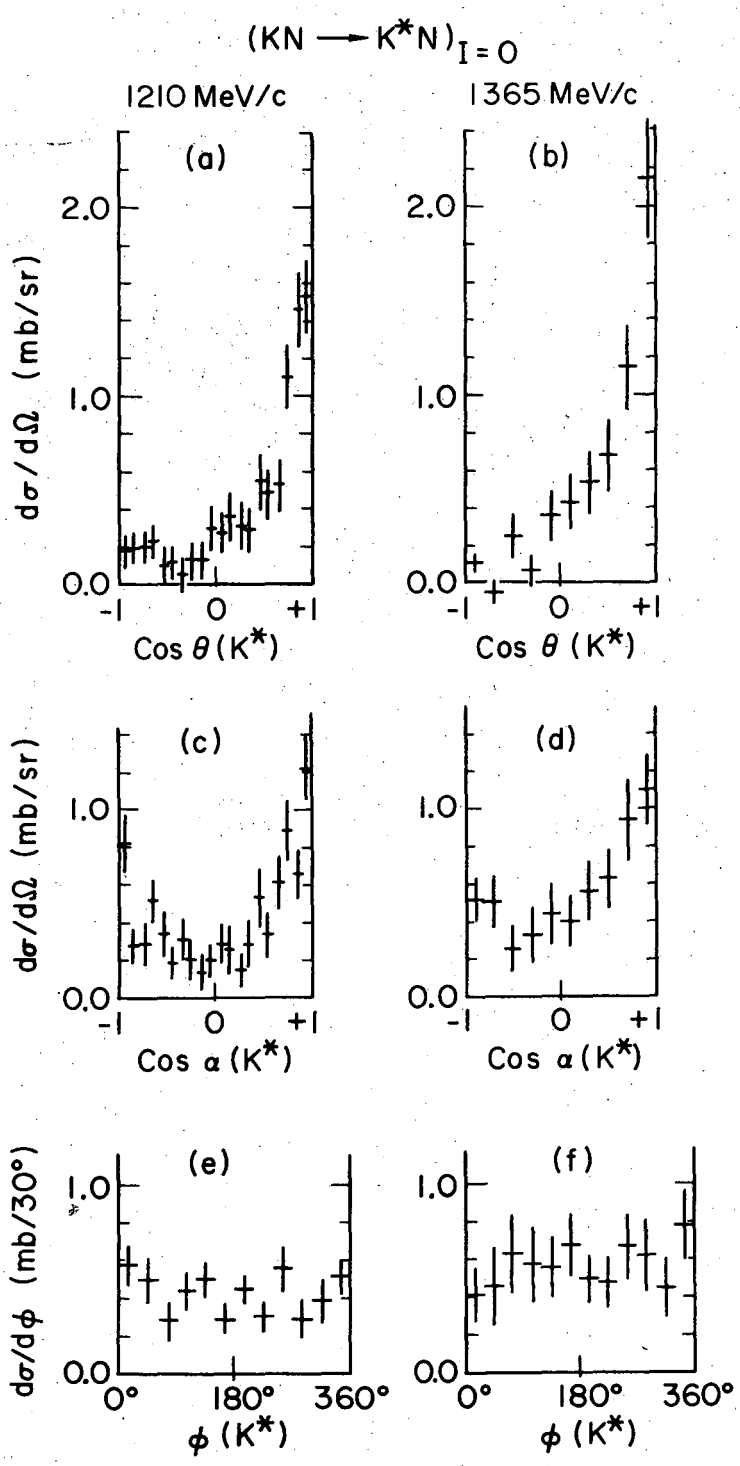

Fig. 37

XBL697-3213

$(KN \to K^* N)_{I=0}$

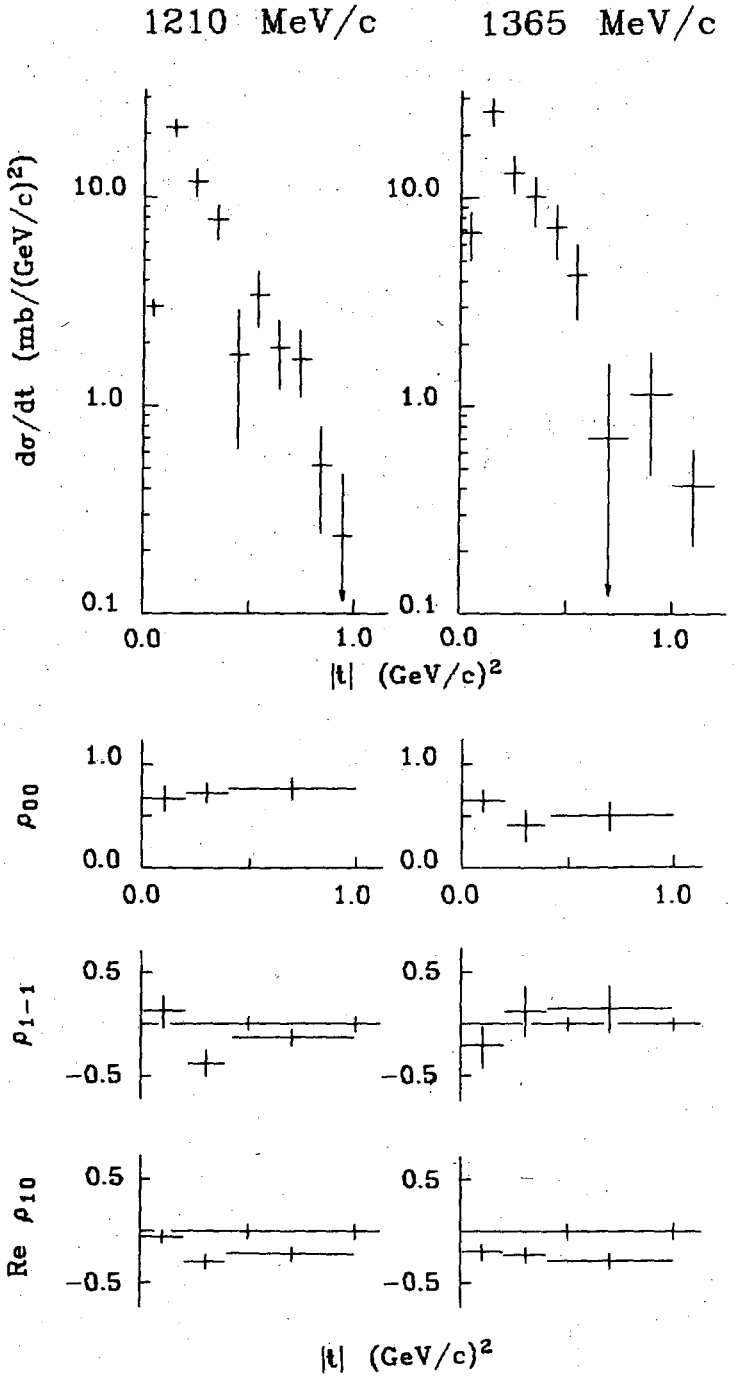

XBL 7010-6682

Fig. 38

TECHNICAL INFORMATION DIVISION
LAWRENCE RADIATION LABORATORY
UNIVERSITY OF CALIFORNIA
BERKELEY, CALIFORNIA 94720